Integrative and comprehensive Understanding on Polar Environments (iCUPE): the concept and initial results

Tuukka Petäjä[1], Ella-Maria Duplissy[1], Ksenia Tabakova[1], Julia Schmale[2,3], Barbara Altstädter[4], Gerard Ancellet[5], Mikhail Arshinov[6], Yurii Balin[6], Urs Baltensperger[2], Jens Bange[7], Alison Beamish[8], Boris Belan[6], Antoine Berchet[9], Rossana Bossi[10], Warren R.L. Cairns[11], Ralf Ebinghaus[12], Imad El Haddad[2], Beatriz Ferreira-Araujo[13], Anna Franck[1], Lin Huang[14], Antti Hyvärinen[15], Angelika Humbert[16,17], Athina-Cerise Kalogridis[18], Pavel Konstantinov[19], Astrid Lampert[4], Matthew MacLeod[20], Olivier Magand[21], Alexander Mahura[1], Louis Marelle[5,21], Vladimir Masloboev[22], Dmitri Moisseev[1], Vaios Moschos[2], Niklas Neckel[16], Tatsuo Onishi[5], Stefan Osterwalder[21], Aino Ovaska[1], Pauli Paasonen[1], Mikhail Panchenko[6], Fidel Pankratov[22], Jakob B. Pernov[10], Andreas Platis[7], Olga Popovicheva[23], Jean-Christophe Raut[5], Aurélie Riandet[9#], Torsten Sachs[8], Rosamaria Salvatori[24], Roberto Salzano[25], Ludwig Schröder[16], Martin Schön[7], Vladimir Shevchenko[26], Henrik Skov[10], Jeroen E. Sonke[13], Andrea Spolaor[11], Vasileios Stathopoulos[18], Mikko Strahlendorff[15], Jennie L. Thomas[21], Vito Vitale[11], Sterios Vratolis[18], Carlo Barbante[11,27], Sabine Chabrillat[8], Aurélien Dommergue[21], Konstantinos Eleftheriadis[18], Jyri Heilimö[15], Kathy S. Law[5], Andreas Massling[10], Steffen M. Noe[28], Jean-Daniel Paris[9], André Prévôt[2], Ilona Riipinen[20], Birgit Wehner[29], Zhiyong Xie[12] and Hanna K. Lappalainen[1,15]

[1]Institute for Atmospheric and Earth System Research/Physics, Faculty of Science, P.O. Box 64, 00014 University of Helsinki, Finland

[2]Laboratory of Atmospheric Chemistry, Paul Scherrer Institute, Villigen PSI, Switzerland

[3]School of Architecture, Civil and Environmental Engineering, École Polytechnique Fédérale de Lausanne, Switzerland

[4]Institute of Flight Guidance, Technische Universität Braunschweig, Germany

[5]LATMOS/IPSL, Sorbonne Université, UVSQ, CNRS, Paris, France

[6]V.E. Zuev Institute of Atmospheric Optics of Siberian Branch of the Russian Academy of Science (IAO SB RAS), Tomsk, Russia

[7]Center for Applied Geoscience, Eberhard-Karls-University, Tübingen, Germany

[8]GFZ German Research Centre for Geosciences, Telegrafenberg, Potsdam, Germany

[9]Laboratoire des Sciences du Climat et de l'Environnement, CEA-CNRS-UVSQ, IPSL, Gif-sur-Yvette, France

[10]Department of Environmental Science, iClimate, Aarhus University, Frederiksborgvej 399, 4000 Roskilde, Denmark

[11]Institute of Polar Sciences, National Research Council of Italy (CNR), Via Torino 155, (I) 30172 Venezia-Mestre (VE), Italy

[12]Helmholtz-Zentrum Geesthacht (HZG), Centre for Materials and Coastal Research, Geesthacht, Germany

[13]Geosciences Environnement Toulouse, CNRS/IRD/Universite Paul Sabatier, Toulouse, France

[14]Climate Research Division, ASTD/STB, Environment & Climate Change Canada (ECCC), Toronto, Canada

[15]Finnish Meteorological Institute (FMI), Helsinki, Finland

[16]Alfred Wegener Institute Helmholtz Centre for Polar and Marine Research (AWI), Bremerhaven, Germany

[17]Department for Geoscience, University of Bremen, Bremen, Germany

[18]Environmental Radioactivity Laboratory, Institute of Nuclear and Radiological Science & Technology, Energy & Safety, NCSR Demokritos, Athens, Greece

[19]Faculty of Geography, Moscow State University, Moscow

[20]Department of Environmental Science and Analytical Chemistry, Stockholm University, Sweden

40   [21]Univ. Grenoble Alpes, CNRS, IRD, Grenoble INP, IGE, 38000 Grenoble, France

[22]Institute of Northern Environmental Problems (INEP), Kola Science Center (KSC), Russian Academy of Sciences (RAS), Apatity, Murmansk region, Russia

[23]Skobeltsyn Institute of Nuclear Physics, Lomonosov Moscow State University, Moscow 119991, Russia

[24]Institute of Polar Sciences, National Research Council of Italy (CNR), Monterotondo (RM), Italy

45   [25]Institute of Atmospheric Pollution Research, National Research Council of Italy (CNR), Sesto Fiorentino (FI), Italy

[26]Shirshov Institute of Oceanology, Russian Academy of Sciences, Moscow, Russia

[27]Ca' Foscari University of Venice, Department of Environmental Sciences, Informatics and Statistics, Via Torino 155, 30172 Mestre, Venice, Italy

[28]Institute of Agricultural and Environmental Sciences, Estonian University of Life Sciences, Tartu, Estonia

50   [29]Leibniz Institute for Tropospheric Research, Leipzig, Germany

Currently at:
[#]Institut Méditerranéen de Biodiversité et d'Ecologie marine et continentale (IMBE), Aix-Marseille Université-Avignon Université-CNRS-IRD, Marseille, France

Abstract. The role of polar regions increases in terms of megatrends such as globalization, new transport routes, demography and use of natural resources consequent effects of regional and transported pollutant concentrations. We set up the ERA-PLANET Strand 4 project "iCUPE - integrative and Comprehensive Understanding on Polar Environments" to provide novel insights and observational data on global grand challenges with an Arctic focus. We utilize an integrated approach combining in situ observations, satellite remote sensing Earth Observations (EO) and multi-scale modeling to synthesize data from comprehensive long-term measurements, intensive campaigns and satellites to deliver data products, metrics and indicators to the stakeholders concerning the environmental status, availability and extraction of natural resources in the polar areas. The iCUPE work consists of thematic state-of-the-art research and provision of novel data in atmospheric pollution, local sources and transboundary transport, characterization of arctic surfaces and their changes, assessment of concentrations and impacts of heavy metals and persistent organic pollutants and their cycling, quantification of emissions from natural resource extraction and validation and optimization of satellite Earth Observation (EO) data streams. In this paper we introduce the iCUPE project and summarize initial results arising out of integration of comprehensive in situ observations, satellite remote sensing and multiscale modeling in the Arctic context.

1 Introduction

The project "iCUPE - integrative and Comprehensive Understanding on Polar Environments" is motivated by the increasing role of Arctic regions in terms of megatrends such as globalization, new transport routes, demography and use of natural resources. These megatrends will rapidly and drastically affect the environment. In particular, the Arctic will face such grand challenges as the soil and water pollution, climate change, land use change, higher demand for resource extraction, increased anthropogenic emissions due to year-round shipping in the Arctic Ocean and other local sources as well as long-range transported pollution from Europe, Asia and North America (e.g. Buixade Farré et al., 2014). Overall, land and ocean areas located in the polar latitudes are currently undergoing and will undergo substantial changes due to increased anthropogenic activities and shipping during the next decades. These activities will put the fragile Arctic environment and the population living in this area in a vulnerable position. The changes will pose unpredictable consequences on food chains, biodiversity and the primary production of different plant ecosystems and ecosystem capacity to recover from the pollution exposure and environmental changes (e.g. Arnold et al., 2016).

The future warming of the Arctic will affect demographic trends by increasing urbanization and migration to northern regions, and by accelerating changes in societal issues and air quality (Schmale et al., 2018). One major consequence of warming in the northern latitudes is related to changes in the cryosphere, including ice sheet mass loss (Helm et al., 2014), the thawing of permafrost and the Arctic Ocean becoming sea ice free part of the year (Kokelj et al., 2017; Meier et al., 2014; Kulmala et al., 2015; Lappalainen et al., 2016; Boy et al., 2019). Even with limiting global warming to 1.5° or 2° C, temperatures over the high Arctic, in particular north Greenland, will rise by 3-4° C by 2100 due to the polar amplification, enhancing impacts like mass loss of the ice sheet (Rückamp et al., 2018). This will accelerate global trade activities in the Arctic region then likely the northern sea route is seasonally opened for shipping between the Atlantic and Asia's Far East. Northern ecosystems and Arctic regions are a source of major natural resources such as oil, natural gas and minerals. The availability and exploitation of natural resources depends also on how significantly the permafrost thaw will damage existing infrastructure.

Human activities have had a profound impact on the composition of the atmosphere and the pollution in the environment through the introduction of increasing quantities of heavy metals and other trace elements (Barbante et al., 2001), radioactive nuclides (Ezerinkis et al., 2014), synthesized organic compounds (Hermanson et al., 2010), aerosols such as black carbon (McConnell and Edwards, 2008), trace gases and greenhouse gases. Anthropogenic contaminants can be transported over long distances and accumulate into polar areas. Persistent Organic Pollutants (POPs), such as Polybrominated Diphenyl Ethers

(PBDE), Polycyclic Aromatic Hydrocarbons (PAH), Polychlorinated Biphenyl (PCB) and persistent Contaminants of Emerging Concern (CEC) (Sauve and Desrosiers, 2014) are rarely produced in the Arctic, but have been found in Arctic wildlife, lake sediments, annual snow and ice (Herbert et al., 2005; Ma et al., 2011; Seki et al., 2015). Mercury and other heavy metals, such as As, Cd, and Pb, are considered toxic at any level. Their presence is generally determined by local geochemistry, but they can be emitted by human activities resulting in their increased abundance in the polar areas (Barbante et al., 2001; Zheng et al., 2015; Angot et al., 2016). Black carbon (BC), a fine component of almost pure carbon from incomplete combustion, is able to modify the snow albedo by absorbing incoming solar radiation (Bond et al., 2013; Jiao et al., 2014). Human activities are impacting the net abundance of these pollutants in the atmosphere, but there is a lack of data exploring the deposition patterns and the abundance of anthropogenic contaminants in polar areas. We also need an improved understanding about their redistribution into different environmental spheres including the biota of the Arctic and Antarctic and the full life cycle of these pollutants (Wöhrnschimmel et al., 2013).

Local emissions make currently only a small contribution to the atmospheric loadings of various pollutants in polar areas, but this might change in the near future as Arctic ice-free areas will extend and more extensive Arctic shipping will become possible (Corbett et al., 2010; Yumashev et al., 2018). Nevertheless, air pollutants from other areas in the world do reach high Arctic regions and have been estimated to have significant impacts on the regional ecosystem and climate (Di Pierro et al., 2011; Breider et al., 2014). Knowledge about source contribution of atmospheric pollution is very limited and further efforts in terms of detailed source identification are urgently needed to formulate and settle mitigation strategies (e.g. Law et al., 2014). The measurements of short-lived climate forcers (SLCF), and their precursors, are necessary for evaluating the impacts of increased regional and international activities, e.g. in relation to natural resource extraction, especially in fragile Arctic environments. Correspondingly, similar activities need to be carried out in Antarctica, which has a minimal amount of anthropogenic influences and can provide clean reference observations.

The existing observational networks with comprehensive in situ observational capacity for the measurements of atmospheric concentrations of air pollutants extend to Arctic and Antarctic environments (e.g. Uttal et al., 2016). However, there are still large gaps in the current measurement networks (Lappalainen et al., 2016), and the interaction between the networks, made up of different national activities, needs to be improved. Polar activities are often based on national activities and missing synergistic benefits of cooperation in the challenging environments. In summary, the methodology of data acquisition, data quality control and future strategies on data flows and data streams are not harmonized on either the European or global scale. Furthermore, particularly in the polar areas, measurements are not always continuous but often carried out campaign-wise due to economic, environmental or logistical challenges.

Satellite remote sensing in the Arctic is based on active and passive missions of varying spatial resolution, repeat visit times and coverage of high latitudes. Monitoring the surface properties and its variations in the Arctic region is a powerful tool to assess the impacts of changes induced into this vulnerable environment. The distribution of different types of land cover (snow, ice, vegetation, soil) can be efficiently analyzed using optical data obtained from the new satellite missions merged with data collected during field campaigns and data acquired from cooperative observer networks. In particular, different patterns of snow cover (as well as soil and vegetation cover) exercise considerable influence on the surface energy balance, since variations in land cover change the surface albedo. While there are established methods for retrieving basic variables, changing snow and ice surfaces and ice-free areas are still challenging and the large variability of system itself is limiting the accuracy of such retrievals (Bokhorst et al., 2016). New Sentinel series of Copernicus sensors in the orbit make it possible to retrieve improved land surface variables due to increased capacities in terms of spatial, temporal, spectral and angular observations. As a consequence, new Earth Observation (EO) technics will lead to multi-mission time series needed for data assimilation into models of the Earth system compartments in the Arctic.

In summary, in order to address the current state of the environment in the polar areas and to provide fact-based decision-making tools for the society in the future, comprehensive high-quality observations of atmospheric concentrations of aerosols,

trace gases and related environmental variables from in situ observations are required in concert with EO from space (Petäjä et al., 2014; Hari et al., 2016). The EO data can be used to study the interactions between different types of surfaces and the atmosphere. The results obtained allow us to evaluate the impact of pollutants on the equilibrium of the Arctic system and provide an important input for the evolutionary scenarios of Arctic environment. The picture needs to be harmonized and supported with complementary multi-scale modeling (e.g. Kulmala et al., 2011a; Kulmala, 2018). The need to establish and maintain long-term, coherent and coordinated observations and research activities on environmental quality and natural resources in polar areas drives iCUPE activities. The core idea of iCUPE is the development of novel, integrated, quality-controlled and harmonized in situ observations and satellite data in the polar areas, as well as supply of data products to the end users. The impact of this integrated Arctic Observing System needs to be demonstrated for changing campaign practices to continuous monitoring activities. The Sustaining Arctic Observing Networks (SAON) initiative under the auspices of the Arctic Council has been developing an assessment framework for this since 2017 and iCUPE has been helping in making the first full value tree analysis for this. It connects observing activities in situ and from satellites through modeling and services to key objectives of societal benefit areas. This will help greatly in forming impact assessments in the future.

The iCUPE project aims to synthesize data from comprehensive long-term measurements, intensive campaigns and satellites, collected during the project or provided by on-going international initiatives. The aim of this paper is to introduce an on-going project iCUPE and summarize its initial results. We put a specific emphasis on black carbon and persistent pollutants in the Arctic context. We explore snow and ice core samples to put the current concentrations in longer perspective. We underline the capacity of the continuous observations to monitor the impact of policies to reduce the emissions. We showcase the potential to address the pollution in the Arctic environment by integrating satellite remote sensing, airborne observations, in-situ data and modeling. The modern comprehensive source apportionment can resolve the different sources of atmospheric aerosols and differentiate between sources within and outside the Arctic environment. We also discuss the iCUPE impact and relevance for the Arctic research and for the stakeholder communities.

2 The concept

The motivation behind iCUPE stems from the need to answer the global environmental challenges in a polar context (Fig. 1). The underpinning concept of iCUPE is that transdisciplinary research utilizing the full capacity of comprehensive in situ observations together with state-of-the-art satellite observations is required to make advances in the understanding of atmospheric and cryospheric processes in the Arctic environment (Fig. 2). Therefore, the work in iCUPE utilizes both expertise in in situ observations and satellite remote sensing in a close connection to modeling frameworks to answer this need (Fig. 3). The work is closely connected to on-going activities such as Integrated Arctic Observation System (INTAROS, Sandven et al., 2018) and Multidisciplinary drifting Observatory for the Study of Arctic Climate (MOSAiC, Shupe et al., 2018) expedition conducted in polar areas through collaboration. These connections enable the iCUPE consortium partners to facilitate interactions and strengthen coordination between the national and international activities in the polar areas. The wide spectrum of observational quantities, data products and modeled variables are required to enable the delivery of integrated data required for decisions related to the Arctic pollution.

3 iCUPE initial results

In this section we summarize results and findings of iCUPE-project regarding the in situ observations (Sect 3.1-3.6) and the satellite component (Sect 3.7). Then we selected integrating examples in Sect. 3.8, which include also method development and conceptualization. This is consistent with the iCUPE concept as a whole (multiplatform observations, modeling, synthesis, Fig. 2).

3.1 Atmospheric observation capacity in the Arctic

180 Fig. 3 depicts year-round monitoring aerosol measurements in the Arctic. Within the International Arctic Systems for Observing the Atmosphere, IASOA (Uttal et al., 2016), there are 14 stations all around the Arctic with a clear prevalence of the west longitudes. In addition to the IASOA sites, Stations for Measuring Ecosystem – Atmosphere Relations (SMEAR, Hari et al., 2016) observation network extends to the Arctic as the SMEAR I in Värriö, Finnish Lapland, has provided aerosol and trace gas observations since 1992 (Hari et al., 1994). Many of these observation sites contribute to the World

185 Meteorological Organization's Global Atmospheric Watch (WMO-GAW) as well as to many thematic European Research infrastructures, such as Integrated Carbon Observation System (ICOS), Aerosols, Clouds and Trace Gases Research Infrastructure (ACTRIS). Regionally Svalbard Integrated Arctic Observing System (SIOS) provides a platform for comprehensive measurement activities within Svalbard area. Overall, the length and breadth of monitoring programs vary greatly from site to site. Some of these sites have been operational for almost 30 years now, measuring a large number of

190 parameters, while others, such as Cape Baranova, have only been open for the past 2−3 years. A historical perspective of aerosol measurements in the Arctic (and Antarctica) is presented by several review papers via the POLAR-AOD network (Tomasi et al., 2007, 2012, 2015) and Pan Eurasian Experiment (PEEX, Lappalainen et al., 2018; Vihma et al., 2019).

A geographically representative distribution of measurements is of particular importance. The atmospheric in situ observation network in the Arctic has developed during the last three decades by individual scientists and groups utilizing the resources

195 available. National interests and logistical possibilities have played a role in the initial establishment of the stations and their maintenance. Considering all this, it is somewhat surprising to see that the distribution of measurement sites covers the entire Arctic circle with a relative high homogeneity. Few gaps can be identified in the Canadian coast and in Russian Arctic along the eastern edge of Siberia and Russian Far East (Petäjä et al., 2019).

The coastline of the Russian Arctic is over 24 000 kilometers long, thus being a significant region where more comprehensive

200 atmospheric and aerosol observations are needed. Within the PEEX program, we have performed a gap analysis in terms of atmospheric and environmental observations within the Russian Arctic (Alekseychik et al., 2016). The work is on-going and the PEEX catalogue consists of metadata from 59 stations altogether at the moment. The stations are operated by universities, Russian Academy of Sciences and Roshydromet. The most comprehensive stations in the Russian Arctic providing atmospheric observations and aerosol data are The Tiksi Hydrometeorological Observatory, Russian Far East (71.6° N, 128.9°

205 E) and the Cherskii, the Northeast Science Station (68.73° N, 161.38° E).

3.2 Long-term atmospheric in situ observations

As an example, we present results from long-term observations of atmospheric aerosol particle measurements at the high Arctic site Villum Research Station (VRS) in North Greenland, and long-term data of black carbon data from Mt Zeppelin at Svalbard. Furthermore, we summarize recent mass spectrometric analyses of organic matter collected on filters within the

210 Arctic during iCUPE and present results from vertical measurements of aerosol particle number concentrations

3.2.1 Aerosol particle number concentrations at the high Arctic site Villum Research Station (VRS) in North Greenland

Particle number size distributions (PNSDs) have been continuously measured at VRS from July 2010 onwards. The aerosol number size distributions were determined with a Scanning Mobility Particle Sizer (SMPS) in the size range from 9 to 915 nm following standardization presented in Wiedensohler et al. (2012).

215 The long-term data shows that the seasonality of the atmospheric aerosol number concentration at VRS is largely governed by synoptic weather patterns. Particularly important is the location of the Arctic Front, which describes the boundary between the cold Arctic air masses and the mid-latitude atmosphere. The Arctic Front effectively blocks atmospheric transport from the mid-latitudes to the high Arctic (e.g. Law and Stohl, 2007). There is considerable variability on the location of the Arctic Front

geographically and seasonally (e.g. Klonecki et al., 2003). This leads to a variable contribution between local emissions and the long-range transported aerosols consequently affecting the observed aerosol number size distribution at VRS (Nguyen et al., 2016). The described seasonality is evident from Fig. 4, which displays the monthly averaged particle number concentration in the accumulation mode (Fig. 4a) and ultrafine modes (Fig. 4b).

Our results from VRS show that in the wintertime (October–April), efficient meridional transport coupled with inefficient wet removal processes permits emissions from anthropogenic sources in the mid-latitudes to reach VRS (Freud et al., 2017). This Arctic Haze is characterized by high concentrations of sulfate, black carbon, and accumulation mode (particle diameter > 100 nm) aerosol particles (Fig. 4a). The expansion of the Polar Front and inefficient wet removal in the High Arctic allows for the transport and build-up of relatively high concentrations of accumulation mode particles at VRS. This mode increases in concentration from November until it reaches a maximum in April. When the Polar Front retreats, transport of anthropogenic emissions is limited to the High Arctic as only emissions north of the Polar Front can find a direct way to high Arctic sites and the front is located much further north. Also, wet removal processes reduce the build-up of high concentrations. Other transport processes would only be pathways in high altitudes and then penetrating the Polar Dome by descending air masses through entrainment reaching high Arctic sites, which is rarely being observed.

The decrease in Arctic Haze, coupled with increases in sunlight and the melting of sea ice/snowpack, allows natural sources of aerosols and their corresponding precursor gasses to become an important source to the atmospheric burden of Arctic aerosols. During the summer months, local and regional emissions from natural sources govern the aerosol burden (Barrie, 1986). There is a minimum of ultrafine mode aerosol concentrations in the winter months followed by an increase in April/May, reaching a maximum in July, before decreasing during August/September until reaching a minimum again in October. The aerosol and precursor sources for the ultrafine aerosols (aerosol particle diameter < 100 nm) particularly during the summer can arise from primary marine aerosols as well as secondary sources such as gas-to-particle conversion of precursor gases (e.g. dimethyl sulfide, oxygenated volatile organic compounds, and halogenated compounds) (Dall 'Osto et al., 2018a; Giamarelou et al., 2016; Mungall et al., 2017; Sipilä et al., 2016).

Due to anthropogenically induced climate change, Arctic sea ice extent is rapidly decreasing as well as thickness with the proportion shifting from multi-year ice to first-year ice (IPCC, 2014). There are also indications for a high contribution of Atlantic warm water contributions to the sea ice loss in the Arctic (Polyakov et al., 2017). This has consequences for the atmospheric burden of ultrafine mode aerosols or their precursors originating during the summer from open waters, ice edges or open leads. In general, these changes are expected to impact on precursor gas emission rates and therefore new particle formation events (Dall 'Osto et al., 2018), which implies that the clean Arctic lower troposphere may have a large impact on the radiative balance if the newly formed particles reach accumulation mode sizes and therefore act as Cloud Condensation Nuclei (CCN). Elucidating the impact of sea ice loss to the aerosol population are needed to understand the radiative forcing of Arctic aerosol in the future. Furthermore, climate change may impact on the Arctic atmospheric circulation systems and consequently change the atmospheric transport patterns or intensity of those with respect to the occurrence of accumulation mode aerosol in late winter and early spring in the High Arctic (Arnold et al., 2016). The long-term observation record on the atmospheric aerosol number size distribution in the Arctic will enable us to resolve these interactions and feedbacks in the future.

3.2.2 Black Carbon concentrations at Mt Zeppelin, Svalbard

Black Carbon (BC) is one of the key short-lived climate forcers contributing to the warming of the Arctic both by absorbing the solar radiation but also by enhancing snow and ice melt by surface deposition (e.g. Bond et al., 2013). As part of the atmospheric observations, the ACTRIS and IASOA networks (Fig. 3) operates a network of aethalometers to determine the atmospheric concentration of BC in the air (Uttal et al., 2016). Although BC is the common term we use for light absorbing carbon, it is now more appropriate to report mass concentrations in terms of equivalent black carbon (eBC), especially when

filter-based optical techniques are employed. Equivalent black carbon mass concentration is considered to be the mass of an equivalent amount of light absorbing carbon with a given mass absorption efficiency causing the attenuation of light observed by the instrument at a given wavelength (Petzold, 2013). The quality assurance of data for eBC and the corresponding aerosol absorption coefficient has greatly improved over the last years. Compensation schemes for measurement artifacts as well as harmonization of data obtained by different instruments have been established (Backman et al., 2017) and are continuously updated (Zanatta et al., 2018).

The results from long-term observations at Zeppelin have been discussed and assessed in several works elaborating on the climatology of BC in the Arctic i.e. (Eleftheriadis et al., 2009.; Sharma et al., 2013; Breider et al., 2017; Schmeisser et al., 2018). The results presented here is the longest continuous eBC reported record by a single instrument in the European High Arctic (Torseth at al., 2019) and globally the second longest after those obtained between 1989-2009 in Alert (Sharma et al., 2019). As an example of long-term observations of BC, we show the latest eBC concentration time series from Zeppelin Station at Svalbard (Fig. 5). The results show a continued gradual reduction in the annual mean value of observed eBC, while the time series is strongly modulated by a seasonal cycle well known in the Arctic with minima in the summer and maximum in late winter spring. One can observe this long-term decline with a linear trend line applied only as a crude estimate for these data. The long-term data series we present here makes it possible to derive some descriptive statistics. The eBC annual mean value has been reduced from an annual mean value of 31 ng m^{-3} at the beginning of the previous decade to 12 ng m^{-3} during the last years with an average reduction of 7 ng m^{-3} per decade which amounts to a reduction 4 % annually or approximately 44 % per decade. However, trend analysis for aerosol climatology records need to be practiced with caution in order to remove the effects of the seasonal cycle. When the extracted absorption coefficient from our data was thoroughly examined for a shorter period (2005-2018) the trend was not found to be statistically significant (Collaud Coen et al., 2020). Minimum values over the summer often drop below the detection limits of the instrument while maximum values vary greatly with their occurrence usually related to large scale biomass burning events across Siberia and Alaska. The continuous reduction in fossil fuel usage is a reason for this reduction but it is well known that emissions are not uniformly changing on a global scale or at least in the Northern hemisphere (Evangeliou et al., 2018).

The long-term observations can provide important insight into how abatement strategies for emission reductions or anthropogenic activities enhanced in certain areas can be responsible for the observed changes. Reverse air mass transport modelling using the FLEXPART model (Stohl et al., 2005) can provide the means to combine eBC observations at a remote station like Zeppelin and the source areas globally. We simulate the backward transport of a Black Carbon (BC) and an air tracer at the arctic station of Zeppelin during a period representative of the high measured concentrations (spring of 2012). The analysis is done using reanalysis meteorological inputs from the European Center for Medium-range Weather Forecasts (ECMWF) on a resolution of one degree. The Potential Source Contribution Function (PSCF) is applied on both tracers. Western Siberia appears as the main source region on the PSCF analysis (Fig 6).

Differences in emission sensitivities between the two tracers stress the importance of deposition mechanisms in aerosol transport. Wet scavenging occurs in the presence of clouds and precipitation. Wet deposition is determined from a scavenging coefficient, which is also dependent on the precipitation rate. The sub-grid variability of precipitation rate is calculated as an area fraction in each grid that experiences precipitation. Both large scale and convective precipitation rates are accounted for. We observed that the difference in areal distribution of source areas, the potential significance of the key emission areas to contribute to eBC in the High Arctic and their estimated climate impact is very much dependent on the microphysical parameterization of the model since the air tracer result is considered a simplified representation of the transport and the metrics above greatly affect the result we observe, when the BC tracer parameterization is applied.

3.3 Results from targeted atmospheric field studies in the Arctic

3.3.1 Mass spectrometric measurements for offline source apportionment based on Arctic organic aerosols

Organic compounds are of high importance because they contribute between one and two thirds to the submicron aerosol mass in the Arctic (Willis et al., 2018; Schmale et al., 2018; Popovicheva et al., 2019) and may be co-emitted or interact with other aerosol species, such as black carbon (AMAP, 2015), sulfate (Kirpes et al., 2018) and metals (Shaw et al., 2010). If imported from lower latitudes, they also act as a vehicle of transport for Persistent Organic Pollutants (POPs) to the Arctic (Westgate et al., 2013). Organic aerosols (OA) also absorb (Moschos et al., 2018) and scatter light, thereby changing the radiative balance (Myhre et al., 2013) and may act as cloud condensation nuclei. OA might become increasingly important in a warming Arctic due to anthropogenic activities (Schmale et al., 2018) and natural emissions, e.g., as a result of expanded vegetation (Bhatt et al., 2010), intensified wildfires (Warneke et al., 2010), decreasing sea ice extent and thickness leading to higher release of marine volatile organic compounds (Mungall et al., 2017), and thawing tundra soils (permafrost) along shores and rivers (Peñuelas et al., 2014; Kramshøj et al., 2018). The continuous monitoring of organic carbon (OC) along with a detailed chemical analysis to determine its natural and anthropogenic sources, seasonal variability and inter-annual evolution in the Arctic is of prime importance for improved climate simulations and a realistic assessment of the effectiveness of potential mitigation or adaptation actions.

Offline mass spectrometric aerosol analysis

The OA chemical composition and corresponding sources remain largely unknown, partly due to the challenging measurement conditions (Uttal et al., 2016; Kulmala, 2018). For example, tremendous effort is required for the deployment of online aerosol mass spectrometry at various environments for long time periods. To overcome this challenge an offline Aerodyne aerosol mass spectrometer (AMS) technique has been introduced based on re-aerosolized liquid filter extracts (Daellenbach et al., 2016). The method is capable of covering broad spatial and seasonal observations as well as determining the sources of OA (e.g. primary versus secondary, biogenic versus anthropogenic) (Moschos et al., 2018; Bozzetti et al., 2017). This is achieved with positive matrix factorization, a bilinear un-mixing receptor model used to describe the input mass spectra time series as a linear combination of static OA source (factor) profiles and their time-dependent contributions to the total OA loading (Canonaco et al., 2013). Within iCUPE, we aim to extend the coverage of this technique to the most climate change sensitive region worldwide. The offline AMS analysis will be combined for the first time with ultra-high-resolution mass spectrometry coupled with liquid chromatography, for a two-dimensional molecular identification of primary aerosol tracers and secondary organic aerosol precursors.

Sampling sites

We have collected quartz fiber filter samples around the Arctic. This unparalleled effort is expected to produce data for the chemical and source characterization of OA at nine sites within six countries (Pallas - Finland, Zeppelin and Gruvebadet - Norway, Villum - Greenland, Alert - Canada, Barrow/Utqiagvik - USA, Tiski and Cape Baranova - Russia) from 68° N to 83° N (Fig. 3) covering the period from 2014 to 2019. These include both coastal/archipelago high Arctic stations and boreal forest Eurasian sites near the Arctic Circle with different emission exposure characteristics. Here we show offline AMS data for samples collected at two stations: Ice Base Cape Baranova (Russia) and Alert (Canada).

The research station Cape Baranova was built in 2013. It is located near the cape Baranova, on the coast of the Shokal Strait which divides Bolshevik and October Revolution islands of the Archipelago Severnaya Zemlya (79.16° N, 101.45° E). The area adjacent to the station is characterized by the presence of sea ice, dome-shaped glaciers and icebergs. Polar night and day at the station Cape Baranova last from October 22 to February and from April 22 to August 22, respectively. The air temperature in summer (June–August) is from 0 to 4° C. In winter (October–April) temperatures range from -25 to -45° C. The area of the station is characterized by stable winds mainly from southern direction with an average speed of 10-15 m s^{-1}. During the transition periods of the year, the wind speed can reach 50 m s^{-1}.

Alert was opened in 1986 as Canadian's first research station for the continuous monitoring of background concentrations of trace gases and aerosols. It is located at 82.5° N, 62.37° W (210 m a.s.l.) with prevailing winds from the southwest, which usually bring clear skies and warmer temperatures. North winds off the ocean are typically accompanied by fog and sudden drops in temperature.

Preliminary results from the filter sampling

In Fig. 7, we show offline AMS-based fragment relative contributions of the different organic families in October 2015 (transition to polar night), for the station Cape Baranova (a) and for Alert (b). Even though only limited conclusions can be drawn from the analyses of single filter samples, there is considerable variability in the composition of organic fragments between the two samples. During the same autumn period, the 2-day Cape Baranova filter sample contains more than one third hydrocarbon-like fragments (family CH) and about 50 % oxygenated species (families CHO, CHOgt1). The 2-week Alert filter sample contains more, i.e. roughly 90 %, and more strongly oxygenated fragments (especially mass to charge ratio m/z 44, family CHOgt1). This can be an indication for the extreme remoteness of the site, because OA has to be advected over long distances before it reaches Alert and can hence be oxidized during transport.

The difference spectrum for Cape Baranova (Fig 7c) emphasizes potential seasonal differences in fragments which have relatively high overall contribution to the organic mass. Specifically, the relative abundance of N-containing fragments is indicative for May (2-day filter), whereas the October sample contains more oxygenated fragments. The former might potentially be linked to transported anthropogenic (e.g., fossil fuel) emissions. No marked significant differences are observed for the CH fragments. Ongoing analyses including the other Arctic stations suggest significant variability among the different sites and seasons in the relative fraction of fragments that are markers of certain sources, indicating largely regionally specific sources of OA across the Arctic land surface.

The data analysis is in its early stages but we anticipate a number of outcomes that are valuable for the upcoming assessment by the Expert Group on Short-Lived Climate Forcers of the Arctic Monitoring and Assessment Programme (AMAP), future ultra-high-resolution mass spectrometric measurements of OA in the Arctic, comparison of atmospheric OA with OA in ice cores for historical trends of sources and composition.

3.3.2 Vertical measurements of aerosol particle number concentrations at Svalbard

Ground based measurements are performed continuously at specific sites around the Arctic, but vertical measurements are still rare. To investigate the spatial distribution of aerosol particles in an Arctic environment a four-week measurement campaign was conducted with two different types of unmanned aerial systems (UAS) between April and May in 2018 in Ny-Ålesund (Spitsbergen, Norway). The UAS ALADINA (see Fig. 8a) is equipped with miniaturized aerosol instrumentation (two condensation particle counters with different lower detection limits, optical particle spectrometer, aethalometer) and meteorological sensors (Altstädter et al., 2015; Lampert et al., 2020). A second fixed-wing UAS of type MASC3 (Fig. 8b) was operated in parallel focusing on meteorological measurements. MASC3 probed the lower atmosphere from around 20 to 600 m a.g.l. with flight times of up to 1.5 hours. It carried a sensor payload for measuring turbulent quantities of pressure, temperature, humidity, and the 3D wind vector, providing 100-Hz data (Rautenberg et al., 2019).

ALADINA flights were focussing on aerosol profiles while MASC3 flew at several fixed altitudes and over a large horizontal extent with high spatial resolution (less than one meter for the wind vector and the temperature). The 3D data series show the spatial horizontal and vertical variability of the different layers, which enable characterizing the complex flow properties in the fjord around Ny-Ålesund.

The resulting data also provides a spatial variability of turbulent properties (sensible heat, turbulent kinetic energy, momentum flux). The UAS data improve the understanding of sources and transport processes of aerosol particles in the Arctic, link the observations close to the fjord and at the Zeppelin mountain station (Ström et al., 2009; Tunved et al., 2013), and help to detect regions where new particle formation takes place. Around 200 vertical profiles were performed with the UAS ALADINA

between ground and 850 m a.g.l., thus connecting the ground-based measurements at Gruvebadet laboratory, located near the village of Ny-Ålesund and the data sampled at the Zeppelin observatory at the height of 474 m a.s.l. Further measurement flights were operated horizontally above snow cover and above open water in order to capture the possible impact of biogenic activity on the NPF, as shown along the flight path in Fig. 9.

Fig. 10 shows selected profiles of preliminary data of one selected measurement day. The potential temperature and water vapor mixing ratio profiles show that the boundary layer at Svalbard consists of a shallow unstable layer with elevated humidity at the surface. This layer grows higher during the day. However, even at 11:17 UTC the mixing reaches only 150 m and higher than that, the boundary layer remains stably stratified. Number concentration of accumulation mode particles remained rather constant as a function of height. However, nanoparticles between the sizes of 4–12 nm varied and several distinct layers were identified. The nanoparticle concentrations were the highest at the elevation closest to the surface, but high number concentrations were observed at altitudes up to 500 m. High nanoparticle concentrations in the residual layer has been observed in different environments as well (e.g. Wehner et al., 2010; Altstädter et al., 2018, Leino et al., 2019; Carnerero et al., 2019). Further analysis needs to be done to conclude if this is caused by anthropogenic pollution or locally restricted NPF events. If NPF events occur on such small scales vertical measurements of aerosol particles are needed to estimate the contribution of such small particles on the regional aerosol balance because many of these layers are not captured by the ground-based measurement sites.

3.4 Mercury in the Arctic

High concentrations of mercury (Hg) in Arctic biota pose a threat to local populations and wildlife (Douglas et al., 2012; AMAP, 2012). The scarce anthropogenic Hg emission sources in the Arctic have left scientists to wonder how mid-latitude emissions reach the Arctic Ocean marine ecosystem (e.g. Durnford et al., 2010). The discovery of massive Arctic atmospheric Hg depletion events in 1998 (Schroeder et al., 1998) that are associated with sea-ice derived reactive halogen oxidants (Skov et al., 2004), have fueled a paradigm where mid-latitude urban-industrial Hg emissions reach the Arctic exclusively via the atmosphere. However, subsequent research has shown that 70-80 % of the deposited Hg is photochemically reemitted back to the atmosphere only hours after deposition (Obrist et al., 2017; Brooks et al., 2006). In iCUPE, we performed observations on the Hg concentrations in the Arctic cryosphere, explored the role of river systems to the Arctic Ocean mercury load and explored the interactions between halogen compounds and Hg.

3.4.1 Arctic Mercury cycle

In 2012, a coupled 3-D Ocean-atmosphere model of the arctic Hg cycle suggested that a source of Hg to the Arctic Ocean was missing (Fisher et al., 2012). The missing source was suggested to be Arctic Rivers, in particular Russian rivers that account for 80 % of river run-off to the Arctic Ocean. We monitored year-round Hg levels in the Yenisei and Severnaya Dvina rivers from 2012 to 2016 and confirm that Russian rivers transport large amounts of Hg to the Arctic Ocean (Sonke et al. 2018, Fig. 11b). As part of the iCUPE project these results were integrated into a 3D Arctic mercury model, developed by co-workers from Harvard University (Sonke et al., 2018). We showed that anthropogenic Hg emissions from mid-latitude industrial sources do not directly reach the Arctic Ocean ecosystem. Instead, atmospheric elemental Hg^0 is taken-up year-round by arctic tundra vegetation and soils (Obrist et al., 2017; Jiskra et al., 2018). Springtime snow melt mobilizes the tundra soil mercury, which is bound to plant-derived carbon, via rivers to the Arctic Ocean, where it becomes partly available to the marine food web.

As a summary, the 3D model suggests that a large portion of riverine Hg is photochemically reduced in the surface Arctic Ocean and emitted into the atmosphere. The river Hg budget, together with recent observations on tundra Hg uptake and Arctic Ocean Hg dynamics, provide a consistent view of the Arctic Hg cycle where continental ecosystems traffic anthropogenic Hg emissions to the Arctic Ocean via rivers, and where the Arctic Ocean exports Hg to the atmosphere, to the Atlantic Ocean, and

to marine sediments (Sonke et al., 2018, Fig. 11). Recent iCUPE research suggests that Arctic warming and permafrost thaw risk doubling tundra soil Hg run-off to the Arctic Ocean via rivers, thereby potentially increasing health risks to humans (Lim et al., 2019).

3.4.2 Mercury deposition to the Svalbard snowpack

430   To expand the knowledge on the role of snowpack in the Hg life cycle, we performed targeted field studies (Spolaor et al., 2018, 2019) to determine the seasonality of Hg deposition as well the total Hg deposition from the atmosphere to snow preserved in the Arctic environment in the Svalbard archipelago, specifically in the Spitsbergen region (Fig. 12). The annual snowpack is defined as the snow that accumulates over a glacier surface during the winter. The snow season in Svalbard changes year by year but typically accumulation of snow starts at the end of September and ends at the end of May in

435   concomitance with the temperature rise and the start of snow melting (Spolaor et al., 2016). The snow season is dependent on altitude, and sites at a higher elevation can preserve part of the annual snowpack throughout the year. The equilibrium line, which is the altitude above which snow accumulated during the snow season is partially preserved and is located at approximately 600 m a.s.l in the Svalbard region, below this height the snow is completely removed.

In this study we selected five locations to study the Hg concentration in the snow pack (Fig. 13). The lower snow pit was dug

440   in the Midtre Lovenbreen glacier (MLB) at an altitude of 401 m a.s.l., the Austre brogerbreen (BRG) snow pit at 484 m a.s.l., the snow pit on the EdithBreen (EDB) at 620 m a.s.l., the Kongsvegen (KNG) snow-pit at 710 m a.s.l. and the Holthedalfonna (HDF) snow-pit at 1100 m a.s.l. The sampling was done following a constant sampling step of 5 cm starting from the top to the bottom of the snowpack (identified as the glacier icy surface or by the snow preserved from the previous year, the latter case only for the KNG and HDF sites). The results show that the Hg concentrations (Fig. 13, lower panel) ranged from 0.5 pg

445   g^{-1} up to 5 pg g^{-1} with an average concentration of 1.5 pg g^{-1}. The higher concentrations were detected at the EDB location $(2.00 \pm 0.56$ pg $g^{-1})$. The MLB and BRG had a concentration of 1.69 ± 1.04 pg g^{-1} and 1.72 ± 0.76 pg g^{-1}, respectively. The lower mean concentration was found in the HDF and KNG snowpack with a concentration of 0.80 ± 0.69 pg g^{-1} and 1.38 ± 0.61 pg g^{-1}, respectively. The snowpack sampled approximately at or below 600 m a.s.l. had rather constant Hg concentrations ranging from 1.7 to 2.0 pg g^{-1} while at higher altitude (from 700 to 1100 m a.s.l.) the concentration decreased in the range

450   between 1.4 to 0.8 pg g^{-1}. We found a linear relationship between altitude and mean Hg concentration with an R^2 of 0.78. However, the concentration of Hg is not the correct parameter to evaluate the deposition flux from different sites since higher snow accumulation might induce to a dilution effect. Therefore, the average Hg concentration was converted into Hg flux considering the annual snowpack depth and its density. The estimated flux represent the total Hg load preserved in the annual snowpack. The results suggest that the Hg deposition flux is similar at all the sites investigated (BRG 0.54; EDB 0.78; MLB

455   0.94; KNG 0.70; and HDF 0.58 µg m^{-2} $year^{-1}$) and the elevation gradient is not statistically significant ($R^2 = 0.28$). In the snow pit, the snow at the bottom is representative of the fall season, the middle of the winter deposition and the upper part corresponds to the snow accumulated during the spring. The results show that the Hg concentration in all snow pits tend to increase in the upper, most recent snow layer, in general from 0 to 40 cm depth. The upper part of the snowpack (the sampling was done in April 2018) is more representative of the spring deposition, potentially influenced by Atmospheric mercury

460   depletion events (AMDE). More data analysis is required to verify this hypothesis.

3.4.3 Mercury in air of the Russian Arctic (Amderma)

Since June, 2001, a long-term monitoring of gaseous elemental Hg^0 in the troposphere was carried out near the Amderma settlement (69.45° N, 61.39° E, 49 m a.s.l, Nenets Autonomous District, Russia), which is located on the Yugor Peninsula on the shore of the Kara Sea and close to the Arctic border between Europe and Asia. A Tekran 2537A Hg^0 vapor analyzer, which

465   is a cold vapor atomic fluorescence spectrometer, was used. We carried out analysis of monthly, seasonal, and inter-annual variability of concentration patterns, occurrence of both atmospheric Hg depletion (AMDE) and elevated (AMEE) events,

determined Hg fluxes to the atmosphere and evaluated concentration trends, and identified possible long-range transport cases originating from Icelandic volcanic eruption with HYSPLIT - Hybrid Single-Particle Lagrangian Integrated Trajectory model (Pankratov et al., 2015).

470   During the entire period of operation at this station, the location of the analyzer was changed three times, at different distances of the Kara Sea coastline. The results show that the frequency of AMDE occurrence was shown to depend on the distance to the coastline. From 2001 to 2004 the analyzer was located at a distance of about 9 km from the coast. The number of AMDEs for this period was 10 % of the total number (6765) of measurements. During 2005−2010 period, the analyzer was placed at 2.5 km from the coast. As a result, the depletion events were registered more frequently, and especially during spring−summer

475   period. In 2006 and 2007 such depletion events were recorded in winter with a frequency of 20 % of the total number (1898) of measurements. Starting from 2010 the analyzer was located at a distance of 200 m from the coast. As a result of this relocation, more events were recorded (30 % of 67986 measurements) (Fig. 14a). For the first time in the Russian Arctic, we identified the intensification of the AMDE frequency as a function of distance to the sea. The results are consistent with observations in other polar stations such as Ny-Alesund and Andoya (Norway), Alert (Canada), and Pallas (Finland)

480   (Pankratov, 2015; Nguyen et al., 2009).

The histograms of the Hg^0 concentration at Amderma during the different years is presented in Fig. 14b. The probability density distribution of the Hg^0 concentration was lognormal for the monitoring period from June 2010 to October 2013. There is a significant asymmetry in the left-hand region of the Hg^0 concentration probability distribution relative to the arithmetic average, pointing to the fact that low Hg^0 concentrations are measured more frequently. In 2013 this asymmetry was especially

485   evident. The shift of the concentration to lower values was due to the increased amount of Hg^0 depletion events recorded during the winter seasons of 2010–2013. To assess the dynamics of Hg^0, a linear approximation of the average annual Hg^0 concentrations for the lognormal distribution was calculated with the reliability coefficient $R^2 = 0.7$ (Fig. 14b)

3.5 Halogens in the Arctic

Polar halogen activation occurs when halide ions originating from seawater are released via chemistry on snow/ice/aerosols to

490   the atmospheric boundary layer (e.g. Simpson et al., 2007; Abbatt et al. 2012). Bromide is a source of atmospheric bromine (Br_2), which is known to be an important species that controls the atmospheric ozone and Hg cycles in Arctic (see reviews of Abbatt et al., 2012 and Simpson et al., 2015). Nearly complete ozone depletion events (ODEs) are regularly observed during Arctic spring, when molecular bromine is released to the atmosphere through a complex multiphase process, which may require the presence of sunlight and/or acids. Elevated concentrations of reactive halogens in the atmosphere are often co-observed

495   with atmospheric Hg^0 depletion events (Saiz-Lopez and von Glasow, 2012).

While observations are numerous, the ability of models to reproduce halogen activation and impacts has remained limited. For example, WRF-Chem (Weather Research and Forecasting model coupled to Chemistry, Grell et al., 2005; Fast et al., 2006; Peckham et al., 2011) is frequently used to study Arctic aerosol and trace gas cycling. Recently, WRF-Chem was improved specifically for modeling ozone in the Arctic region (Marelle et al., 2017) although at present it does not include any description

500   of the impact of reactive halogens on the Arctic ozone cycle. Fig. 15 shows the current ozone-predicting capability of the model during spring and summer, compared to surface ozone observations at two Arctic sites. Within iCUPE, we aim to improve model predictions of Arctic halogen activation and related ozone depletion in the atmosphere using the WRF-Chem model. The ultimate goal is to improve the ability to predict the role of halogens in controlling the Arctic atmospheric mercury cycle.

3.6 Persistent organic pollutants (POPs) and emerging contaminants (EOC) in the Arctic

Persistent organic pollutants (POPs) and newly emerging organic contaminants (EOCs) were analyzed from five Arctic research stations, Alert (Canada), Pallas (Finland), Storhofdi (Iceland) and Zeppelin (Svalbard/Norway) since 1993 (Hung et al., 2010) and at VRS (Greenland) since 2008 (Hung et al., 2016). Air concentration of polychlorinated biphenyls (PCBs), organochlorine pesticides showed a more or less consistent decline in the 1990s. This reduction is, however, less apparent in recent years. In contrast, concentrations of polybrominated diphenyl ethers (PBDEs), hexachlorobenzene (HCB) and some PCB congeners were still found to be increased. The results indicate that both temporal and spatial pattern of POPs in Arctic air is affected by anthropogenic emissions and may be affected by various processes driven by climate change, such as reduced ice cover, increasing seawater temperature and increasing biomass burning in boreal regions.

EOCs such as poly- and perfluorinated alkyl substances (PFAS), novel brominated flame-retardants (BFR) and organophosphate flame-retardants and plasticizers (OPFR) were investigated in the Arctic environment (Xie et al., 2015; Li et al., 2017; Bossi et al., 2016). Long-range atmospheric processes may have moved particle-bound BFRs to the site, probably during the Arctic haze season. Several modeling studies have been conducted in an attempt to resolve the dominant transport pathway of PFASs to the Arctic, namely atmospheric transport of precursors versus direct transport via ocean currents (Wania, 2007; Armitage et al., 2009; Stemmler et al., 2010). Atmospheric measurements have shown the widespread occurrence of PFAS precursors, e.g. fluorotelomer alcohol (FTOHs) and perfluorinated sulfonamide alcohols (FOSE/FOSA) (Shoeib et al., 2006; Cai et al., 2012). The detection of perfluorocarboxylic acids (PFCAs), perfluorinated sulfonic acids (PFSAs) and neutral PFAS in snow deposition is consistent with the volatile precursor transport hypothesis (Young et al., 2007; Xie et al., 2015). The measurements of PFCAs and PFSAs in seawater from the Greenland Sea indicated melting snow and ice tend to be an input source (Zhao et al., 2012). The inconsistent temporal and spatial trends between regions may be representative of differences in emissions from source regions (Woehrnschimmel et al., 2013).

The decline of legacy POPs in the environment is expected in response to global efforts to reduce emissions. Whereas, with their persistence in environmental matrices, such as water, sediment, soil, vegetation and ice/snow, warming Arctic may drive them again into environmental circulation. Consequently, future research should be focused on quantifying remobilization fluxes and sinks for both legacy POPs and emerging contaminants in the Arctic, and on developing a quantitative understanding of global exposure pathways for POPs to support risk assessments (McLachlan et al. 2018).

3.7 Satellite remote sensing

Satellite remote sensing is a very useful tool for Earth observation in the Arctic, given the vast size of the area and constraints in accessibility. The sensors that are typically applied are ranging from radar sensors of different frequency, typically X- and C-band (TerraSAR-X, Tandem-X, Sentinel-1) to optical sensors (Landsat, MODIS, Sentinel-2 and -3) and altimeters (CryoSat-2, ICESat-2, Sentinel-3). In future a hyperspectral mission (EnMAP) will survey the Arctic. In the framework of iCUPE, we utilize satellite remote sensing data on the topics ranging from Arctic vegetation, snow-cover monitoring, and supraglacial melt of glaciers. Beyond the development of products and assessment of existing approaches, also new techniques like polarimetry for glaciers were assessed, which will serve for recommendations for future satellite missions. Furthermore, we present an example for integration of satellite remote sensing, airborne observation and modelling, applied to a case of anthropogenic emissions from oil/gas extraction in northern Russia. An analysis of the current observing systems and future needs are summarized, including value chains of satellite missions.

3.7.1 Arctic vegetation

As part of iCUPE, we are working beyond the recent retrievals of satellite remote sensing data to include advanced current and upcoming optical remote sensing missions with improved spatial, temporal and spectral resolutions and their potential for

characterization of Arctic regions. In particular, hyperspectral remote sensing (or imaging spectroscopy) has been shown to provide superior derivation of key biophysical surface variables in snow-free permafrost areas during the summer months based on field and airborne remote sensing data (Buchhorn et al., 2013; Bratsch et al., 2016; Liu et al., 2017; Beamish et al., 2019a). The datasets compiled as part of the iCUPE project (see Sect 3.8) consist of four years of field data including canopy-level spectral reflectance data, as well as aerial hyperspectral images (Alaska and Canada) and a dense Sentinel-2 time series (Siberia). Additional ground-based data includes leaf-level photosynthetic pigment data from multiple phenological phases, as well as aboveground biomass and detailed species composition data. The study sites include Toolik Lake Alaska, Qikiqtaruk-Herschel Island (QHI) Canada, and Lena Delta, Siberia. All three sites represent key low Arctic research stations with the Toolik and QHI sites having pre-established long-term vegetation monitoring plots. This dataset is unique and provides the potential for further work given the freely available nature of much of the ancillary data and the intensive international research being conducted at all locations. The main goal of this work was to provide an initial characterization and exploration of the application of hyperspectral remote sensing data in Arctic terrestrial ecosystems where existing research is limited.

As a first step to improve the estimation and monitoring of Arctic tundra vegetation, we conducted a detailed spectral characterization of dominant vegetation communities at Toolik Lake, Alaska with the aim of better informing current and upcoming hyperspectral remote sensing platforms such as the PRISMA (Italy) mission (Loizzo et al., 2018) that started in 2019 and the EnMAP (Germany) satellite planned to be launched mid 2021 (Guanter et al., 2015). To be noted, as part of the High Priority candidate missions for the Copernicus Sentinel expansion, the ESA is considering a hyperspectral mission named CHIME for 'Copernicus Hyperspectral Imaging Mission for the Environment' (Rast et al., 2019). To accomplish the ground spectral characterization, we collected canopy-based spectral reflectance in five dominant low Arctic vegetation communities at three major phenological phases of leaf-out, maximum canopy, and senescence (Fig. 16) and simulated upcoming EnMAP and Sentinel-2 spectral reflectance. We then examined within and between community variability to determine the most discriminative wavelengths and phenological phase for the ground-based, EnMAP, and Sentinel-2 reflectance.

The results suggest that for imaging spectroscopy (ground-based and simulated EnMAP) the senescent phase imagery is superior to leaf-out and maximum canopy for differentiating vegetation types, while for Sentinel-2 maximum canopy was superior. The difference between the narrow and broadband data is likely due to the extreme color differences observed during senescence that are well captured by imaging spectroscopy but not by broadband data. These results provide important information for better interpreting current broadband and future narrowband spectral reflectance data for more accurate estimation of vegetation composition, vigor and biomass (Beamish et al., 2017).

As a second step, we explored the relationship between spectral information from imaging spectroscopy and digital cameras data to biochemical variables at Toolik Lake, Alaska to assess the utility of low-tech cameras as a ground-based validation tool. To do this we looked at the relationships between narrowband and RGB indices and in turn the relationship of these indices to changes in photosynthetic pigments of chlorophyll and carotenoids. We were again interested in how these relationships vary by phenological phase and vegetation type. The results showed that vegetation color contributes strongly to changes in both narrowband and RGB indices and that these changes are related to changes in photosynthetic pigment concentration (Fig. 17). We conclude that digital cameras can be used to estimate and track pigment development and degradation in low Arctic vegetation serving as a crucial in situ validation for hyperspectral remote sensing.

In a final effort to explore applications of hyperspectral remote sensing to characterization of Arctic vegetation, we explored the spectral sensitivity of airborne hyperspectral imagery to fractional cover of plant functional types at Toolik Lake, Alaska (Fig. 18, Beamish et al., 2019b).

Using detailed plant compositional data, we explored the sensitivity using simple linear regression of individual wavelength and two-band spectral indices to varying fractional vegetation cover. We found that wavelengths and spectral indices showed overlapping areas of sensitivity to vascular and non-vascular functional types which could confound the extraction of vegetation properties derived from vegetation indices. We also found that two-band vegetation indices do not provide

consistent information across vegetation community types and the contribution of non-vascular and non-photosynthetic components influences indices values (Fig. 19). The findings of this research point to the importance of *a priori* knowledge of species composition and phenological phase to accurately interpret vegetation properties derived from imaging spectroscopy. Using data from the Lena River Delta and Qikiqtaruk-Herschel Island, within iCUPE we plan to expand characterization of Arctic vegetation using imaging spectroscopy to include biodiversity and biomass estimates. Using detailed species composition data and destructive biomass sampling in combination with spectral variables we will explore relationships at the ground, airborne and satellite scale to best estimate these key biophysical variables (Fig. 20).

In the next step, we aim to provide best practices and proxies for mapping vegetation status and aboveground biomass in the low Arctic at landscape scales with aerial imagery, Sentinel-2 and upcoming hyperspectral satellite imagery. The biomass data will also be compared to volatile organic compound and atmospheric chemistry datasets.

3.7.2 Snow cover in the Arctic

Snow cover is an important component of the cryosphere that plays a key role for climate dynamics and the resources availability: the seasonality of the snow cover influences weather patterns, hydro-power generation, agriculture, forestry, tourism, and aquatic ecosystems (Beniston et al., 2018). The snow cover characterization and its annual spatial-evolution represent important factors to be considered in the framework of climate modelling at a global scale. Furthermore, the snow cover has been officially declared as an Essential Climate Variable (ECV) by the Global Climate Observing System (GCOS) and high priority is assigned to enhancing and maintaining snow cover observations (WMO, 2010; 2011). From this perspective, the continuous monitoring of snow cover is a major challenge of these last years and the advances in remote sensing explain why optical data are so diffusely used to monitor the snow covers.

The description of the snow cover implies two variables: the extent and the albedo. These variables, in the framework of the iCUPE project, are critical inputs for pollutant transport and climate change models. Remote sensing is the most common tool for the routine estimation of the snow cover extent, but two different aspects must be considered for the selection of the most appropriate input: time and spatial resolutions. Both components, using remotely sensed data, are connected to each other, since the higher the spatial resolution (below hundreds of meters), the lower the revisit time interval (more than 1 week) (Dietz et al., 2012). Concerning the albedo, the spectral behavior of the snow reflectance in the visible and short-wave infrared ranges supports the discrimination of snowed surfaces from other matrices and, moreover, the characterization of the snow surface (Painter et al., 2003; Tedesco & Kokhanovsky, 2007). In details, the reflectance of pure snow in the visible range of the electromagnetic spectrum (400–700 nm) is approximately 100 % and it decreases as a function of the amount of impurity content in the snow and slightly increasing in the size of the snow grains with ageing. In the short-wave infrared part of the solar spectrum (700–2500 nm), snow reflectance decreases rapidly and it is mostly controlled, in this case, by the snow grain size (Warren & Wiscombe, 1980; Wiscombe & Warren, 1980; Warren, 1982).

The state-of-the-art snow products concerning the snow extent are derived using remotely sensed data and they are based mainly on multispectral optical sensors. They can investigate the snow cover and give information about the size and the shape of snow grains (Dozier et al., 2009), the presence of impurity soot, the age of the snow, and the presence of depth hoar. Furthermore, the short-wave infrared signal can support the discrimination between snow and clouds (Rodell et al., 2004). Considering that snow-covered surfaces are highly reflective in the visible range and low reflective in the Short-Wave InfraRed (SWIR) (Salomonson & Appel, 2006), it is possible to define an index that enhances the discrimination between snow and not snow in a single pixel. This index, defined as Normalized Difference Snow Index (NDSI), is calculated as follows:

$$NDSI = \frac{R_G - R_{SWIR}}{R_G + R_{SWIR}} \tag{1}$$

The green and the SWIR parameters are the bands available for each satellite sensor and their selection includes generally wavelength ranges centered at 500–600 nm (R_G) and 1500–1600 nm (R_{swir}). The estimation of the snow extent from remotely sensed multispectral images is based on the relation between the radiative behavior of the surfaces and the Fractional Snow Cover (FSC). This parameter describes the percentage of surface covered by snow (Painter et al., 2009) in a pixel element of a remotely sensed image. The relation between the FSC and the NDSI represents the most common inference required by remote sensing studies. There are two options for estimating the NDSI—FSC relation: the first one consists in combining satellite products with different spatial resolution (Yin et al 2013); and the second one can be approached having a ground truth information. The first solution is based on (Salomonson & Appel, 2006) combining Landsat and MODIS data and a NDSI to FSC relation is defined as:

$$FSC = 1.45 \times NDSI - 0.01 \tag{2}$$

This knowledge was implemented in the SNOWMAP algorithm (Hall et al., 2016), which is the core of the MODIS data chain for the definition of remotely sensed snow products. This approach is replicated also on Landsat data (Vermote et al., 2016) and in the NASA VIIRS ATBD (Riggs et al., 2015), derived by Suomi NPP satellite platform. Similarly, it is included in the SC algorithm, which is part of the Sentinel 2A data chain (Main-Korn et al., 2017). The second solution can be approached defining an empirical reflectance-to-snow-cover model that requires a calibration having a number of reference sites in the satellite image (Solberg et al., 2006), which is the core of the GlobSnow Snow Extent (SE) data chain (Metsämäki et al., 2015). The occurrence of different interferences (cloud cover or snow metamorphism for example) requires the availability of additional proxies, like webcam networks (Salzano et al., 2019), that can improve the calibration and validation processes of remotely sensed products.

Several satellite products are available for the remote sensing of the cryosphere and for this study we considered products obtained by optical sensors, characterized by different spatial resolutions: high (< 100 m); intermediate (100 m - 1 km); and low (> 1 km). The integration between those products and ground-based imagery will be tested, in order to improve the dataset concerning the snow cover over a decade.

As part of iCUPE, we aim to develop a semi-automatic procedure focused on preparing a snow product useful for monitoring spatial and spectral variations of the snow cover. The first year was concerned on data collection and analysis of terrestrial images that will be complementary to Sentinel multispectral images (Fig. 21). We selected a study area located close to Ny-Ålesund (Svalbard, Norway) where the Italian Arctic Station represents an important scientific facility and experimental activities are appropriately supported. The site is characterized by intense international research collaborations and different data sources can be included as input for the integration between remotely sensed data and terrestrial images collected by webcam. We performed an overview about the algorithms focused on processing multispectral images and snow index calculation as well as on the automatic geo-rectification of ground-based photography and on the routinely estimation of the fractional snow cover. From this perspective, we carried out a first field campaign aimed to survey the available webcams in the study site and to deploy a new webcam on the CNR Climate Change Tower. This site has proved to be the most suitable for the collection of ancillary data necessary for a correct interpretation of both satellite and terrestrial images. This CNR infrastructure is equipped with different meteorological sensors as well as instruments focused on detecting the radiative properties of the atmosphere and of the snow-covered surface.

The core of this activity was the development of a procedure suitable to collect remotely-sensed data and match these images to FSC estimations obtained using terrestrial photography. The resampling of snow - no snow pixels, provided by webcams (Fig. 22 a and c), using grids associated with satellite imagery, provided a continuous dataset of FSC to NDSI relations (Fig. 22 b and d) that can enhance the recognition of different snow cover types in the considered site. From this point of view,

670 terrestrial photography represents a term available daily or hourly in common for all the imagery that can be obtained by different satellites, with different revisit time (from 1 to 10 days) and under intense cloud cover (up to 80% of cloudy conditions per year in Svalbard islands (Salzano et al., 2016). The final output will support the definition of the snow cover extent including shadowed areas and variations associated with the snow metamorphism. Furthermore, we will be able to describe the evolution of the snow cover year by year, with complete timelines that could assess the melt cycle variability over the last

675 decades, on a local scale with terrestrial photography, or over the last few years, on a regional scale using remotely sensed data.

3.7.3 Supraglacial lakes in Greenland

The surface of ice sheets and glaciers in the Arctic, e.g. in Greenland, is prone to melt during summer. As part of iCUPE we focused on the Greenland ice sheet, given its current contribution to sea level rise and the polar amplification making this are

680 to a hot spot of future warming. Whereas the entire ice sheet surface is experiencing melt only rarely, like in the extreme melt year 2012, the margins of the Greenland ice sheet is melting between May and August. Melt water may either percolate into the porous firn matrix or may run-off along the surface and accumulate in topographic sinks forming supraglacial lakes. These supraglacial lakes may freeze over during winter, being covered with a lid of lake ice, or drain and deliver vast amounts of water acting as a lubricant to the glacier base. Whatever route the melt water takes, it also transports previously deposited

685 pollutants during snow accumulation. There are three major questions that we addressed within iCUPE: (i) how much water is drained? (ii) How often does the lake drainage occur? (iii) What are the opportunities and limitations of satellite radar remote sensing to answer these questions?

Within iCUPE we studied an area in northeast Greenland, which contains lakes of the size of 21 km^2 and of up to 40 m depth, containing volumes of up to 108 m^3 of water (Humbert et al., in review). The availability of water at the glacier base leads to

690 an immediate speed of 9-22 %, that is declining over time as the water has been discharged (Neckel et al., in review). Estimating the volume of lakes has been done with differencing digital elevation models (DEM's) obtained from TanDEM-X at different acquisition times. With revisit time of 11 days, we can limit the drainage duration with this no better than 11 days, however, the combination between optical (Sentinel-2) and TerraSAR-X data allowed to constrain the duration of one particular drainage event to be shorter than 1 day (Neckel et al., in review).

695 With Copernicus' Sentinel program, continuation of satellite missions is assured, which makes the development of methods to derive time series of lake drainage events based on these sensors a desirable approach for obtaining long time series in future, as formation, filling and drainage of supraglacial lakes will increase in future under warming. Radar remote sensing is most attractive for observing polar areas, as it is independent of clouds and daylight. While the Copernicus program does not contain a bistatic radar mission required for lake volume estimates, Sentinel-1 is a C-band dual polarimetric mission, for which

700 we explore the potential to retrieve quantities for the supraglacial hydrological cycle. Polarimetry allows to separate surface reflections from volume reflections, using transmission and retrieval of horizontal (H) and vertical (V) polarised radar waves (Fig.23b,c).

The hypothesis we based our analysis on is that supraglacial lakes act as surface reflectors, whereas the surrounding glacier surface acts as a volume scattering material (Fig. 23a). With Sentinel-1 being only a dual polarimetric mission (HH, HV), the

705 full decomposition cannot be conducted. However, the difference in amplitude between HH-HV has been used to derive a time series from May 2017 to September2019 over 79° N Glacier and Zacharias Isstrøm, two outlet glaciers of the North-East Greenland Ice Stream. Fig. 23 displays the difference HH-HV in April, thus before the onset of melt. Bright yellow color represents areas where surface scattering is dominating, whereas darker purple color represents volume scattering. The time series (not shown in Fig. 23) of difference in amplitude is prone to saturation during the melt period, consequently the

710 difference HH-HV can also not be assessed. The areas with large differences HH-HV are coincident with lake locations detected with the DEM differencing, as well as optical satellite imagery, serving as a validation of this method. The vertical

polarization is arising from the reflection at the transition between lake ice and water. This is another indication for the lakes only being covered with a lid of lake ice and not freezing through entirely, which we also found in airborne radar surveys using AWI's ultra-wide band radar (UWB) on 2018-04-11.

We find polarimetry being a promising approach for detecting multi-annual lakes of large volume. Polarimetric SAR is likely to improve lake detection during the melt season and is currently investigated. From our assessment, it would be most beneficial to have a full-polarimetric bistatic L-mission with short repeat cycles covering the polar areas, allowing even for SAR tomography, in order to be able to observe englacial aquifers and refrozen melt layers and their evolution in the next decades.

3.8 Integrating examples

This section presents a suite of integrative examples developed during the iCUPE project, which utilized the comprehensive observation capacities and combined technologies in order to address satellite data validation task based on in situ observations, assessment of aerosol emissions from flaring in the Arctic in a combination of aircraft observations, satellite retrievals and modeling tools. We also present work towards development of proxy variables from the comprehensive observations and performed a value tree analysis for the Arctic observation network as a whole.

3.8.1 Satellite data validation

The SMEAR II station (Hari and Kulmala, 2005) in Hyytiälä is the ground-validation site for the current NASA Global Precipitation Mission (GPM, Skofronick-Jackson et al., 2018) and upcoming ESA EarthCARE satellites (Illingworth et al., 2015). The satellite calibration/validation activities can be divided into two main approaches, i.e. validation and verification of the assumptions and parameterizations used in the retrieval algorithms and direct validation of satellite observations.

Within iCUPE, the main focus of our satellite validation activities was on the microphysical assumptions and parameterizations used in the ice cloud and snowfall retrievals. Given the climate and comprehensive surface-based observations of precipitating ice particles, our observations allowed us to constrain retrievals and refine these parametrizations. Following the work of von Lerber et al., (2017), the snowflake masses and size distribution were retrieved and used to derive event specific radar reflectivity-snowfall rate relations. These relations were applied in the validation of ice cloud and precipitation retrieval algorithms. For example, the performance of the "unified" algorithm that combines the radar and lidar observations of EarthCARE, in a variety of snowfall conditions (Moisseev et al., 2017; Li et al., 2018), was tested using the snowfall data as shown in Mason et al. (2018; 2019). Using these studies showed that the measurements collected at Hyytiälä, namely combined observations of the surface snowfall observations and multi-frequency radar observations, show the potential for verification of satellite cloud and precipitation retrieval algorithms in the future.

Direct validation of satellite precipitation products was carried out by applying tuned relations between radar reflectivity and snowfall rate, as derived from surface precipitation measurements, to the Finnish Meteorological Institute Ikaalinen radar observations. This method was developed by von Lerber et al. (2018) and applied to validate GPM snowfall rate estimates at Hyytiälä, SMEAR II station. Using these observations, we showed that the current NASA GPM algorithms underestimates snowfall intensity, but showed good skill in detecting falling snow.

To prepare for the upcoming ESA Earthcare validation activities, preparatory studies were performed on how ground-based radar observations can be used to validate space-based radar observations of vertical profiles of clouds and precipitation. A comparison between such observations, in this case we use CloudSat, is shown in Fig. 24. The figure shows vertical profiles of radar reflectivity as observed using ground-based and satellite-based cloud radars. As can be noticed there are detectable differences in the observed values. The CloudSat observed values are higher at cloud tops and lower in precipitation if compared to the ground-based radar. These differences are caused by attenuation of ground-based radar measurements in rain and melting layer and in cloud and melting layer for CloudSat observations. Therefore, a direct comparison of observed vertical

profiles requires a method that can into account the attenuation. As a part of iCUPE Li et al., (2019) has studied the impact of melting layer of precipitation on cloud radar observations. The results of this study will be used for the EarthCare validation in the future.

3.8.2 Anthropogenic emissions from oil/gas extraction over northern Russia: a combined approach using aircraft, satellite data and modelling

Aircraft data collected for the first time over northern Russian oil and gas producing regions was used to examine the validity of available emission inventories. The data was collected in October 2014 and July 2017 as part of the French-Russian YAK-AEROSIB program (Paris et al., 2010; Antokhina et al., 2018, Fig. 25). A combination of different approaches was applied involving joint analysis of aircraft and satellite data together with source-receptor modeling using FLEXPART/FLEXPART-WRF and regional WRF-Chem modeling (Marelle et al., 2017, 2018) to investigate discrepancies in both black carbon (BC) and methane (CH_4) anthropogenic emissions over Russia, from where only very little data is available to date.

Analysis of Equivalent BC data collected over Northern Siberia in October 2014 showed clear signatures of enhanced concentrations in the lower troposphere especially near the surface (Antokhina et al., 2018). The origins of polluted air masses sampled during flights over the Ob Valley, Yamal and Kara Sea regions during October 2014 were analysed using WRF-Chem BC tracer runs with emissions from different sectors using the ECLIPSEv5 (Klimont et al., 2017) and Arctic Black Carbon (ABC) (Huang et al., 2015) inventories with several plumes clearly identified as coming from the gas flaring regions. Backward FLEXPART-WRF simulations from the plumes were used to compare emission footprints for the Huang ABC and the ECLIPSE BC flaring emissions. Discrepancies were identified in both inventories and in some cases completely missing emissions, particularly over the Nenets region (Onishi et al., 2019, in prep.). The data is being further analysed using daily VIIRS (Visible Infrared Imaging Radiometer Suite) satellite night-light data (provided courtesy of Earth Observation Group, Payne Institute for Public Policy, https://eogdata.mines.edu/download_dnb_composites.html) to examine the sensitivity of modelled BC to daily variability in flaring emissions. Preliminary results suggest that the simulated BC is highly sensitive to significant observed variability.

Methane emissions from oil and gas activities are similarly poorly known, and their spatial and temporal distribution is related to that of BC (e.g. Gvakharia et al., 2017). Inventories are affected by 1) highly variable emission factors, 2) highly variable scheduled or unscheduled operations leading to release of methane and 3) the uncertain spatial distribution of regional totals (Fig. 26a). The inventory EDGAR v4.3.2 (Janssens-Maenhout et al., 2017) predicts a total emission for energy in Western Siberia of 2.8 MtCH4 yr^{-1} whereas ECLIPSE v5a (Höglund-Isaksson et al., 2012) yields 14.1 MtCH4 yr^{-1} (Fig. 26b). Similar to BC, the YAK-AEROSIB campaigns were used to integrate in situ observations in methane inventory validation. A comparison between observations and modelled methane enhancement using the FLEXPART model revealed overall that the most descriptive signals are contained in the occurrences of boundary layer measurements. Typically, the methane enhancements in these measurements are estimated by a tagged tracer analysis to originate for approximately 60 % from regional wetland emissions. We used the ORCHIDEE model (Poulter et al., 2017) to subtract the contribution of these widespread ecosystems to the methane enhancements detected in the boundary layer and estimate the compatibility of emission inventories with the airborne measurements. However, this introduces a significant uncertainty in the constraint that can be applied to methane emissions from oil and gas that needs to be investigated though comparison with a different wetland model.

3.8.3. Aerosol vertical profiling in Russia and in Finland

Within iCUPE, data collected at ground-based lidar sites in Siberia and in Southern Finland provided new insights into aerosol sources affecting atmospheric composition in the Arctic and sub-Arctic regions.

Russia

Aerosol backscatter vertical profile data collected in Tomsk, Siberia and corresponding aerosol optical depth (AOD) have been derived using a micropulse lidar at 808 nm and a novel lidar data processing approach based on a careful system calibration and an aerosol source apportionment based on FLEXPART backward transport simulations of an aerosol tracer including dry and wet removal processes (Ancellet et al., 2019). The potential emission sensitivity maps from the FLEXPART simulations were coupled with the spatial distribution of five aerosol sources to obtain the aerosol source apportionment: urban pollution map (cities of more than 500,000 inhabitants), biomass burning daily maps (NASA Fire Information for Resource Management System (FIRMS) using MODIS (Giglio et al., 2003) and the Visible Infrared Imaging Radiometer Suite (VIIRS) (Schroeder et al., 2014)), forest and desert maps (Advanced Very High Resolution Radiometer (AVHRR) database (Sertel et al., 2010)), and gas flaring emission map (ECLIPSEv54 database (Evaluating the CLimate and air quality ImPacts of Short-livEd pollutants) described in Klimont et al., 2017).

An example of lidar aerosol vertical profile is shown in Fig. 27a for a mixture of gas flaring emissions from the Ob Valley below 3 km (Fig. 27e) and a dust layer transported from Kazakhstan above 3 km (Fig. 27c) during a time period with no forest fires in Siberia. Aerosol scattering ratios at 808 nm increased by a factor of 3 due to this event while the corresponding AOD reached 0.3 in good agreement with the Tomsk AERONET sun photometer observations and the MODIS hot spot near TOMSK (Fig. 27b). Elevated CO columns seen by IASI above the Ob valley and Tomsk also support gas flaring emissions during this period. A CALIOP overpass (black line in Fig. 27b and d) also provides a latitudinal distribution on the aerosol layers showing the limited vertical extent (2 km) of the aerosol layer at 55° N transported from the gas flaring region, while dust layers reached 4 km at latitudes below 50° N over Kazakhstan.

The fraction of all the aerosol layers detected by the lidar from April 2015 to October 2016 were derived for the five aerosol types observed in Ancellet et al. (2019). The results show that the occurrence of layers was linked to natural emissions (vegetation, forest fires and dust) and their contribution was high (56 %). However, anthropogenic emissions still contributed up to 44 % of the detected layers (1/3 from flaring and 2/3 from urban emissions). In Tomsk, the frequency of dust events is very low (5 %). The contribution to the largest AOD (> 0.1) showed that the frequency of forest fires (25 %) and urban pollution events (25 %) were dominant, while the frequency of flaring (10 %) and dust emission (13 %) are equivalent and two times lower in frequency. The flaring emissions are indeed frequent but do not contribute very much to the large optical depth cases. Our results show that the aerosol particles originating from the urban and flaring emissions remain confined below 2.5 km, while the aerosol particles related to dust events were mainly observed above 2.5 km. The aerosols from forest fire emissions are on the opposite observed both within and above the PBL.

Finland

Based on a combination of ground-based High Spectral Resolution Lidar (HSRL, Shipley et al., 1983) observations and airborne in situ measurements, we have analyzed the boundary layer and aerosol layers aloft over a relatively clean SMEAR II station. An HSRL was one of the deployed instruments during BAECC (Biogenic Aerosols – Effects on Cloud and Climate) Campaign (Petäjä et al., 2016) that was organized at the station from February to September 2014. A Scanning Mobility Particle Sizer (SMPS) and Optical Particle Sizer (OPS) were installed onboard Cessna FR172F aircraft (Schobesberger et al., 2013, Leino et al. 2019) to measure aerosol size distribution from 0.1 to 0.23 μm and 0.3 to 5 μm, respectively. The flights were conducted in the vicinity of the station not higher than 4 km in altitude with relatively low speed of 200 km/h, thus, providing observations with good spatial resolution.

We analyzed a set of clear-sky and cloudy cases (Nikandrova et al., 2018) at Hyytiälä during the BAECC campaign. HYSPLIT 96 h backward trajectories were calculated every 50 m and combined into layers based on the similarities in the origin and traveling path, and compared with the layers recognized with HSRL. Most of the layers were recognized in both approaches yet arrival heights of the back trajectories were not always similar to the heights of the layers of HSRL. These discrepancies are due to the small-scale vertical motions that are not resolved in the HYSPLIT model (Stein et al., 2015).

835 In both clear-sky and cloudy cases, elevated layers with high aerosol concentrations were detected with both the HSRL and with the airborne measurements. One of the clear-sky case studies of 9 April 2014 is shown in fig. 28. The boundary layer can be visually recognized from the backscatter coefficient to be around 1.4 km in the afternoon when the flight took place (Fig. 28a). Fig. 28b shows HYSPLIT backward trajectories divided into three layers and their arrival heights. The aircraft data showed a similar shape of the size distribution for the elevated layers and in the boundary layer during the flight with higher

840 aerosol concentration in the boundary layer (Fig. 28c). Small variability of the size distribution in the BL suggest a well-mixed BL, whereas in the elevated layers the internal variability was larger and the layers were not mixed as thoroughly. Back trajectories analyses showed that the air mass origin was similar regardless of the arrival height, which indicated that both the BL and the elevated layers were affected by similar aerosol sources (Fig. 28d). Therefore, the differences in the number concentration and size distribution were mostly due to differences in their dilution during transport to Hyytiälä. Nucleation

845 mode particles are also seen in the middle layer, and, assuming that this layer did not experience strong mixing for several days, we suppose that these new particles were formed in this elevated layer.

Certainly, higher aerosol concentrations within the elevated layers are periodically present in Finland. These layers can influence for example the columnar optical closure in the boreal environment (Zieger et al., 2015). More detailed analysis is needed in order to address the relative contribution of different aerosol sources to these layers and to be able to compare the

850 results with the data available in Tomsk, Russia.

3.8.4 Deriving proxy variables from in situ and satellite data

In iCUPE, we developed proxies for atmospheric variables from the in situ data gathered in Finnish measurement sites. In practice, this means that we derive formulas that describe the proxy variables as functions of more commonly measured parameters. Previously, the proxies have been derived mainly for concentrations of gas phase molecules, such as sulfuric acid

855 (Petäjä et al., 2009; Mikkonen et al., 2011) and monoterpenes (Kontkanen et al., 2016). In iCUPE, we are developing proxies for condensation sink (CS), boundary layer height (BLH) and ecosystem level gross primary production (GPP). The aim is to produce proxies that rely on variables that can also be retrieved from the satellite data in order to produce proxies with good spatial coverage (e.g. Kulmala et al. 2011b). Here, we describe the CS proxy development, while the proxies for BLH and GPP remain under development.

860 Condensation sink (CS) describes the loss rate of vapor molecules due to their condensation on the aerosol particle surfaces (Kulmala et al., 2001). Therefore, it depends strongly on the particle surface area, which is determined mainly by the concentration of particles with diameters close to or over 100 nm. Particles in this size range are introduced into atmosphere directly from various combustion sources, especially from residential combustion of wood and other biofuel (Paasonen et al., 2016), and grown from smaller sizes by condensation of mainly biogenic vapors (Riipinen et al., 2011; Paasonen et al., 2013).

865 In our proxy we use carbon monoxide (CO) as a tracer for aerosols produced in combustion processes, and air temperature for estimating the formation of biogenic secondary organic aerosol. Air temperature has been shown to correlate with the concentrations of the particles in the relevant size range in various continental environments (Paasonen et al., 2013).

We determined the proxy for daily averages of CS for measurement sites at SMEAR II in Hyytiälä (Southern Finland), at SMEAR I in Värriö and in Pallas (Northern Finland). When determining the dependence between CO concentration and CS,

870 we observed a clear pattern in the seasonal minima of CO concentration at both sites (Fig. 29a). Since this pattern is not reflected in CS, but originates presumably from longer atmospheric lifetime of CO during dark months, we proceeded with inspecting the relation between CS and ΔCO, which describes the difference between the observation and the 5th percentile of concentrations at the respected time of year. In Fig. 29b we show the dependence of CS on ΔCO in different temperature bins in Värriö. We calculated average slopes (b_{ave}) for the fittings in Fig. 29b for each measurement site, and evaluated the intercepts

of the new fittings, where this average slope was applied. These intercepts are depicted for the sites in Fig. 29c. These intercepts reflect the expected temperature dependence, where CS is not impacted by temperature at T < 5°C, when ecosystem emissions are generally low, and increasing positive temperatures cause increase in CS. Finally, we formulated the temperature dependent part of the proxy ($a_1(T)$) by calculating the average intercepts in T < 5°C and making fit to the intercepts in positive temperatures (Fig. 29c). This produces the final proxies for CS (Fig. 29d), with form:

$$CS_{proxy} = a_1(T) + b_{ave} \times \Delta CO. \tag{3}$$

As a next step for the CS proxies, we will derive and test a proxy derived from a data set combined from all different sites, study how the proxies work for data from other polar stations, and investigate whether CO and temperature retrieved from the satellite data can be applied for the proxies.

3.8.5 iCUPE data flow

One of the main outcomes of iCUPE are new data products developed based on the comprehensive use of in situ and satellite remote sensing. The new iCUPE data products, which will fill e.g. observational gap of the key variables of Persisting Organic Pollutants (POPs), Chemicals of Emerging Concern (CECs), Short-Lived Climate Forcers (SLCFs), and atmospheric trace gases in the polar context, are being co-designed together with different end users. The list of data products is presented in Table 1. End-users for the iCUPE data sets include European Environment Agency, geoengineering bodies, decision makers, intergovernmental organizations, local government and environmental administration (ministries), citizens and National and European weather services. The data can be used to improve models, to advance our scientific understanding of the Arctic regions, support policy making and improve weather predictions and mechanisms in risk control of natural hazards, in sea traffic control, in tourism and in chemical weather prediction.

iCUPE will provide in total more than 20 datasets as products usable for researchers, decision- and policy makers, stakeholders and end-users communities. These will be a valuable and important contribution from the iCUPE project activities in piloting open access to Arctic data. All these datasets will be publicly available for different applications and services. Focusing on the Arctic region territories, the planned datasets will include e.g. novel data on anthropogenic contaminants in snow and ice cores and organic contaminants in the air-snow-water and concentrations of different chemical species and aerosols as well as their characteristics including vertical profiles. Within iCUPE we will also develop specific datasets focusing on selected geographical areas in northern latitudes. The data provision is open and Russian iCUPE collaborators have also provided data from the Russian Arctic, such as atmospheric mercury measurements at Amderma station, elemental and organic carbon over the north-western coast of the Kandalaksha Bay of the White Sea and micro-climatic features and Urban Heat Island intensity in cities of Arctic region.

Each of the data sets are promoted through "teasers" (www.atm.helsinki.fi/icupe/index.php/submitted-datasets), which provides the metadata information pertinent to the data sets. Majority of archived datasets (as products) are directly linked (and downloadable) and corresponding metadata information included. The University of Helsinki will take responsibility for long-term storage, accessibility, and maintenance. The raw data will be hosted and maintained by the dataset providers.

As soon as a larger fraction of iCUPE data products are available, we explore different platforms to disseminate the iCUPE data sets. To facilitate and standardize access to data cloud-based online platforms, known as the Data and Information Access Services (DIAS), providing storage, centralized access and handling to data, and processing tools. The DIAS platforms (CREODIAS - creodias.eu; SOBLOO - sobloo.eu; MUNDI - mundiwebservices.com; ONDA - www.onda-dias.eu/cms; and WEkEO - www.wekeo.eu) allow users to explore, process, and download Copernicus data and information as well as to have the ability to process and combine with data from other sources. It is also possible to develop and host new applications on such platforms. Other tested platforms for pre/post-processing/analysis of iCUPE data include the Virtual Laboratory (vlab.geodab.org) Google Earth Engine (earthengine.google.com), Polar Thematic Exploitation Platform (portal.polartep.io),

Global Earth Observation System of Systems Portal (www.geoportal.org). We will continue to explore these options for the iCUPE data provision in the future.

All final data products and proxies developed will follow interoperability and data sharing principles endorsed by GEOSS. We explore possibilities to maximize the use of new data products and advertising these to larger communities, such as in several community portals such as Sustaining Arctic Observation Networks (SAON) Arctic Observation System and Arctic Portal and Pan Eurasian Experiment (PEEX) Program- the Arctic-Boreal Hub Portal. The SAON portal expands the visibility of the iCUPE data to the circumpolar context and PEEX to Russian and Chinese research and other end-user communities. For selected topical data sets, some will be included in the University of Helsinki smart-SMEAR platform (Junninen et al. 2009) and disseminated via metadata catalogs to a wider audience. As a whole we need to utilize the full capacity of the multi-platform approach (in situ, satellites and models) to address the fate of pollutants in the Arctic. This will provide tools to perform targeted reductions, but can also provide new insights into the lifecycle of the pollutants in the Arctic environment.

3.8.6 Observation system analysis

In addition to investigate new observation capabilities, iCUPE was tasked to evaluate the connectivity and scale of satellite observations for Arctic needs. This task was expanded and elaborated by the SAON initiative "Arctic observing system assessment framework" (STPI/SAON, 2017). The framework links societal benefits to the observing system. Within the framework we identified 170 common objectives classified under 12 Societal Benefit Areas from international Arctic strategy documents. These objectives identify a need for earth observation information to enable informed decision-making in the Arctic context. In this work, a team of domain experts from SAON, AMAP and iCUPE evaluated the assessment framework value tree for atmosphere and ocean variables.

The basis of the analysis includes the observation capacity. Earth Observation (EO) inputs like SYNOP station measurements of physical atmosphere and in other stations, ocean variables, were linked to key products / outcomes / services such as numerical weather prediction and through groups like in this case weather service connected to key objectives of the assessment framework (Fig. 30), such as weather service or environmental information service.

We weighted the analysis by annual costs for operation. Representative yearly unit costs of EO inputs and modelling components were estimated by station experts or estimated based on European Union projects or Copernicus program tenders. As the observational capacity and its monetary value, we utilized the WMO OSCAR database for satellite and surface observation systems (https://www.wmo-sat.info/oscar/) north of 60° N. This provided us the volume of stations in different station and mission categories in the Arctic (Table 2). Based on our analysis, the total yearly value of this observation system including EO inputs and modeling is over 204 million €. Compared to the observing system estimated costs in the area 30° N to 60° N this is only about one fifth.

Another way to scale Arctic needs is to look at the distribution of stations globally for operational networks: WMO has organized in the integrated ground observing system WIGOS stations on land, co-sponsoring is mainly with IMO for marine platforms and the non-affiliated are research organizations distributing information in near-real-time. The Arctic slice compared to Northern mid-latitudes has about one sixth of the stations on about one third of aerial coverage compared with the mid-latitude costs. Doubling current observing efforts would be needed to achieve a similar coverage in the Arctic.

The value chain from the observations through modeling frameworks into services and decision-making is presented in Fig. 30. It is an estimation of the data flows from different stations and satellites to modeling systems and onwards to services carrying the weight of the total investment forward divided on the importance that the next step places on the information. The costs of modeling have been estimated and added to the value tree. Services are an important element, included by giving each connection in the tree a value of 1 million annually. This cost represents the global effort and with the included connections amounts to 81 million EUR per year. To compare this value, it corresponds to the annual costs of the Finnish Meteorological

Institute at 74 million €, which operates 429 meteorological stations, all included as part of Arctic observation capacity in Table 2. In addition to FMI, there is at least 6 similar other institutes serving for the Arctic, the estimate is reasonable.

The decision-making step in the value tree is channeled through 6 services, which include research activities and the efforts to consolidate research results in Arctic Council working group reports or the International Panel on Climate Change or the IPBES for biodiversity as one-off actions. Continuous services are established in weather, climate, marine and environmental information. The full value tree that connects all services to 170 key objectives from the Societal Benefit Areas is complex, but could help to attribute the costs of an observing system fairly to all the areas that use it. Browsing the full tree is there much better on the web under http://arctic-obs.fmi.fi/ and in the publication (Strahlendorff et al., 2019). iCUPE activities are grouped in the value tree under research stations, observation grids and research services. The costs could not be determined in detail, but the activities fit into the research station estimate although the in situ monitoring activities are very diverse. Travel costs can be substantial, but this component could not be averaged usefully over the range of different research stations.

In conclusion a doubling of Arctic observing efforts both from satellites as well as in situ is necessary and reasoned. This amounts to a yearly increase of 200 million € to observing infrastructure and the production value chain. The European Union Space program is planning for additions to the satellite component with Sentinel Expansion missions, but additions to the in situ component are missing a funding action.

4 Summary and Outlook

The polar regions are facing changes in the future, both in terms of climate change influenced by Arctic amplification but also due to on-going megatrends such as globalization that drive development e.g. of new transport routes through the fragile Arctic environment and extensive utilization of natural resources within the Arctic. The environment in the Arctic is at risk. To address aspects related to the Arctic change, we set up the ERA-PLANET Strand 4 project "iCUPE - integrative and Comprehensive Understanding on Polar Environments" to provide novel insights and observational data on global grand challenges with a polar focus.

In iCUPE, our concept is to utilize an integrated approach combining in situ observations, satellite remote sensing Earth Observations (EO) and multi-scale modeling to synthesize data from comprehensive long-term measurements, intensive campaigns and satellites to deliver data products, metrics and indicators to the stakeholders concerning the environmental status, availability and extraction of natural resources in the polar areas.

The circumpolar coverage of in situ atmospheric observations has developed during the last decades. In selected locations, such as Svalbard, observations are available for assessing the decadal variability of key observables, such as black carbon. The geographical coverage should be particularly expanded in the Russian Arctic (Petäjä et al., 2019) although a lot of observation sites are operated already (Alekseychik et al., 2016). However, the connection of various continuous national activities and intensive campaigns within the Arctic should be coordinated in order to reduce operation costs. The observations should take advantage of data harmonization procedures set up e.g. by WMO-GAW and European Research infrastructures (ICOS, ACTRIS, eLTER). Work towards open data sharing should be continued.

Harmonized and open data is crucial for development of services based on the observations within the Arctic. We need to maintain and improve comprehensive and continuous observations network of in situ observations in the Arctic that is sustained for extended periods of time to monitor the concentration of atmospheric pollutants. This gives us verification data on the political decisions to reduce the emissions of harmful compounds but also enables us to respond to arising new threats to the environment. The in situ observations analyzed and performed within iCUPE underlined that we need to utilize the full capacity of the multi-platform approach (in situ, satellites and models) to address the fate of pollutants in the Arctic. New observational needs should be analyzed e.g. in the framework of Essential Variables (EVs) that connect to sustainable development goals of the United Nations.

The long-term observations at Svalbard revealed the aerosol concentrations are strongly modulated with seasons. This is apparent in Svalbard Equivalent Black Carbon concentrations as well as in aerosol number concentrations detected at Villum Station in Northern Greenland. The comprehensive source apportionment of the organic aerosol fraction at different observation sites in the Arctic indicated that the concentrations are affected by a combination of regionally specific sources and long-range transport of anthropogenic aerosol particles. Vertical profiling can provide novel insights into pollution transport and dispersion in the Arctic environment. The combined use of aircraft observations, modeling tools and emission inventory analysis can provide novel insights into variability of atmospheric pollutants within the Arctic.

Similar to the decrease in black carbon, the decline of legacy POPs in the environment is expected under global efforts. Whereas, with their persistence in environmental matrices, such as water, sediment, soil, vegetation and ice/snow, warming Arctic may drive them again available for environmental circulation. Consequently, future research should be focused on quantifying these remobilization fluxes and sinks for both legacy POPs and emerging contaminants in the Arctic.

Within iCUPE, we determined concentrations of mercury in different compartments and fluxes between these compartments in the land-atmosphere continuum. The mercury flux to the Arctic environment through riverine discharge was found to be important. The concentration of mercury in the snow varied as a function of snow depth indicating a crucial role of atmospheric deposition. Long-term observations of atmospheric mercury in the Russian Arctic were found to be connected with the distance to the sea. The modeling results underline the interconnected life-cycle between mercury halogen compounds and atmospheric oxidants.

Furthermore, the remote sensing activities in the iCUPE project highlighted the need of a ground truth concerning the fractional snow cover. This kind of information can be obtained by terrestrial photography and it represents a tool in common between remotely-sensed products useful for integrating satellite data with different spatial and time resolutions. This approach can be very effective in high-latitude areas where illuminating conditions, topography and cloud cover limit the use of optical remote sensing.

The satellite remote sensing work within iCUPE revealed that imaging spectroscopy also known as hyperspectral remote sensing for Arctic vegetation provides valuable information on vegetation status and biomass that can improve our understanding of long-term vegetation trends derived from broadband data. Spectral information stored in the narrow wavelengths of the visible spectrum are the most promising for differentiating spectrally similar vegetation communities and for delivering information on photosynthetic activity and biomass. The lack of ground-validated datasets and an overall scarcity of dense, high quality image time series remains a challenge. The increasing availability of hyperspectral data will face similar challenges and given the limited number of hyperspectral remote sensing studies in the Arctic, high quality, ground-validated data is required to accurately interpret these dense and complex datasets. The rise of more advanced classification methods such as machine-learning techniques are highly promising for Arctic vegetation mapping using advanced remote sensing platforms. An increased effort to develop Arctic-specific algorithms is needed.

Within iCUPE, the benefits of combining in situ and satellite remote sensing and multiscale modeling in cryospheric, terrestrial and marine regimes as well as atmospheric domain are clear. Such integrative activities need to be expanded and continued in order to provide verified environmental data and services in the changing Arctic.

Data availability. The data presented in this paper is available through the authors upon request. The iCUPE data products are available through iCUPE-webpage: https://www.atm.helsinki.fi/icupe/index.php/datasets.

Author contributions. TP had the initial idea. All authors contributed in specific sections of the paper and commented on the manuscript. TP, E-MD, KT, JS and HKL formed the editorial team consolidating the text.

Competing interests. The authors declare no competing interests.

Acknowledgements

This project has received funding from the European Union's Horizon 2020 research and innovation programme under grant agreement No 689443 via project iCUPE (Integrative and Comprehensive Understanding on Polar Environments)" and through ACTRIS2 is gratefully acknowledged. Additional financial support through Academy of Finland (Center of Excellence in Atmospheric Sciences) and through Academy of Finland project NANOBIOMASS (decision number 307537), Belmont Forum project "Community Resilience to Boreal Environmental change: Assessing Risks from fire and disease" (ACRoBEAR) via Academy of Finland, decision number 334792 are gratefully acknowledged. P.O. thanks for partial support from project Russian Foundation for Basic Research (RFBR) No. 18-05-60084. Ground-based lidar observations in Siberia were supported in part by Ministry of Science of Education of the Russian Federation (Agreement No. 14.616.21.0104, unique identifier RFMEFI61618X0104). We thank J. Pelon for assistance with research conducted at LATMOS and IGE. French groups also acknowledge support from the French Arctic Initiative project Pollution in the Arctic System (PARCS). Part of this study was founded by the Danish Environmental Protection Agency and the Danish Energy Agency by means of DANCEA funds for Environmental Support to the Arctic Region. The Royal Danish Air Force is acknowledged for providing free transport of equipment to Station Nord, and the staff at Station Nord is especially acknowledged for excellent support. Part of this study was funded by the German Science Foundation (Deutsche Forschungsgemeinschaft, DFG) as project with the number LA 2907/5-3, BA 1988/14-3, WI 1449/22-3. For UAV measurements in Ny-Ålesund we thank the whole AWIPEV team and Kingsbay crew for support during preparation and for hosting us.

References

Abbatt, J. P. D., Thomas, J. L., Abrahamsson, K., Boxe, C., Granfors, A., Jones, A. E., King, M. D., Saiz-Lopez, A., Shepson, P. B., Sodeau, J., Toohey, D. W., Toubin, C., von Glasow, R., Wren, S. N., and Yang, X.: Halogen activation via interactions with environmental ice and snow in the polar lower troposphere and other regions, Atmos. Chem. Phys., 12, 6237-6271, https://doi.org/10.5194/acp-12-6237-2012, 2012.

Alekseychik, P., Lappalainen, H. K., Petäjä, T., Zaitseva, N., Heimann, M., Laurila, T., Lihavainen, H., Asmi, E., Arshinov, M., Shevchenko, V., Makshtas, A., Dubtsov, S., Mikhailov, E., Lapshina, E., Kirpotin, S., Kurbatova, Y., Ding, A., Guo, H., Park, S., Lavric, J. V., Reum, F., Panov, A., Prokushkin, A., and Kulmala, M.: Ground-based station network in Arctic and Subarctic Eurasia, Geography, Environment and Sustainability, 9, https://doi.org/10.15356/2071-9388_02v09_2016_06, 2016.

Altstädter, B., Platis, A., Wehner, B., Scholtz, A., Wildmann, N., Hermann, M., Käthner, R., Baars, H., Bange, J., and Lampert, A.: ALADINA - an unmanned research aircraft for observing vertical and horizontal distributions of ultrafine particles within the atmospheric boundary layer, Atmos. Meas. Tech., 8, 1627-1639, https://doi.org/10.5194/amt-8-1627-2015, 2015.

Altstädter, B., Platis, A., Jähn, M., Baars, H., Lückerath, J., Held, A., Lampert, A., Bange, J., Hermann, M., and Wehner, B.: Airborne observations of newly formed boundary layer aerosol particles under cloudy conditions, Atmos Chem Phys, 18, 8249-8264, https://doi.org/10.5194/acp-18-8249-2018, 2018.

AMAP, 2011. AMAP Assessment 2011: Mercury in the Arctic. Arctic Monitoring and Assessment Programme (AMAP), Oslo, Norway. xiv + 193 pp.

AMAP Assessment 2015: Black carbon and ozone as Arctic climate forcers. Arctic Monitoring and Assessment Programme (AMAP), Oslo, Norway. vii + 116 pp.

Ancellet, G., Penner, I. E., Pelon, J., Mariage, V., Zabukovec, A., Raut, J. C., Kokhanenko, G., and Balin, Y. S.: Aerosol monitoring in Siberia using an 808 nm automatic compact lidar, Atmos. Meas. Tech., 12, 147-168, https://doi.org/10.5194/amt-12-147-2019, 2019.

Angot, H., Magand, O., Helmig, D., Ricaud, P., Quennehen, B., Gallée, H., Del Guasta, M., Sprovieri, F., Pirrone, N., Savarino, J., and Dommergue, A.: New insights into the atmospheric mercury cycling in central Antarctica and implications on a continental scale, Atmos. Chem. Phys., 16, 8249-8264, https://doi.org/10.5194/acp-16-8249-2016, 2016.

1085 Antokhina, O. Y., Antokhin, P. N., Arshinova, V. G., Arshinov, M. Y., Belan, B. D., Belan, S. B., Belov, V. V., Gridnev, Y. V., Davydov, D. K., Ivlev, G. A., Kozlov, A. V., Law, K. S., Nédélec, P., Paris, J.-D., Rasskazchikova, T. M., Savkin, D. E., Simonenkov, D. V., Sklyadneva, T. K., Tolmachev, G. N., and Fofonov, A. V.: Comparison between the distributions of atmospheric gases measured with remote and contact tools over the Russian Arctic. (in Russian), Atmos Ocean Opt, 31, 507-510, https://doi.org/10.15372/AOO20180707, 2016.

Antokhina, O. Y., Antokhin, P. N., Arshinova, V. G., Arshinov, M. Y., Belan, B. D., Belan, S. B., Davydov, D. K., Ivlev, G. 1090 A., Kozlov, A. V., Nedelec, P., Paris, J. D., Rasskazchikova, T. M., Savkin, D. E., Simonenkov, D. V., Sklyadneva, T. K., Tolmachev, G. N., and Fofonov, A. V.: Vertical Distributions of Gaseous and Aerosol Admixtures in Air over the Russian Arctic, Atmos Ocean Opt, 31, 300-310, https://doi.org/10.1134/S102485601803003x, 2018.

Armitage, J. M., MacLeod, M., and Cousins, I. T.: Comparative Assessment of the Global Fate and Transport Pathways of Long-Chain Perfluorocarboxylic Acids (PFCAs) and Perfluorocarboxylates (PFCs) Emitted from Direct Sources, Environ. 1095 Sci. Technol., 43, 5830-5836, https://doi.org/10.1021/es900753y, 2009.

Arnold, S. R., Law, K. S., Brock, C. A., Thomas, J. L., Starkweather, S. M., von Salzen, K., Stohl, A., Sharma, S., Lund, M. T., Flanner, M. G., Petäjä, T., Tanimoto, H., Gamble, J., Dibb, J. E., Melamed, M., Johnson, N., Fidel, M., Tynkkynen, V. P., Baklanov, A., Eckhardt, S., Monks, S. A., Browse, J., and Bozem, H.: Arctic air pollution: Challenges and opportunities for the next decade, Elementa-Sci. Anthrop., 4, 1-17, https://doi.org/10.12952/journal.elementa.000104, 2016.

1100 Backman, J., Schmeisser, L., Virkkula, A., Ogren, J. A., Asmi, E., Starkweather, S., Sharma, S., Eleftheriadis, K., Uttal, T., Jefferson, A., Bergin, M., Makshtas, A., Tunved, P., and Fiebig, M.: On Aethalometer measurement uncertainties and an instrument correction factor for the Arctic, Atmos. Meas. Tech., 10, 5039-5062, https://doi.org/10.5194/amt-10-5039-2017, 2017.

Barbante, C., Veysseyre, A., Ferrari, C., Van de Velde, K., Morel, C., Capodaglio, G., Cescon, P., Scarponi, G., and Boutron, 1105 C.: Greenland snow evidence of large scale atmospheric contamination for platinum, palladium, and rhodium, Environ. Sci. Technol., 35, 835-839, https://doi.org/10.1021/es000146y, 2001.

Barrie, L. A.: Arctic Air-Pollution - an Overview of Current Knowledge, Atmos. Environ., 20, 643-663, https://doi.org/10.1016/0004-6981(86)90180-0, 1986.

Barsi, J. A., Lee, K., Kvaran, G., Markham, B. L., and Pedelty, J. A.: The Spectral Response of the Landsat-8 Operational 1110 Land Imager, Remote Sens., 6, 10232-10251, https://doi.org/10.3390/rs61010232, 2014.

Beamish, A. L., Coops, N., Chabrillat, S., and Heim, B.: A Phenological Approach to Spectral Differentiation of Low-Arctic Tundra Vegetation Communities, North Slope, Alaska, Remote Sens., 9, https://doi.org/10.3390/rs9111200, 2017.

Beamish, A. L., Coops, N. C., Hermosilla, T., Chabrillat, S., and Heim, B.: Monitoring pigment-driven vegetation changes in a low-Arctic tundra ecosystem using digital cameras, Ecosphere, 9, https://doi.org/10.1002/ecs2.2123, 2018.

1115 Beamish, A. L.: Recent trends and remaining challenges for optical remote sensing of Arctic tundra vegetation: A review and outlook., Remote Sens. Environ., under review, RSE-D-19-01752, 2019.

Beamish, A. L., Chabrillat, S., Brell, M., Coops, N. C., T., H., and Heim, B.: Spectral sensitivity of airborne hyperspectral data to plant functional types in a low Arctic tundra ecosystem: Implications for landscape scale vegetation monitoring., Int. J. Appl. Earth Obs., under review, JAG_2019_812, 2019.

1120 Beniston, M., Farinotti, D., Stoffel, M., Andreassen, L. M., Coppola, E., Eckert, N., Fantini, A., Giacona, F., Hauck, C., Huss, M., Huwald, H., Lehning, M., López-Moreno, J. I., Magnusson, J., Marty, C., Morán-Tejéda, E., Morin, S., Naaim, M., Provenzale, A., Rabatel, A., Six, D., Stötter, J., Strasser, U., Terzago, S., and Vincent, C.: The European mountain cryosphere:

a review of its current state, trends, and future challenges, Cryosphere, 12, 759-794, https://doi.org/10.5194/tc-12-759-2018, 2018.

1125 Bhatt, U. S., Walker, D. A., Raynolds, M. K., Comiso, J. C., Epstein, H. E., Jia, G. S., Gens, R., Pinzon, J. E., Tucker, C. J., Tweedie, C. E., and Webber, P. J.: Circumpolar Arctic Tundra Vegetation Change Is Linked to Sea Ice Decline, Earth Interact., 14, https://doi.org/10.1175/2010ei315.1, 2010.

Bokhorst, S., Pedersen, S. H., Brucker, L., Anisimov, O., Bjerke, J. W., Brown, R. D., Ehrich, D., Essery, R. L. H., Heilig, A., Ingvander, S., Johansson, C., Johansson, M., Jónsdóttir, I. S., Inga, N., Luojus, K., Macelloni, G., Mariash, H., McLennan, D.,

1130 Rosqvist, G. N., Sato, A., Savela, H., Schneebeli, M., Sokolov, A., Sokratov, S. A., Terzago, S., Vikhamar-Schuler, D., Williamson, S., Qiu, Y. B., and Callaghan, T. V.: Changing Arctic snow cover: A review of recent developments and assessment of future needs for observations, modelling, and impacts, Ambio, 45, 516-537, https://doi.org/10.1007/s13280-016-0770-0, 2016.

Bond, T., Doherty, S. J., Fahey, D., Forster, P., Berntsen, T., DeAngelo, B., Flanner, M., Ghan, S., Kärcher, B., Koch, D.,

1135 Kinne, S., Kondo, Y., Quinn, P., Sarofim, M., Schultz, M., Schulz, M., Venkataraman, C., Zhang, H., Zhang, S., Bellouin, N., Guttikunda, S., Hopke, P., Jacobson, M., Kaiser, J., Klimont, Z., Lohmann, U., Schwarz, J., Shindell, D., Storelvmo, T., Warren, S., and Zender, C.: Bounding the role of black carbon in the climate system: A scientific assessment, J. Geophys. Res.-Atmos., 118, 5380-5552, https://doi.org/10.1002/jgrd.50171, 2013.

Bossi, R., Vorkamp, K., and Skov, H.: Concentrations of organochlorine pesticides, polybrominated diphenyl ethers and

1140 perfluorinated compounds in the atmosphere of North Greenland, Environ. Pollut., 217, 4-10, https://doi.org/10.1016/j.envpol.2015.12.026, 2016.

Boy, M., Thomson, E. S., Navarro, J. C. A., Arnalds, O., Batchvarova, E., Bäck, J., Berninger, F., Bilde, M., Brasseur, Z., Dagsson-Waldhauserova, P., Castarède, D., Dalirian, M., de Leeuw, G., Dragosics, M., Duplissy, E. M., Duplissy, J., Ekman, A. M. L., Fang, K. Y., Gallet, J. C., Glasius, M., Gryning, S. E., Grythe, H., Hansson, H. C., Hansson, M., Isaksson, E., Iversen,

1145 T., Jonsdottir, I., Kasurinen, V., Kirkevåg, A., Korhola, A., Krejci, R., Kristjansson, J. E., Lappalainen, H. K., Lauri, A., Leppäranta, M., Lihavainen, H., Makkonen, R., Massling, A., Meinander, O., Nilsson, E. D., Olafsson, H., Pettersson, J. B. C., Prisle, N. L., Riipinen, I., Roldin, P., Ruppel, M., Salter, M., Sand, M., Seland, O., Seppä, H., Skov, H., Soares, J., Stohl, A., Ström, J., Svensson, J., Swietlicki, E., Tabakova, K., Thorsteinsson, T., Virkkula, A., Weyhenmeyer, G. A., Wu, Y. S., Zieger, P., and Kulmala, M.: Interactions between the atmosphere, cryosphere, and ecosystems at northern high latitudes,

1150 Atmos. Chem. Phys., 19, 2015-2061, https://doi.org/10.5194/acp-19-2015-2019, 2019.

Bozzetti, C., Sosedova, Y., Xiao, M., Daellenbach, K. R., Ulevicius, V., Dudoitis, V., Mordas, G., Byčenkienė, S., Plauškaitė, K., Vlachou, A., Golly, B., Chazeau, B., Besombes, J. L., Baltensperger, U., Jaffrezo, J. L., Slowik, J. G., El Haddad, I., and Prévôt, A. S. H.: Argon offline-AMS source apportionment of organic aerosol over yearly cycles for an urban, rural, and marine site in northern Europe, Atmos. Chem. Phys., 17, 117-141, https://doi.org/10.5194/acp-17-117-2017, 2017.

1155 Bratsch, S. N., Epstein, H. E., Buchhorn, M., and Walker, D. A.: Differentiating among Four Arctic Tundra Plant Communities at Ivotuk, Alaska Using Field Spectroscopy, Remote Sens., 8, https://doi.org/10.3390/rs8010051, 2016.

Breider, T. J., Mickley, L. J., Jacob, D. J., Wang, Q. Q., Fisher, J. A., Chang, R. Y. W., and Alexander, B.: Annual distributions and sources of Arctic aerosol components, aerosol optical depth, and aerosol absorption, J. Geophys. Res.-Atmos., 119, 4107-4124, https://doi.org/10.1002/2013jd020996, 2014.

1160 Breider, T. J., Mickley, L. J., Jacob, D. J., Ge, C., Wang, J., Sulprizio, M. P., Croft, B., Ridley, D. A., McConnell, J. R., Sharma, S., Husain, L., Dutkiewicz, V. A., Eleftheriadis, K., Skov, H., and Hopke, P. K.: Multidecadal trends in aerosol radiative forcing over the Arctic: Contribution of changes in anthropogenic aerosol to Arctic warming since 1980, J. Geophys. Res.-Atmos., 122, 3573-3594, https://doi.org/10.1002/2016jd025321, 2017.

Brooks, S. B., Saiz-Lopez, A., Skov, H., Lindberg, S. E., Plane, J. M. C., and Goodsite, M. E.: The mass balance of mercury

1165 in the springtime arctic environment, Geophys. Res. Lett., 33, https://doi.org/10.1029/2005gl025525, 2006.

Buchhorn, M., Walker, D. A., Heim, B., Raynolds, M. K., Epstein, H. E., and Schwieder, M.: Ground-Based Hyperspectral Characterization of Alaska Tundra Vegetation along Environmental Gradients, Remote Sens., 5, 3971-4005, https://doi.org/10.3390/rs5083971, 2013.

Buixadé Farré, A., Stephenson, S. R., Chen, L., Czub, M., Dai, Y., Demchev, D., Efimov, Y., Graczyk, P., Grythe, H., Keil, K., Kivekäs, N., Kumar, N., Liu, N., Matelenok, I., Myksvoll, M., O'Leary, D., Olsen, J., Pavithran.A.P, S., Petersen, E., Raspotnik, A., Ryzhov, I., Solski, J., Suo, L., Troein, C., Valeeva, V., van Rijckevorsel, J., and Wighting, J.: Commercial Arctic shipping through the Northeast Passage: routes, resources, governance, technology, and infrastructure, Polar Geogr., 37, 298-324, https://doi.org/10.1080/1088937X.2014.965769, 2014.

Cai, M. H., Xie, Z. Y., Möller, A., Yin, Z. G., Huang, P., Cai, M. G., Yang, H. Z., Sturm, R., He, J. F., and Ebinghaus, R.: Polyfluorinated compounds in the atmosphere along a cruise pathway from the Japan Sea to the Arctic Ocean, Chemosphere, 87, 989-997, https://doi.org/10.1016/j.chemosphere.2011.11.010, 2012.

Canonaco, F., Crippa, M., Slowik, J. G., Baltensperger, U., and Prévôt, A. S. H.: SoFi, an IGOR-based interface for the efficient use of the generalized multilinear engine (ME-2) for the source apportionment: ME-2 application to aerosol mass spectrometer data, Atmos. Meas. Tech., 6, 3649-3661, https://doi.org/10.5194/amt-6-3649-2013, 2013.

Carnerero, C., Pérez, N., Petäjä, T., Laurila, T. M., Ahonen, L. R., Kontkanen, J., Ahn, K.-H., Alastuey, A., and Querol, X.: Relating high ozone, ultrafine particles, and new particle formation episodes using cluster analysis, Atmos. Environ.: X, 4, 100051, https://doi.org/10.1016/j.aeaoa.2019.100051, 2019.

Collaud Coen, M., Andrews, E., Alastuey, A., Arsov, T. P., Backman, J., Brem, B. T., Bukowiecki, N., Couret, C., Eleftheriadis, K., Flentje, H., Fiebig, M., Gysel-Beer, M., Hand, J. L., Hoffer, A., Hooda, R., Hueglin, C., Joubert, W., Keywood, M., Kim, J. E., Kim, S.-W., Labuschagne, C., Lin, N.-H., Lin, Y., Lund Myhre, C., Luoma, K., Lyamani, H., Marinoni, A., Mayol-Bracero, O. L., Mihalopoulos, N., Pandolfi, M., Prats, N., Prenni, A. J., Putaud, J.-P., Ries, L., Reisen, F., Sellegri, K., Sharma, S., Sheridan, P., Sherman, J. P., Sun, J., Titos, G., Torres, E., Tuch, T., Weller, R., Wiedensohler, A., Zieger, P., and Laj, P.: Multidecadal trend analysis of aerosol radiative properties at a global scale, Atmos. Chem. Phys. Discuss., https://doi.org/10.5194/acp-2019-1174, in review, 2020.

Corbett, J., Lack, D., Winebrake, J., Harder, S., Silberman, J., and Gold, M.: Arctic shipping emissions inventories and future scenarios, Atmos. Chem. Phys., 10, 9689-9704, https://doi.org/10.5194/acp-10-9689-2010, 2010.

Daellenbach, K. R., Bozzetti, C., Křepelova, A. K., Canonaco, F., Wolf, R., Zotter, P., Fermo, P., Crippa, M., Slowik, J. G., Sosedova, Y., Zhang, Y., Huang, R. J., Poulain, L., Szidat, S., Baltensperger, U., El Haddad, I., and Prévôt, A. S. H.: Characterization and source apportionment of organic aerosol using offline aerosol mass spectrometry, Atmos. Meas. Tech., 9, 23-39, https://doi.org/10.5194/amt-9-23-2016, 2016.

Dall'Osto, M., Geels, C., Beddows, D. C. S., Boertmann, D., Lange, R., Nøjgaard, J. K., Harrison, R. M., Simo, R., Skov, H., and Massling, A.: Regions of open water and melting sea ice drive new particle formation in North East Greenland, Sci. Rep.-UK, 8, https://doi.org/10.1038/s41598-018-24426-8, 2018a.

Dall'Osto, M., Simo, R., Harrison, R. M., Beddows, D. C. S., Saiz-Lopez, A., Lange, R., Skov, H., Nøjgaard, J. K., Nielsen, I. E., and Massling, A.: Abiotic and biotic sources influencing spring new particle formation in North East Greenland, Atmos. Environ., 190, 126-134, https://doi.org/10.1016/j.atmosenv.2018.07.019, 2018b.

Di Pierro, M., Jaeglé, L., and Anderson, T. L.: Satellite observations of aerosol transport from East Asia to the Arctic: three case studies, Atmos. Chem. Phys., 11, 2225-2243, https://doi.org/10.5194/acp-11-2225-2011, 2011.

Dietz, A. J., Kuenzer, C., Gessner, U., and Dech, S.: Remote sensing of snow - a review of available methods, Int. J. Remote Sens., 33, 4094-4134, https://doi.org/10.1080/01431161.2011.640964, 2012.

Douglas, T. A., Loseto, L. L., Macdonald, R. W., Outridge, P., Dommergue, A., Poulain, A., Amyot, M., Barkay, T., Berg, T., Chételat, J., Constant, P., Evans, M., Ferrari, C., Gantner, N., Johnson, M. S., Kirk, J., Kroer, N., Larose, C., Lean, D., Nielsen,

T. G., Poissant, L., Rognerud, S., Skov, H., Sørensen, S., Wang, F. Y., Wilson, S., and Zdanowicz, C. M.: The fate of mercury in Arctic terrestrial and aquatic ecosystems, a review, Environ. Chem., 9, 321-355, https://doi.org/10.1071/En11140, 2012.

1210 Dozier, J., Green, R. O., Nolin, A. W., and Painter, T. H.: Interpretation of snow properties from imaging spectrometry, Remote Sens. Environ., 113, S25-S37, https://doi.org/10.1016/j.rse.2007.07.029, 2009.

Durnford, D., Dastoor, A., Figueras-Nieto, D., and Ryjkov, A.: Long range transport of mercury to the Arctic and across Canada, Atmos. Chem. Phys., 10, 6063-6086, https://doi.org/10.5194/acp-10-6063-2010, 2010.

Eleftheriadis, K., Vratolis, S., and Nyeki, S.: Aerosol black carbon in the European Arctic: Measurements at Zeppelin station,
1215 Ny-Alesund, Svalbard from 1998-2007, Geophys. Res. Lett., 36, https://doi.org/10.1029/2008gl035741, 2009.

ESA: Sen2Cor Configuration and User Manual. https://step.esa.int/thirdparties/sen2cor/2.4.0/Sen2Cor_240_Documenation_PDF/S2-PDGS-MPC-L2A-SUM-V2.4.0.pdf, 2018.

Evangeliou, N., Thompson, R. L., Eckhardt, S., and Stohl, A.: Top-down estimates of black carbon emissions at high latitudes
1220 using an atmospheric transport model and a Bayesian inversion framework, Atmos. Chem. Phys., 18, 15307-15327, https://doi.org/10.5194/acp-18-15307-2018, 2018.

Ežerinskis, Ž., Spolaor, A., Kirchgeorg, T., Cozzi, G., Vallelonga, P., Kjær, H. A., Šapolaitė, J., Barbante, C., and Druteikienė, R.: Determination of I-129 in Arctic snow by a novel analytical approach using IC-ICP-SFMS, J. Anal. Atom. Spectrom., 29, 1827-1834, https://doi.org/10.1039/c4ja00179f, 2014.

1225 Fast, J. D., Gustafson, W. I., Easter, R. C., Zaveri, R. A., Barnard, J. C., Chapman, E. G., Grell, G. A., and Peckham, S. E.: Evolution of ozone, particulates, and aerosol direct radiative forcing in the vicinity of Houston using a fully coupled meteorology-chemistry-aerosol model, J. Geophys. Res.-Atmos., 111, https://doi.org/10.1029/2005jd006721, 2006.

Fisher, J. A., Jacob, D. J., Soerensen, A. L., Amos, H. M., Steffen, A., and Sunderland, E. M.: Riverine source of Arctic Ocean mercury inferred from atmospheric observations, Nat. Geosci., 5, 499-504, https://doi.org/10.1038/ngeo1478, 2012.

1230 Freud, E., Krejci, R., Tunved, P., Leaitch, R., Nguyen, Q. T., Massling, A., Skov, H., and Barrie, L.: Pan-Arctic aerosol number size distributions: seasonality and transport patterns, Atmos. Chem. Phys., 17, 8101-8128, https://doi.org/10.5194/acp-17-8101-2017, 2017.

Giglio, L., Descloitres, J., Justice, C. O., and Kaufman, Y. J.: An enhanced contextual fire detection algorithm for MODIS, Remote Sens. Environ., 87, 273-282, https://doi.org/10.1016/S0034-4257(03)00184-6, 2003.

1235 Grell, G. A., Peckham, S. E., Schmitz, R., McKeen, S. A., Frost, G., Skamarock, W. C., and Eder, B.: Fully coupled "online" chemistry within the WRF model, Atmos. Environ., 39, 6957-6975, https://doi.org/10.1016/j.atmosenv.2005.04.027, 2005.

Guanter, L., Kaufmann, H., Segl, K., Foerster, S., Rogass, C., Chabrillat, S., Kuester, T., Hollstein, A., Rossner, G., Chlebek, C., Straif, C., Fischer, S., Schrader, S., Storch, T., Heiden, U., Mueller, A., Bachmann, M., Mühle, H., Müller, R., Habermeyer,
1240 M., Ohndorf, A., Hill, J., Buddenbaum, H., Hostert, P., van der Linden, S., Leitão, P. J., Rabe, A., Doerffer, R., Krasemann, H., Xi, H. Y., Mauser, W., Hank, T., Locherer, M., Rast, M., Staenz, K., and Sang, B.: The EnMAP Spaceborne Imaging Spectroscopy Mission for Earth Observation, Remote Sens., 7, 8830-8857, https://doi.org/10.3390/rs70708830, 2015.

Gvakharia, A., Kort, E. A., Brandt, A., Peischl, J., Ryerson, T. B., Schwarz, J. P., Smith, M. L., and Sweeney, C.: Methane, Black Carbon, and Ethane Emissions from Natural Gas Flares in the Bakken Shale, North Dakota, Environ. Sci. Technol., 51, 5317-5325, https://doi.org/10.1021/acs.est.6b05183, 2017.

1245 Hall, D. K., and Riggs, G. A.: MODIS/Terra Snow Cover Daily L3 Global 500m SIN Grid, Version 6. Boulder, Colorado USA. NASA National Snow and Ice Data Center Distributed Active Archive Center. https://doi.org/10.5067/MODIS/MOD10A1.006. [accessed 19.12.2019], 2016.

Hari, P., Aalto, P., Hämeri, K., Kulmala, M., Lahti, T., Luoma, S., Palva, L., Pohja, T., Pulliainen, E., Siivola, E., and Vesala, T.: Air pollution in eastern Lapland: challenge for an environmental measurement station, Silva Fenn., 28,
1250 https://doi.org/10.14214/sf.a9160, 1994.

Hari, P., Petäjä, T., Back, J., Kerminen, V. M., Lappalainen, H. K., Vihma, T., Laurila, T., Viisanen, Y., Vesala, T., and Kulmala, M.: Conceptual design of a measurement network of the global change, Atmos. Chem. Phys., 16, 1017-1028, https://doi.org/10.5194/acp-16-1017-2016, 2016.

Helm, V., Humbert, A., and Miller, H.: Elevation and elevation change of Greenland and Antarctica derived from CryoSat-2, Cryosphere, 8, 1539-1559, https://doi.org/10.5194/tc-8-1539-2014, 2014.

Herbert, B. M. J., Halsall, C. J., Villa, S., Jones, K. C., and Kallenborn, R.: Rapid changes in PCB and OC pesticide concentrations in Arctic snow, Environ. Sci. Technol., 39, 2998-3005, https://doi.org/10.1021/es040076l, 2005.

Hermanson, M. H., Isaksson, E., Forsström, S., Texeira, C., Muir, D. C. G., Pohjola, V. A., and van de Wal, R. S. V.: Deposition history of brominated flame retardant compounds in an ice core from Holtedahlfonna, Svalbard, Norway, Environ. Sci. Technol., 44, 7405-7410, https://doi.org/10.1021/es1016608, 2010.

Höglund-Isaksson, L.: Global anthropogenic methane emissions 2005-2030: technical mitigation potentials and costs, Atmos. Chem. Phys., 12, 9079-9096, https://doi.org/10.5194/acp-12-9079-2012, 2012.

Huang, K., Fu, J. S., Prikhodko, V. Y., Storey, J. M., Romanov, A., Hodson, E. L., Cresko, J., Morozova, I., Ignatieva, Y., and Cabaniss, J.: Russian anthropogenic black carbon: Emission reconstruction and Arctic black carbon simulation, J. Geophys. Res.-Atmos., 120, 11306-11333, https://doi.org/10.1002/2015jd023358, 2015.

Humbert, A., Neckel, N., Dörr, N., Binder, T., and Beyer, S.: Persistent englacial channels and subglacial water storage in North-East Greenland, Geophys. Res. Lett., in review, 2019.

Hung, H., Kallenborn, R., Breivik, K., Su, Y. S., Brorström-Lundén, E., Olafsdottir, K., Thorlacius, J. M., Leppänen, S., Bossi, R., Skov, H., Manø, S., Patton, G. W., Stern, G., Sverko, E., and Fellin, P.: Atmospheric monitoring of organic pollutants in the Arctic under the Arctic Monitoring and Assessment Programme (AMAP): 1993-2006, Sci.Total Environ., 408, 2854-2873, https://doi.org/10.1016/j.scitotenv.2009.10.044, 2010.

Hung, H., Katsoyiannis, A. A., Brorström-Lundén, E., Olafsdottir, K., Aas, W., Breivik, K., Bohlin-Nizzetto, P., Sigurdsson, A., Hakola, H., Bossi, R., Skov, H., Sverko, E., Barresi, E., Fellin, P., and Wilson, S.: Temporal trends of Persistent Organic Pollutants (POPs) in Arctic air: 20 years of monitoring under the Arctic Monitoring and Assessment Programme (AMAP), Environ. Pollut., 217, 52-61, https://doi.org/10.1016/j.envpol.2016.01.079, 2016.

IDA Science and Technology Policy Institute and Sustaining Arctic Observing Networks. International Arctic Observations Assessment Framework, IDA Science and Technology Policy Institute, Washington, DC, U.S.A., and Sustaining Arctic Observing Networks, Oslo, Norway, 73pp., 2017.

Illingworth, A. J., Barker, H. W., Beljaars, A., Ceccaldi, M., Chepfer, H., Clerbaux, N., Cole, J., Delanoë, J., Domenech, C., Donovan, D. P., Fukuda, S., Hirakata, M., Hogan, R. J., Huenerbein, A., Kollias, P., Kubota, T., Nakajima, T., Nakajima, T. Y., Nishizawa, T., Ohno, Y., Okamoto, H., Oki, R., Sato, K., Satoh, M., Shephard, M. W., Velázquez-Blázquez, A., Wandinger, U., Wehr, T., and van Zadelhoff, G.-J.: The EarthCARE Satellite the next step forward in global measurements of clouds, aerosols, precipitation, and radiation, Bull. Am. Meteorol. Soc., 96, 1311-1332, https://doi.org/10.1175/Bams-D-12-00227.1, 2015.

IPCC, 2014: Climate Change 2014: Synthesis Report. Contribution of Working Groups I, II and III to the Fifth Assessment Report of the Intergovernmental Panel on Climate Change [Core Writing Team, R.K. Pachauri and L.A. Meyer (eds.)]. 151 pp.

Janssens-Maenhout, G., Crippa, M., Guizzardi, D., Muntean, M., Schaaf, E., Dentener, F., Bergamaschi, P., Pagliari, V., Olivier, J. G. J., Peters, J. A. H. W., van Aardenne, J. A., Monni, S., Doering, U., Petrescu, A. M. R., Solazzo, E., and Oreggioni, G. D.: EDGAR v4.3.2 Global Atlas of the three major greenhouse gas emissions for the period 1970-2012, Earth Syst. Sci. Data, 11, 959-1002, https://doi.org/10.5194/essd-11-959-2019, 2019.

Jiao, C., Flanner, M. G., Balkanski, Y., Bauer, S. E., Bellouin, N., Berntsen, T. K., Bian, H., Carslaw, K. S., Chin, M., De Luca, N., Diehl, T., Ghan, S. J., Iversen, T., Kirkevåg, A., Koch, D., Liu, X., Mann, G. W., Penner, J. E., Pitari, G., Schulz,

M., Seland, Ø., Skeie, R. B., Steenrod, S. D., Stier, P., Takemura, T., Tsigaridis, K., van Noije, T., Yun, Y., and Zhang, K.:

1295 An AeroCom assessment of black carbon in Arctic snow and sea ice, Atmos. Chem. Phys., 14, 2399-2417, https://doi.org/10.5194/acp-14-2399-2014, 2014.

Jiskra, M., Sonke, J. E., Obrist, D., Bieser, J., Ebinghaus, R., Myhre, C. L., Pfaffhuber, K. A., Wängberg, I., Kyllönen, K., Worthy, D., Martin, L. G., Labuschagne, C., Mkololo, T., Ramonet, M., Magand, O., and Dommergue, A.: A vegetation control on seasonal variations in global atmospheric mercury concentrations, Nat. Geosci., 11, 244-+,

1300 https://doi.org/10.1038/s41561-018-0078-8, 2018.

Junninen, H., Lauri, A., Keronen, P., Aalto, P., Hiltunen, V., Hari, P., and Kulmala, M.: Smart-SMEAR: on-line data exploration and visualization tool for SMEAR stations, Boreal Environ. Res., 14, 447-457, 2009.

Kirpes, R. M., Bondy, A. L., Bonanno, D., Moffet, R. C., Wang, B. B., Laskin, A., Ault, A. P., and Pratt, K. A.: Secondary sulfate is internally mixed with sea spray aerosol and organic aerosol in the winter Arctic, Atmos. Chem. Phys., 18, 3937-

1305 3949, https://doi.org/10.5194/acp-18-3937-2018, 2018.

Klimont, Z., Kupiainen, K., Heyes, C., Purohit, P., Cofala, J., Rafaj, P., Borken-Kleefeld, J., and Schöpp, W.: Global anthropogenic emissions of particulate matter including black carbon, Atmos. Chem. Phys., 17, 8681-8723, https://doi.org/10.5194/acp-17-8681-2017, 2017.

Klonecki, A., Hess, P., Emmons, L., Smith, L., Orlando, J., and Blake, D.: Seasonal changes in the transport of pollutants into

1310 the Arctic troposphere-model study, J. Geophys. Res.-Atmos., 108, https://doi.org/10.1029/2002jd002199, 2003.

Kokelj, S. V., Lantz, T. C., Tunnicliffe, J., Segal, R., and Lacelle, D.: Climate-driven thaw of permafrost preserved glacial landscapes, northwestern Canada, Geology, 45, 371-374, https://doi.org/10.1130/G38626.1, 2017.

Kontkanen, J., Paasonen, P., Aalto, J., Bäck, J., Rantala, P., Petäjä, T., and Kulmala, M.: Simple proxies for estimating the concentrations of monoterpenes and their oxidation products at a boreal forest site, Atmos. Chem. Phys., 16, 13291-13307,

1315 https://doi.org/10.5194/acp-16-13291-2016, 2016.

Kramshøj, M., Albers, C. N., Holst, T., Holzinger, R., Elberling, B., and Rinnan, R.: Biogenic volatile release from permafrost thaw is determined by the soil microbial sink, Nat. Commun., 9, https://doi.org/10.1038/s41467-018-05824-y, 2018.

Kulmala, M., Dal Maso, M., Mäkelä, J. M., Pirjola, L., Väkevä, M., Aalto, P., Miikkulainen, P., Hämeri, K., and O'Dowd, C. D.: On the formation, growth and composition of nucleation mode particles, Tellus B, 53, 479-490,

1320 https://doi.org/10.1034/j.1600-0889.2001.530411.x, 2001.

Kulmala, M., Asmi, A., Lappalainen, H. K., Baltensperger, U., Brenguier, J. L., Facchini, M. C., Hansson, H. C., Hov, Ø., O'Dowd, C. D., Pöschl, U., Wiedensohler, A., Boers, R., Boucher, O., de Leeuw, G., van der Gon, H. A. C. D., Feichter, J., Krejci, R., Laj, P., Lihavainen, H., Lohmann, U., McFiggans, G., Mentel, T., Pilinis, C., Riipinen, I., Schulz, M., Stohl, A., Swietlicki, E., Vignati, E., Alves, C., Amann, M., Ammann, M., Arabas, S., Artaxo, P., Baars, H., Beddows, D. C. S.,

1325 Bergström, R., Beukes, J. P., Bilde, M., Burkhart, J. F., Canonaco, F., Clegg, S. L., Coe, H., Crumeyrolle, S., D'Anna, B., Decesari, S., Gilardoni, S., Fischer, M., Fjaeraa, A. M., Fountoukis, C., George, C., Gomes, L., Halloran, P., Hamburger, T., Harrison, R. M., Herrmann, H., Hoffmann, T., Hoose, C., Hu, M., Hyvärinen, A., Hõrrak, U., Iinuma, Y., Iversen, T., Josipovic, M., Kanakidou, M., Kiendler-Scharr, A., Kirkevåg, A., Kiss, G., Klimont, Z., Kolmonen, P., Komppula, M., Kristjánsson, J. E., Laakso, L., Laaksonen, A., Labonnote, L., Lanz, V. A., Lehtinen, K. E. J., Rizzo, L. V., Makkonen, R., Manninen, H. E.,

1330 McMeeking, G., Merikanto, J., Minikin, A., Mirme, S., Morgan, W. T., Nemitz, E., O'Donnell, D., Panwar, T. S., Pawlowska, H., Petzold, A., Pienaar, J. J., Pio, C., Plass-Duelmer, C., Prévôt, A. S. H., Pryor, S., Reddington, C. L., Roberts, G., Rosenfeld, D., Schwarz, J., Seland, Ø., Sellegri, K., Shen, X. J., Shiraiwa, M., Siebert, H., Sierau, B., Simpson, D., Sun, J. Y., Topping, D., Tunved, P., Vaattovaara, P., Vakkari, V., Veefkind, J. P., Visschedijk, A., Vuollekoski, H., Vuolo, R., Wehner, B., Wildt, J., Woodward, S., Worsnop, D. R., van Zadelhoff, G. J., Zardini, A. A., Zhang, K., van Zyl, P. G., Kerminen, V. M., Carslaw,

1335 K. S., and Pandis, S. N.: General overview: European Integrated project on Aerosol Cloud Climate and Air Quality interactions

(EUCAARI) - integrating aerosol research from nano to global scales, Atmos. Chem. Phys., 11, 13061-13143, https://doi.org/10.5194/acp-11-13061-2011, 2011a.

Kulmala, M., Arola, A., Nieminen, T., Riuttanen, L., Sogacheva, L., de Leeuw, G., Kerminen, V.-M., and Lehtinen, K.E.J. The first estimates of global nucleation mode aerosol concentrations based on satellite measurements, Atmos. Chem. Phys., 1340   11, 10791–10801, doi:10.5194/acp-11-10791-2011, 2011b.

Kulmala, M., Lappalainen, H. K., Petäjä, T., Kurten, T., Kerminen, V. M., Viisanen, Y., Hari, P., Sorvari, S., Bäck, J., Bondur, V., Kasimov, N., Kotlyakov, V., Matvienko, G., Baklanov, A., Guo, H. D., Ding, A., Hansson, H. C., and Zilitinkevich, S.: Introduction: The Pan-Eurasian Experiment (PEEX) - multidisciplinary, multiscale and multicomponent research and capacity-building initiative, Atmos. Chem. Phys., 15, 13085-13096, https://doi.org/10.5194/acp-15-13085-2015, 2015.

1345   Kulmala, M.: Build a global Earth observatory, Nature, 553, 21-22, https://doi.org/10.1038/d41586-017-08967-y, 2018.

Lange, R., Dall'Osto, M., Skov, H., Nøjgaard, J. K., Nielsen, I. E., Beddowse, D. C. S., Simob, R., Harrison, R. M., and Massling, A.: Characterization of distinct Arctic aerosol accumulation modes and their sources, Atmos. Environ., 183, 1-10, https://doi.org/10.1016/j.atmosenv.2018.03.060, 2018.

Lampert, A., Altstädter, B., Bärfuss, K., Bretschneider, L., Sandgaard, J., Michaelis, J., Lobitz, L., Asmussen, M., Damm, E., 1350   Käthner, R., Krüger, T., Lüpkes, C., Nowak, S., Peuker, A., Rausch, T., Reiser, F., Scholtz, A., Sotomayor Zakharov, D.; Gaus, D., Bansmer, S., Wehner, B., and Pätzold, F.: Unmanned aerial systems for investigating the Polar atmospheric boundary layer - technical challenges and examples of applications, Atmosphere, 11, 1-25, https://doi.org/10.3390/atmos11040416, 2020.

Lappalainen, H. K., Kerminen, V. M., Petäjä, T., Kurten, T., Baklanov, A., Shvidenko, A., Bäck, J., Vihma, T., Alekseychik, 1355   P., Andreae, M. O., Arnold, S. R., Arshinov, M., Asmi, E., Belan, B., Bobylev, L., Chalov, S., Cheng, Y. F., Chubarova, N., de Leeuw, G., Ding, A. J., Dobrolyubov, S., Dubtsov, S., Dyukarev, E., Elansky, N., Eleftheriadis, K., Esau, I., Filatov, N., Flint, M., Fu, C. B., Glezer, O., Gliko, A., Heimann, M., Holtslag, A. A. M., Hõrrak, U., Janhunen, J., Juhola, S., Järvi, L., Järvinen, H., Kanukhina, A., Konstantinov, P., Kotlyakov, V., Kieloaho, A. J., Komarov, A. S., Kujansuu, J., Kukkonen, I., Duplissy, E. M., Laaksonen, A., Laurila, T., Lihavainen, H., Lisitzin, A., Mahura, A., Makshtas, A., Mareev, E., Mazon, S., 1360   Matishov, D., Melnikov, V., Mikhailov, E., Moisseev, D., Nigmatulin, R., Noe, S. M., Ojala, A., Pihlatie, M., Popovicheva, O., Pumpanen, J., Regerand, T., Repina, I., Shcherbinin, A., Shevchenko, V., Sipilä, M., Skorokhod, A., Spracklen, D. V., Su, H., Subetto, D. A., Sun, J. Y., Terzhevik, A. Y., Timofeyev, Y., Troitskaya, Y., Tynkkynen, V. P., Kharuk, V. I., Zaytseva, N., Zhang, J. H., Viisanen, Y., Vesala, T., Hari, P., Hansson, H. C., Matvienko, G. G., Kasimov, N. S., Guo, H. D., Bondur, V., Zilitinkevich, S., and Kulmala, M.: Pan-Eurasian Experiment (PEEX): towards a holistic understanding of the feedbacks 1365   and interactions in the land-atmosphere-ocean-society continuum in the northern Eurasian region, Atmos. Chem. Phys., 16, 14421-14461, https://doi.org/10.5194/acp-16-14421-2016, 2016.

Lappalainen, H. K., Altimir, N., Kerminen, V., Petäjä, T., Makkonen, R., Alekseychik, P., Zaitseva, N., Bashmakova, I., Kujansuu, J., Lauri, A., Haapanala, P., Mazon, S. B., Borisova, A., Konstantinov, P., Chalov, S., Laurila, T., Asmi, E., Lihavainen, H., Bäck, J., Arshinov, M., Mahura, A., Arnold, S., Vihma, T., Uotila, P., de Leeuw, G., Kukkonen, I., 1370   Malkhazova, S., Tynkkynen, V., Fedorova, I., Hansson, H. C., Dobrolyubov, S., Melnikov, V., Matvienko, G., Baklanov, A., Viisanen, Y., Kasimov, N., Guo, H., Bondur, V., Zilitinkevich, S., and Kulmala, M.: Pan-eurasian experiment (peex) program: An overview of the first 5 years in operation and future prospects, Geography, Environment and Sustainability, 11, 6-19, https://doi.org/10.24057/2071-9388-2018-11-1-6-19, 2018.

Law, K. S., and Stohl, A.: Arctic air pollution: Origins and impacts, Science, 315, 1537-1540, 1375   https://doi.org/10.1126/science.1137695, 2007.

Law, K. S., Stohl, A., Quinn, P. K., Brock, C. A., Burkhart, J. F., Paris, J. D., Ancellet, G., Singh, H. B., Roiger, A., Schlager, H., Dibb, J., Jacob, D. J., Arnold, S. R., Pelon, J., and Thomas, J. L.: Arctic Air Pollution: New Insights from POLARCAT-IPY, B. Am. Meteorol. Soc., 95, 1873-+, https://doi.org/10.1175/Bams-D-13-00017.1, 2014.

Leino, K., Lampilahti, J., Poutanen, P., Väänänen, R., Manninen, A., Mazon, S. B., Dada, L., Franck, A., Wimmer, D., Aalto,
1380   P. P., Ahonen, L. R., Enroth, J., Kangasluoma, J., Keronen, P., Korhonen, F., Laakso, H., Matilainen, T., Siivola, E., Manninen, H. E., Lehtipalo, K., Kerminen, V. M., Petäjä, T., and Kulmala, M.: Vertical profiles of sub-3nm particles over the boreal forest, Atmos. Chem. Phys., 19, 4127-4138, https://doi.org/10.5194/acp-19-4127-2019, 2019.

Li, H. R., Moisseev, D., and von Lerber, A.: How does riming affect dual-polarization radar observations and snowflake shape?, J. Geophys. Res.-Atmos., 123, 6070-6081, https://doi.org/10.1029/2017jd028186, 2018.

1385   Li, H. R., and Moisseev, D.: Melting layer attenuation at Ka- and W-Bands as derived from multifrequency radar doppler spectra observations, J. Geophys. Res.-Atmos., 124, 9520-9533, https://doi.org/10.1029/2019jd030316, 2019.

Li, J., Xie, Z. Y., Mi, W. Y., Lai, S. C., Tian, C. G., Emeis, K. C., and Ebinghaus, R.: Organophosphate Esters in Air, Snow, and Seawater in the North Atlantic and the Arctic, Environ. Sci.Technol., 51, 6887-6896, https://doi.org/10.1021/acs.est.7b01289, 2017.

1390   Lim, A. G., Sonke, J. E., Krickov, I. V., Manasypov, R. M., Loiko, S. V., and Pokrovsky, O. S.: Enhanced particulate Hg export at the permafrost boundary, western Siberia, Environ. Pollut., 254, https://doi.org/10.1016/j.envpol.2019.113083, 2019.

Liu, N. F., Budkewitsch, P., and Treitz, P.: Examining spectral reflectance features related to Arctic percent vegetation cover: Implications for hyperspectral remote sensing of Arctic tundra, Remote Sens. Environ., 192, 58-72, https://doi.org/10.1016/j.rse.2017.02.002, 2017.

1395   Loizzo, R., Guarini, R., Longo, F., Scopa, T., Formaro, R., Facchinetti, C., and Varacalli, G.: Prisma: the Italian hyperspectral mission, Int Geosci Remote Se, 2018, 175-178,

Ma, J. M., Hung, H. L., Tian, C., and Kallenborn, R.: Revolatilization of persistent organic pollutants in the Arctic induced by climate change, Nat. Clim. Change, 1, 255-260, https://doi.org/10.1038/Nclimate1167, 2011.

Main-Knorn, M., Pflug, B., Louis, J., Debaecker, V., Muller-Wilm, U., and Gascon, F.: Sen2Cor for Sentinel-2, Image and
1400   Signal Processing for Remote Sensing Xxiii, 10427, https://doi.org/10.1117/12.2278218, 2017.

Marelle, L., Raut, J. C., Law, K. S., Berg, L. K., Fast, J. D., Easter, R. C., Shrivastava, M., and Thomas, J. L.: Improvements to the WRF-Chem 3.5.1 model for quasi-hemispheric simulations of aerosols and ozone in the Arctic, Geosci. Model Dev., 10, 3661-3677, https://doi.org/10.5194/gmd-10-3661-2017, 2017.

Marelle, L., Raut, J. C., Law, K. S., and Duclaux, O.: Current and future Arctic aerosols and ozone from remote emissions and
1405   emerging local sources-modeled source contributions and radiative effects, J. Geophys. Res.-Atmos., 123, 12942-12963, https://doi.org/10.1029/2018jd028863, 2018.

Mason, S. L., Chiu, C. J., Hogan, R. J., Moisseev, D., and Kneifel, S.: Retrievals of riming and snow density from vertically pointing doppler radars, J. Geophys. Res.-Atmos., 123, 13807-13834, https://doi.org/10.1029/2018jd028603, 2018.

Mason, S. L., Hogan, R. J., Westbrook, C. D., Kneifel, S., Moisseev, D., and von Terzi, L.: The importance of particle size
1410   distribution and internal structure for triple-frequency radar retrievals of the morphology of snow, Atmos. Meas. Tech., 12, 4993-5018, https://doi.org/10.5194/amt-12-4993-2019, 2019.

McConnell, J. R., and Edwards, R.: Coal burning leaves toxic heavy metal legacy in the Arctic, P. Natl. Acad. Sci. USA, 105, 12140-12144, https://doi.org/10.1073/pnas.0803564105, 2008.

Meier, W. N., Hovelsrud, G. K., van Oort, B. E. H., Key, J. R., Kovacs, K. M., Michel, C., Haas, C., Granskog, M. A., Gerland,
1415   S., Perovich, D. K., Makshtas, A., and Reist, J. D.: Arctic sea ice in transformation: A review of recent observed changes and impacts on biology and human activity, Rev. Geophys., 52, 185-217, https://doi.org/10.1002/2013rg000431, 2014.

Metsämäki, S., Mattila, O. P., Pulliainen, J., Niemi, K., Luojus, K., and Böttcher, K.: An optical reflectance model-based method for fractional snow cover mapping applicable to continental scale, Remote Sens. Environ., 123, 508-521, https://doi.org/10.1016/j.rse.2012.04.010, 2012.

1420 Metsämäki, S., Pulliainen, J., Salminen, M., Luojus, K., Wiesmann, A., Solberg, R., Böttcher, K., Hiltunen, M., and Ripper, E.: Introduction to GlobSnow Snow Extent products with considerations for accuracy assessment, Remote Sens. Environ., 156, 96-108, https://doi.org/10.1016/j.rse.2014.09.018, 2015.

Mikkonen, S., Romakkaniemi, S., Smith, J. N., Korhonen, H., Petäjä, T., Plass-Duelmer, C., Boy, M., McMurry, P. H., Lehtinen, K. E. J., Joutsensaari, J., Hamed, A., Mauldin, R. L., Birmili, W., Spindler, G., Arnold, F., Kulmala, M., and
1425 Laaksonen, A.: A statistical proxy for sulphuric acid concentration, Atmos. Chem. Phys., 11, 11319-11334, https://doi.org/10.5194/acp-11-11319-2011, 2011.

Moisseev, D., von Lerber, A., and Tiira, J.: Quantifying the effect of riming on snowfall using ground-based observations, J. Geophys. Res.-Atmos., 122, 4019-4037, https://doi.org/10.1002/2016jd026272, 2017.

Moschos, V., Kumar, N. K., Daellenbach, K. R., Baltensperger, U., Prévôt, A. S. H., and El Haddad, I.: Source apportionment
1430 of brown carbon absorption by coupling ultraviolet-visible spectroscopy with aerosol mass spectrometry, Environ. Sci. Tech. Lett., 5, 302-+, https://doi.org/10.1021/acs.estlett.8b00118, 2018.

Mungall, E. L., Abbatt, J. P. D., Wentzell, J. J. B., Lee, A. K. Y., Thomas, J. L., Blais, M., Gosselin, M., Miller, L. A., Papakyriakou, T., Willis, M. D., and Liggio, J.: Microlayer source of oxygenated volatile organic compounds in the summertime marine Arctic boundary layer, P. Natl. Acad. Sci. USA, 114, 6203-6208,
1435 https://doi.org/10.1073/pnas.1620571114, 2017.

Myhre, G., Shindell, D., Bréon, F.-M., Collins, W., Fuglestvedt, J., Huang, J., Koch, D., Lamarque, J.-F., Lee, D., Mendoza, B., Nakajima, T., Robock, A., Stephens, G., Takemura, T., and Zhang, H.: Anthropogenic and Natural Radiative Forcing. In: Climate Change 2013: The Physical Science Basis. Contribution of Working Group I to the Fifth Assessment Report of the Intergovernmental Panel on Climate Change [Stocker, T.F., D. Qin, G.-K. Plattner, M. Tignor, S.K. Allen, J. Boschung, A.
1440 Nauels, Y. Xia, V. Bex and P.M. Midgley (eds.)] Cambridge University Press, Cambridge, United Kingdom and New York, NY, USA., 2013.

Neckel, N., Zeising, O., Steinhage, D., Helm, V., and Humbert, A.: Seasonal observations at 79° N Glacier (Greenland) from remote sensing and in situ measurements, Front. Earth Sci., in review, 2019.

Nguyen, H. T., Kim, K. H., Shon, Z. H., and Hong, S.: A Review of Atmospheric Mercury in the Polar Environment, Crit.
1445 Rev. Env. Sci. Tec., 39, 552-584, https://doi.org/10.1080/10643380701764308, 2009.

Nguyen, Q. T., Glasius, M., Sørensen, L. L., Jensen, B., Skov, H., Birmili, W., Wiedensohler, A., Kristensson, A., Nøjgaard, J. K., and Massling, A.: Seasonal variation of atmospheric particle number concentrations, new particle formation and atmospheric oxidation capacity at the high Arctic site Villum Research Station, Station Nord, Atmos. Chem. Phys., 16, 11319-11336, https://doi.org/10.5194/acp-16-11319-2016, 2016.

1450 Nikandrova, A., Tabakova, K., Manninen, A., Väänänen, R., Petäjä, T., Kulmala, M., Kerminen, V. M., and O'Connor, E.: Combining airborne in situ and ground-based lidar measurements for attribution of aerosol layers, Atmos. Chem. Phys., 18, 10575-10591, https://doi.org/10.5194/acp-18-10575-2018, 2018.

Obrist, D., Agnan, Y., Jiskra, M., Olson, C. L., Colegrove, D. P., Hueber, J., Moore, C. W., Sonke, J. E., and Helmig, D.: Tundra uptake of atmospheric elemental mercury drives Arctic mercury pollution, Nature, 547, 201-+,
1455 https://doi.org/10.1038/nature22997, 2017.

Paasonen, P., Asmi, A., Petäjä, T., Kajos, M. K., Äijälä, M., Junninen, H., Holst, T., Abbatt, J. P. D., Arneth, A., Birmili, W., van der Gon, H. D., Hamed, A., Hoffer, A., Laakso, L., Laaksonen, A., Leaitch, W. R., Plass-Dülmer, C., Pryor, S. C., Räisänen, P., Swietlicki, E., Wiedensohler, A., Worsnop, D. R., Kerminen, V. M., and Kulmala, M.: Warming-induced increase in aerosol number concentration likely to moderate climate change, Nat. Geosci., 6, 438-442,
1460 https://doi.org/10.1038/Ngeo1800, 2013.

Paasonen, P., Kupiainen, K., Klimont, Z., Visschedijk, A., van der Gon, H. A. C. D., and Amann, M.: Continental anthropogenic primary particle number emissions, Atmos. Chem. Phys., 16, 6823-6840, https://doi.org/10.5194/acp-16-6823-2016, 2016.

Painter, T. H., Dozier, J., Roberts, D. A., Davis, R. E., and Green, R. O.: Retrieval of subpixel snow-covered area and grain size from imaging spectrometer data, Remote Sens. Environ., 85, 64-77, https://doi.org/10.1016/S0034-4257(02)00187-6, 2003.

Painter, T. H., Rittger, K., McKenzie, C., Slaughter, P., Davis, R. E., and Dozier, J.: Retrieval of subpixel snow covered area, grain size, and albedo from MODIS, Remote Sens. Environ., 113, 868-879, https://doi.org/10.1016/j.rse.2009.01.001, 2009.

Pankratov, F., Mahura, A., Popov, V., and Katz, O.: Long-term continuous monitoring of mercury in the Russian arctic: winter increase of atmospheric mercury depletion events, EGU General Assembly Conference Abstracts, May 01, 2014, 2014.

Pankratov, F.: Dynamics of Atmospheric Mercury in the Russian Arctic, Ph. D. thesis, Moscow State University, Moscow, https://doi.org/10.13140/RG.2.1.4255.1767, 2015.

Paris, J. D., Ciais, P., Nédélec, P., Stohl, A., Belan, B. D., Arshinov, M. Y., Carouge, C., Golitsyn, G. S., and Granberg, I. G.: New insights on the chemical composition of the Siberian air shed from the Yak-Aerosib aircraft campaigns, Bull. Am. Met. Soc., 91, 625-+, https://doi.org/10.1175/2009bams2663.1, 2010.

Peckham, S. E., Grell, G. A., McKeen, S. A., Barth, M., Pfister, G., Wiedinmyer, C., Fast, J. D., Gustafson, W. I., Zaver, R., Easter, R. C., Barnard, J., Chapman, E., Hewson, M., Schmitz, R., Salzmann, M., and Freitas, S.: WRF/Chem version 3.3 user's guide. NOAA Technical Memo, 98 pp, 2012.

Pedersen, C.: Zeppelin Webcamera Time Series. [Data set]. Norwegian Polar Institute, https://doi.org/10.21334/npolar.2013.9fd6dae0, 2013.

Penuelas, J., Asensio, D., Tholl, D., Wenke, K., Rosenkranz, M., Piechulla, B., and Schnitzler, J. P.: Biogenic volatile emissions from the soil, Plant Cell Environ., 37, 1866-1891, https://doi.org/10.1111/pce.12340, 2014.

Petzold, A., Ogren, J. A., Fiebig, M., Laj, P., Li, S.-M., Baltensperger, U., Holzer-Popp, T., Kinne, S., Pappalardo, G., Sugimoto, N., Wehrli, C., Wiedensohler, A., and Zhang, X.-Y.: Recommendations for reporting "black carbon" measurements, Atmos. Chem. Phys., 13, 8365–8379, https://doi.org/10.5194/acp-13-8365-2013, 2013

Petäjä, T., Mauldin, R. L., Kosciuch, E., McGrath, J., Nieminen, T., Paasonen, P., Boy, M., Adamov, A., Kotiaho, T., and Kulmala, M.: Sulfuric acid and OH concentrations in a boreal forest site, Atmos. Chem. Phys., 9, 7435-7448, https://doi.org/10.5194/acp-9-7435-2009, 2009.

Petäjä, T., de Leeuw, G., Lappalainen, H. K., Moisseev, D., O'Connor, E., Bondur, V., Kasimov, N., Kotlyakov, V., Guo, H. D., Zhang, J. H., Matvienko, G., Kerminen, V. M., Baklanov, A., Zilitinkevich, S., and Kulmala, M.: Connecting ground based in situ observations, ground-based remote sensing and satellite data within the Pan Eurasian Experiment (PEEX) program, Proc. Spie., 9242, https://doi.org/10.1117/12.2068111, 2014.

Petäjä, T., O'Connor, E. J., Moisseev, D., Sinclair, V. A., Manninen, A. J., Väänänen, R., von Lerber, A., Thorntoton, J. A., Nicocoll, K., Petersen, W., Chandrasekar, V., Smith, J. N., Winkler, P. M., Krüger, O., Hakola, H., Timonen, H., Brus, D., Laurila, T., Asmi, E., Riekkola, M. L., Mona, L., Massoli, P., Engelmann, R., Komppula, M., Wang, J., Kuang, C. G., Back, J., Virtanen, A., Levula, J., Ritsche, M., and Hickmon, N.: BAECC: a field campaign to elucidate the impact of biogenic aerosols on clouds and climate, Bull. Am. Met. Soc., 97, 1909-1928, https://doi.org/10.1175/Bams-D-14-00199.1, 2016.

Petäjä, T., Ganzei, K. S., Lappalainen, H. K., Tabakova, K., Makkonen, R., Räisänen, J., Chalov, S., Kulmala, M., Zilitinkevich, S. S., Baklanov, P., Shakirov, R. B., Mishina, N. V., Egidarev, E. G., and Kondrat'ev, I. I.: Research agenda for the Russian Far East and utilization of multi-platform comprehensive environmental observations, J. Digital Earth, submitted, 2020.

Polyakov, I. V., Pnyushkov, A. V., Alkire, M. B., Ashik, I. M., Baumann, T. M., Carmack, E. C., Goszczko, I., Guthrie, J., Ivanov, V. V., Kanzow, T., Krishfield, R., Kwok, R., Sundfjord, A., Morison, J., Rember, R., and Yulin, A.: Greater role for

Atlantic inflows on sea-ice loss in the Eurasian Basin of the Arctic Ocean, Science, 356, 285-+, https://doi.org/10.1126/science.aai8204, 2017.

Popovicheva, O., Diapouli, E., Makshtas, A., Shonija, N., Manousakas, M., Saraga, D., Uttal, T., and Eleftheriadis, K.: East Siberian Arctic background and black carbon polluted aerosols at HMO Tiksi, Sci. Tot. Environ., 655, 924-938, https://doi.org/10.1016/j.scitotenv.2018.11.165, 2019.

Poulter, B., Bousquet, P., Canadell, J. G., Ciais, P., Peregon, A., Saunois, M., Arora, V. K., Beerling, D. J., Brovkin, V., Jones, C. D., Joos, F., Gedney, N., Ito, A., Kleinen, T., Koven, C. D., McDonald, K., Melton, J. R., Peng, C. H., Peng, S. S., Prigent, C., Schroeder, R., Riley, W. J., Saito, M., Spahni, R., Tian, H. Q., Taylor, L., Viovy, N., Wilton, D., Wiltshire, A., Xu, X. Y., Zhang, B. W., Zhang, Z., and Zhu, Q. A.: Global wetland contribution to 2000-2012 atmospheric methane growth rate dynamics, Environ. Res. Lett., 12, https://doi.org/10.1088/1748-9326/aa8391, 2017.

Rast, M., Nieke, J., Ananasso, C., Bach, H., Ben Dor, E., Chabrillat, S., Colombo, R., Feret, J., Giardino, C., Green, R., Guanter, L., Marsh, S., Ong, C., Rum, G., Schaepman, M., Schlerf, M., Skidmore, A., Strobl, P., Gascon, F., Adams, J., Isola, C., and Del Bello, U.: The Copernicus hyperspectral imaging mission for the environment (CHIME). In: Abstract 2019 ESA living planet symposium, Milan, Italy, 13–17 May 2019, 2019.

Rautenberg, A., Schön, M., zum Berge, K., Mauz, M., Manz, P., Platis, A., van Kesteren, B., Suomi, I., Kral, S. T., and Bange, J.: The Multi-Purpose Airborne Sensor Carrier MASC-3 for Wind and Turbulence Measurements in the Atmospheric Boundary Layer, Sensors-Basel, 19, https://doi.org/10.3390/s19102292, 2019.

Riggs, G., Hall, D. K., and Román, M. O.: VIIRS Snow Cover Algorithm Theoretical Basis Document (ATBD). Version 1.0. https://viirsland.gsfc.nasa.gov/PDF/VIIRS_snow_cover_ATBD_2015.pdf, 2015.

Riipinen, I., Pierce, J. R., Yli-Juuti, T., Nieminen, T., Häkkinen, S., Ehn, M., Junninen, H., Lehtipalo, K., Petäjä, T., Slowik, J., Chang, R., Shantz, N. C., Abbatt, J., Leaitch, W. R., Kerminen, V. M., Worsnop, D. R., Pandis, S. N., Donahue, N. M., and Kulmala, M.: Organic condensation: a vital link connecting aerosol formation to cloud condensation nuclei (CCN) concentrations, Atmos. Chem. Phys., 11, 3865-3878, https://doi.org/10.5194/acp-11-3865-2011, 2011.

Rodell, M., and Houser, P. R.: Updating a land surface model with MODIS-derived snow cover, J. Hydrometeorol., 5, 1064-1075, https://doi.org/10.1175/Jhm-395.1, 2004.

Rückamp, M., Falk, U., Frieler, K., Lange, S., and Humbert, A.: The effect of overshooting 1.5 degrees C global warming on the mass loss of the Greenland ice sheet, Earth Syst. Dynam., 9, 1169-1189, https://doi.org/10.5194/esd-9-1169-2018, 2018.

Saiz-Lopez, A., and von Glasow, R.: Reactive halogen chemistry in the troposphere, Chem. Soc. Rev., 41, 6448-6472, https://doi.org/10.1039/c2cs35208g, 2012.

Salomonson, V. V., and Appel, I.: Development of the Aqua MODIS NDSI fractional snow cover algorithm and validation results, Ieee T. Geosci. Remote, 44, 1747-1756, https://doi.org/10.1109/Tgrs.2006.876029, 2006.

Salzano, R., Lanconelli, C., Salvatori, R., Esposito, G., and Vitale, V.: Continuous monitoring of spectral albedo of snowed surfaces in Ny-lesund, Rend Lincei-Sci Fis, 27, 137-146, https://doi.org/10.1007/s12210-016-0513-y, 2016.

Salzano, R., Salvatori, R., Valt, M., Giuliani, G., Chatenoux, B., and Ioppi, L.: Automated Classification of Terrestrial Images: The Contribution to the Remote Sensing of Snow Cover, Geosciences, 9, https://doi.org/10.3390/geosciences9020097, 2019.

Sandven, S., Ludwigsen, C. A., Sagen, H., Hamre, T., and Pirazzini, R.: Assessment of Arctic sea ice and ocean observing systems based on INTAROS survey, American Geophysical Union, Fall Meeting, 2018,

Sauvé, S., and Desrosiers, M.: A review of what is an emerging contaminant, Chem. Cent. J., 8, https://doi.org/10.1186/1752-153x-8-15, 2014.

Schmale, J., Arnold, S. R., Law, K. S., Thorp, T., Anenberg, S., Simpson, W. R., Mao, J., and Pratt, K. A.: Local Arctic air pollution: a neglected but serious problem, Earths Future, 6, 1385-1412, https://doi.org/10.1029/2018ef000952, 2018.

1545   Schmeisser, L., Backman, J., Ogren, J. A., Andrews, E., Asmi, E., Starkweather, S., Uttal, T., Fiebig, M., Sharma, S., Eleftheriadis, K., Vratolis, S., Bergin, M., Tunved, P., and Jefferson, A.: Seasonality of aerosol optical properties in the Arctic, Atmos. Chem. Phys., 18, 11599-11622, https://doi.org/10.5194/acp-18-11599-2018, 2018.

Schobesberger, S., Väänänen, R., Leino, K., Virkkula, A., Backman, J., Pohja, T., Siivola, E., Franchin, A., Mikkilä, J., Paramonov, M., Aalto, P. P., Krejci, R., Petäjä, T., and Kulmala, M.: Airborne measurements over the boreal forest of southern

1550   Finland during new particle formation events in 2009 and 2010, Boreal Environ. Res., 18, 145-163, 2013.

Schroeder, W., Oliva, P., Giglio, L., and Csiszar, I. A.: The New VIIRS 375 m active fire detection data product: Algorithm description and initial assessment, Remote Sens. Environ., 143, 85-96, https://doi.org/10.1016/j.rse.2013.12.008, 2014.

Schroeder, W. H., Anlauf, K. G., Barrie, L. A., Lu, J. Y., Steffen, A., Schneeberger, D. R., and Berg, T.: Arctic springtime depletion of mercury, Nature, 394, 331-332, https://doi.org/10.1038/28530, 1998.

1555   Seki, O., Kawamura, K., Bendle, J. A. P., Izawa, Y., Suzuki, I., Shiraiwa, T., and Fujii, Y.: Carbonaceous aerosol tracers in ice-cores record multi-decadal climate oscillations, Sci. Rep.-UK, 5, https://doi.org/10.1038/srep14450, 2015.

Sertel, E., Robock, A., and Ormeci, C.: Impacts of land cover data quality on regional climate simulations, Int. J. Climatol., 30, 1942-1953, https://doi.org/10.1002/joc.2036, 2010.

Sharma, S., Ishizawa, M., Chan, D., Lavoué, D., Andrews, E., Eleftheriadis, K., and Maksyutov, S.: 16-year simulation of

1560   Arctic black carbon: Transport, source contribution, and sensitivity analysis on deposition, J. Geophys. Res.-Atmos., 118, 943-964, https://doi.org/10.1029/2012jd017774, 2013.

Sharma, S., Barrie, L. A., Magnusson, E., Brattstrom, G., Leaitch, W. R., Steffen, A., and Landsberger, S.: A Factor and Trends Analysis of Multidecadal Lower Tropospheric Observations of Arctic Aerosol Composition, Black Carbon, Ozone, and Mercury at Alert, Canada, J. Geophys. Res.-Atmos., 124, 14133-14161, https://doi.org/10.1029/2019jd030844, 2019.

1565   Shaw, P. M., Russell, L. M., Jefferson, A., and Quinn, P. K.: Arctic organic aerosol measurements show particles from mixed combustion in spring haze and from frost flowers in winter, Geophys. Res. Lett., 37, https://doi.org/10.1029/2010gl042831, 2010.

Shipley, S. T., Tracy, D. H., Eloranta, E. W., Trauger, J. T., Sroga, J. T., Roesler, F. L., and Weinman, J. A.: high spectral resolution lidar to measure optical-scattering properties of atmospheric aerosols .1. Theory and instrumentation, Appl. Optics,

1570   22, 3716-3724, https://doi.org/10.1364/Ao.22.003716, 1983.

Shoeib, M., Harner, T., and Vlahos, P.: Perfluorinated chemicals in the Arctic atmosphere, Environ. Sci. Technol., 40, 7577-7583, https://doi.org/10.1021/es0618999, 2006.

Shupe, M., de Boer, G., Dethloff, K., Hunke, E., Maslowski, W., McComiskey, A., Perrson, O., Randall, D., Tjernstrom, M., Turner, D., and Verlinde, J.: The Multidisciplinary Drifting Observatory for the Study of Arctic Climate (MOSAIC)

1575   Atmosphere Science Plan, ARM Climate Research Facility, Pacific Northwest National Laboratory, Richland, WA; DOE Office of Science Atmospheric Radiation Measurement (ARM) Program (United States), Medium: ED pp., 2018.

Simpson, W. R., von Glasow, R., Riedel, K., Anderson, P., Ariya, P., Bottenheim, J., Burrows, J., Carpenter, L. J., Friess, U., Goodsite, M. E., Heard, D., Hutterli, M., Jacobi, H. W., Kaleschke, L., Neff, B., Plane, J., Platt, U., Richter, A., Roscoe, H., Sander, R., Shepson, P., Sodeau, J., Steffen, A., Wagner, T., and Wolff, E.: Halogens and their role in polar boundary-layer

1580   ozone depletion, Atmos. Chem. Phys., 7, 4375-4418, https://doi.org/10.5194/acp-7-4375-2007, 2007.

Simpson, W. R., Brown, S. S., Saiz-Lopez, A., Thornton, J. A., and von Glasow, R.: Tropospheric Halogen Chemistry: Sources, Cycling, and Impacts, Chem. Rev., 115, 4035-4062, https://doi.org/10.1021/cr5006638, 2015.

Sipilä, M., Sarnela, N., Jokinen, T., Henschel, H., Junninen, H., Kontkanen, J., Richters, S., Kangasluoma, J., Franchin, A., Peräkylä, O., Rissanen, M. P., Ehn, M., Vehkämäki, H., Kurten, T., Berndt, T., Petäjä, T., Worsnop, D., Ceburnis, D.,

1585   Kerminen, V. M., Kulmala, M., and O'Dowd, C.: Molecular-scale evidence of aerosol particle formation via sequential addition of HIO3, Nature, 537, 532-534, https://doi.org/10.1038/nature19314, 2016.

Skofronick-Jackson, G., Kirschbaum, D., Petersen, W., Huffman, G., Kidd, C., Stocker, E., and Kakar, R.: The Global Precipitation Measurement (GPM) mission's scientific achievements and societal contributions: reviewing four years of advanced rain and snow observations, Q. J. Roy. Meteor. Soc., 144, 27-48, https://doi.org/10.1002/qj.3313, 2018.

1590   Skov, H., Christensen, J. H., Goodsite, M. E., Heidam, N. Z., Jensen, B., Wåhlin, P., and Geernaert, G.: Fate of elemental mercury in the arctic during atmospheric mercury depletion episodes and the load of atmospheric mercury to the arctic, Environ. Sci. Technol., 38, 2373-2382, https://doi.org/10.1021/es030080h, 2004.

Solberg, R., Koren, H., and Amlien, J.: A review of optical snow cover algorithms. Norwegian Computing Center Note. Available online: https://www.nr.no/directdownload/4400/Solberg_-_A_review_of_optical_snow_algorithms.pdf (accessed 1595   on 19 December 2019). 2006.

Sonke, J. E., Teisserenc, R., Heimbürger-Boavida, L. E., Petrova, M. V., Maruszczak, N., Le Dantec, T., Chupakov, A. V., Li, C. X., Thackray, C. P., Sunderland, E. M., Tananaev, N., and Pokrovsky, O. S.: Eurasian river spring flood observations support net Arctic Ocean mercury export to the atmosphere and Atlantic Ocean, P. Natl. Acad. Sci. USA, 115, E11586-E11594, https://doi.org/10.1073/pnas.1811957115, 2018.

1600   Spolaor, A., Barbaro, E., Christille, J. M., Kirchgeorg, T., Giardi, F., Cappelletti, D., Turetta, C., Bernagozzi, A., Björkman, M. P., Bertolini, E., and Barbante, C.: Evolution of the Svalbard annual snow layer during the melting phase, Rend. Lincei-Sci. Fis., 27, 147-154, https://doi.org/10.1007/s12210-015-0500-8, 2016.

Spolaor, A., Angot, H., Roman, M., Dommergue, A., Scarchilli, C., Vardè, M., Del Guasta, M., Pedeli, X., Varin, C., Sprovieri, F., Magand, O., Legrand, M., Barbante, C., and Cairns, W. R. L.: Feedback mechanisms between snow and atmospheric 1605   mercury: Results and observations from field campaigns on the Antarctic plateau, Chemosphere, 197, 306-317, https://doi.org/10.1016/j.chemosphere.2017.12.180, 2018.

Spolaor, A., Barbaro, E., Cappelletti, D., Turetta, C., Mazzola, M., Giardi, F., Björkman, M. P., Lucchetta, F., Dallo, F., Pfaffhuber, K. A., Angot, H., Dommergue, A., Maturilli, M., Saiz-Lopez, A., Barbante, C., and Cairns, W. R. L.: Diurnal cycle of iodine, bromine, and mercury concentrations in Svalbard surface snow, Atmos. Chem. Phys., 19, 13325-13339, 1610   https://doi.org/10.5194/acp-19-13325-2019, 2019.

Stein, A. F., Draxler, R. R., Rolph, G. D., Stunder, B. J. B., Cohen, M. D., and Ngan, F.: Noaa's Hysplit Atmospheric Transport and Dispersion Modeling System, Bull. Am. Met. Soc., 96, 2059-2077, https://doi.org/10.1175/Bams-D-14-00110.1, 2015.

Stemmler, I., and Lammel, G.: Pathways of PFOA to the Arctic: variabilities and contributions of oceanic currents and atmospheric transport and chemistry sources, Atmos. Chem. Phys., 10, 9965-9980, https://doi.org/10.5194/acp-10-9965-2010, 1615   2010.

Stohl, A., Forster, C., Frank, A., Seibert, P., and Wotawa, G.: Technical note: The Lagrangian particle dispersion model FLEXPART version 6.2, Atmos. Chem. Phys., 5, 2461-2474, https://doi.org/10.5194/acp-5-2461-2005, 2005.

Strahlendorff, M., Veijola, K., Gallo, J., Vitale, V., Savela, H., Smirnov, A., Tanaka, H., Sueyoshi, T., Nitu, R., and Larsen, J. R.: Value tree for physical atmosphere and ocean observations in the Arctic. Finnish Meteorological Institute. Reports 2019:3. 1620   28 pp. https://helda.helsinki.fi/handle/10138/300768, 2019.

Tedesco, M., and Kokhanovsky, A. A.: The semi-analytical snow retrieval algorithm and its application to MODIS data, Remote Sens. Environ., 111, 228-241, https://doi.org/10.1016/j.rse.2007.02.036, 2007.

Tomasi, C., Vitale, V., Lupi, A., Di Carmine, C., Campanelli, M., Herber, A., Treffeisen, R., Stone, R. S., Andrews, E., Sharma, S., Radionov, V., von Hoyningen-Huene, W., Stebel, K., Hansen, G. H., Myhre, C. L., Wehrli, C., Aaltonen, V., Lihavainen, 1625   H., Virkkula, A., Hillamo, R., Strom, J., Toledano, C., Cachorro, V. E., Ortiz, P., de Frutos, A. M., Blindheim, S., Frioud, M., Gausa, M., Zielinski, T., Petelski, T., and Yamanouchi, T.: Aerosols in polar regions: A historical overview based on optical depth and in situ observations, J. Geophys. Res.-Atmos., 112, https://doi.org/10.1029/2007jd008432, 2007.

Tomasi, C., Lupi, A., Mazzola, M., Stone, R. S., Dutton, E. G., Herber, A., Radionov, V. F., Holben, B. N., Sorokin, M. G., Sakerin, S. M., Terpugova, S. A., Sobolewski, P. S., Lanconelli, C., Petkov, B. H., Busetto, M., and Vitale, V.: An update on

polar aerosol optical properties using POLAR-AOD and other measurements performed during the International Polar Year, Atmos. Environ., 52, 29-47, https://doi.org/10.1016/j.atmosenv.2012.02.055, 2012.

Tomasi, C., Kokhanovsky, A. A., Lupi, A., Ritter, C., Smirnov, A., O'Neill, N. T., Stone, R. S., Holben, B. N., Nyeki, S., Wehrli, C., Stohl, A., Mazzola, M., Lanconelli, C., Vitale, V., Stebel, K., Aaltonen, V., de Leeuw, G., Rodriguez, E., Herber, A. B., Radionov, V. F., Zielinski, T., Petelski, T., Sakerin, S. M., Kabanov, D. M., Xue, Y., Mei, L. L., Istomina, L., Wagener, R., McArthur, B., Sobolewski, P. S., Kivi, R., Courcoux, Y., Larouche, P., Broccardo, S., and Piketh, S. J.: Aerosol remote sensing in polar regions, Earth-Sci. Rev., 140, 108-157, https://doi.org/10.1016/j.earscirev.2014.11.001, 2015.

Torseth, K. et al.: EU Action on Black Carbon in the Arctic, 2019. Review of observation capacities and data availability for Black Carbon in the Arctic region: EU Action on Black Carbon in the Arctic - Technical Report 1. December 2019. iv + 35pp.

Uttal, T., Starkweather, S., Drummond, J. R., Vihma, T., Makshtas, A. P., Darby, L. S., Burkhart, J. F., Cox, C. J., Schmeisser, L. N., Haiden, T., Maturilli, M., Shupe, M. D., De Boer, G., Saha, A., Grachev, A. A., Crepinsek, S. M., Bruhwiler, L., Goodison, B., McArthur, B., Walden, V. P., Dlugokencky, E. J., Persson, P. O. G., Lesins, G., Laurila, T., Ogren, J. A., Stone, R., Long, C. N., Sharma, S., Massling, A., Turner, D. D., Stanitski, D. M., Asmi, E., Aurela, M., Skov, H., Eleftheriadis, K., Virkkula, A., Platt, A., Førland, E. J., Iijima, Y., Nielsen, I. E., Bergin, M. H., Candlish, L., Zimov, N. S., Zimov, S. A., O'Neill, N. T., Fogal, P. F., Kivi, R., Konopleva-Akish, E. A., Verlinde, J., Kustov, V. Y., Vasel, B., Ivakhov, V. M., Viisanen, Y., and Intrieri, J. M.: International Arctic Systems for Observing the Atmosphere: An International Polar Year Legacy Consortium, B. Am. Meteorol. Soc., 97, 1033-1056, https://doi.org/10.1175/Bams-D-14-00145.1, 2016.

Vermote, E., Justice, C., Claverie, M., and Franch, B.: Preliminary analysis of the performance of the Landsat 8/OLI land surface reflectance product, Remote Sens. Environ., 185, 46-56, https://doi.org/10.1016/j.rse.2016.04.008, 2016.

Vermote, E. F., Tanre, D., Deuze, J. L., Herman, M., and Morcrette, J. J.: Second Simulation of the Satellite Signal in the Solar Spectrum, 6S: An overview, Ieee T. Geosci. Remote, 35, 675-686, https://doi.org/10.1109/36.581987, 1997.

Vihma, T., Uotila, P., Sandven, S., Pozdnyakov, D., Makshtas, A., Pelyasov, A., Pirazzini, R., Danielsen, F., Chalov, S., Lappalainen, H. K., Ivanov, V., Frolov, I., Albin, A., Cheng, B., Dobrolyubov, S., Arkhipkin, V., Myslenkov, S., Petäjä, T., and Kulmala, M.: Towards an advanced observation system for the marine Arctic in the framework of the Pan-Eurasian Experiment (PEEX), Atmos. Chem. Phys., 19, 1941-1970, https://doi.org/10.5194/acp-19-1941-2019, 2019.

von Lerber, A., Moisseev, D., Bliven, L. F., Petersen, W., Harri, A. M., and Chandrasekar, V.: Microphysical Properties of Snow and Their Link to Z(e)-S Relations during BAECC 2014, J. Appl. Meteorol. Clim., 56, 1561-1582, https://doi.org/10.1175/Jamc-D-16-0379.1, 2017.

von Lerber, A., Moisseev, D., Marks, D. A., Petersen, W., Harri, A. M., and Chandrasekar, V.: Validation of GMI Snowfall Observations by Using a Combination of Weather Radar and Surface Measurements, J. Appl. Meteorol. Clim., 57, 797-820, https://doi.org/10.1175/Jamc-D-17-0176.1, 2018.

Wania, F.: A global mass balance analysis of the source of perfluorocarboxylic acids in the Arctic ocean, Environ. Sci. Technol., 41, 4529-4535, https://doi.org/10.1021/es070124c, 2007.

Warneke, C., Froyd, K. D., Brioude, J., Bahreini, R., Brock, C. A., Cozic, J., de Gouw, J. A., Fahey, D. W., Ferrare, R., Holloway, J. S., Middlebrook, A. M., Miller, L., Montzka, S., Schwarz, J. P., Sodemann, H., Spackman, J. R., and Stohl, A.: An important contribution to springtime Arctic aerosol from biomass burning in Russia, Geophys. Res. Lett., 37, https://doi.org/10.1029/2009gl041816, 2010.

Warren, S. G., and Wiscombe, W. J.: A Model for the Spectral Albedo of Snow .2. Snow Containing Atmospheric Aerosols, J. Atmos. Sci., 37, 2734-2745, https://doi.org/10.1175/1520-0469(1980)037<2734:Amftsa>2.0.Co;2, 1980.

Warren, S. G.: Optical-Properties of Snow, Rev. Geophys., 20, 67-89, https://doi.org/10.1029/RG020i001p00067, 1982.

Westgate, J. N., Sofowote, U. M., Roach, P., Fellin, P., D'Sa, I., Sverko, E., Su, Y. S., Hung, H., and Wania, F.: In search of potential source regions of semi-volatile organic contaminants in air in the Yukon Territory, Canada from 2007 to 2009 using hybrid receptor models, Environ. Chem., 10, 22-33, https://doi.org/10.1071/En12164, 2013.

Wiedensohler, A., Birmili, W., Nowak, A., Sonntag, A., Weinhold, K., Merkel, M., Wehner, B., Tuch, T., Pfeifer, S., Fiebig, M., Fjäraa, A. M., Asmi, E., Sellegri, K., Depuy, R., Venzac, H., Villani, P., Laj, P., Aalto, P., Ogren, J. A., Swietlicki, E.,

1675 Williams, P., Roldin, P., Quincey, P., Hüglin, C., Fierz-Schmidhauser, R., Gysel, M., Weingartner, E., Riccobono, F., Santos, S., Grüning, C., Faloon, K., Beddows, D., Harrison, R. M., Monahan, C., Jennings, S. G., O'Dowd, C. D., Marinoni, A., Horn, H. G., Keck, L., Jiang, J., Scheckman, J., McMurry, P. H., Deng, Z., Zhao, C. S., Moerman, M., Henzing, B., de Leeuw, G., Löschau, G., and Bastian, S.: Mobility particle size spectrometers: harmonization of technical standards and data structure to facilitate high quality long-term observations of atmospheric particle number size distributions, Atmos. Meas. Tech., 5, 657-

1680 685, https://doi.org/10.5194/amt-5-657-2012, 2012.

Willis, M. D., Leaitch, W. R., and Abbatt, J. P. D.: Processes Controlling the Composition and Abundance of Arctic Aerosol, Rev. Geophys., 56, 621-671, https://doi.org/10.1029/2018rg000602, 2018.

Wiscombe, W. J., and Warren, S. G.: A Model for the Spectral Albedo of Snow. I: Pure Snow, J. Atmos. Sci., 37, 2712-2733, https://doi.org/10.1175/1520-0469(1980)037<2712:Amftsa>2.0.Co;2, 1980.

1685 WMO: World Meteorological Organization report, No. 1074, 2010.

WMO: World Meteorological Organization report, No. 1085, 2011.

Wöhrnschimmel, H., MacLeod, M., and Hungerbuhler, K.: Emissions, Fate and Transport of Persistent Organic Pollutants to the Arctic in a Changing Global Climate, Environ. Sci. Technol., 47, 2323-2330, https://doi.org/10.1021/es304646n, 2013.

Xie, Z. Y., Wang, Z., Mi, W. Y., Möller, A., Wolschke, H., and Ebinghaus, R.: Neutral Poly-/perfluoroalkyl Substances in Air

1690 and Snow from the Arctic, Sci. Rep., 5, https://doi.org/10.1038/srep08912, 2015.

Yin, D. M., Cao, X., Chen, X. H., Shao, Y. J., and Chen, J.: Comparison of automatic thresholding methods for snow-cover mapping using Landsat TM imagery, Int. J. Remote Sens., 34, 6529-6538, https://doi.org/10.1080/01431161.2013.803631, 2013.

Young, C. J., Furdui, V. I., Franklin, J., Koerner, R. M., Muir, D. C. G., and Mabury, S. A.: Perfluorinated acids in arctic

1695 snow: New evidence for atmospheric formation, Environ. Sci. Technol., 41, 3455-3461, https://doi.org/10.1021/es0626234, 2007.

Yumashev, D., van Hussen, K., Gille, J., and Whiteman, G.: Towards a balanced view of Arctic shipping: estimating economic impacts of emissions from increased traffic on the Northern Sea Route, Climatic Change, 143, 143-155, https://doi.org/10.1007/s10584-017-1980-6, 2017.

1700 Zanatta, M., Laj, P., Gysel, M., Baltensperger, U., Vratolis, S., Eleftheriadis, K., Kondo, Y., Dubuisson, P., Winiarek, V., Kazadzis, S., Tunved, P., and Jacobi, H.-W.: Effects of mixing state on optical and radiative properties of black carbon in the European Arctic, Atmos. Chem. Phys., 18, 14037–14057, https://doi.org/10.5194/acp-18-14037-2018, 2018.

Zhao, Z., Xie, Z. Y., Möller, A., Sturm, R., Tang, J. H., Zhang, G., and Ebinghaus, R.: Distribution and long-range transport of polyfluoroalkyl substances in the Arctic, Atlantic Ocean and Antarctic coast, Environ. Pollut., 170, 71-77,

1705 https://doi.org/10.1016/j.envpol.2012.06.004, 2012.

Zheng, W., Xie, Z. Q., and Bergquist, B. A.: Mercury stable isotopes in ornithogenic deposits As tracers of historical cycling of Mercury in Ross Sea, Antarctica, Environ. Sci. Technol., 49, 7623-7632, https://doi.org/10.1021/acs.est.5b00523, 2015.

Zieger, P., Aalto, P. P., Aaltonen, V., Äijälä, M., Backman, J., Hong, J., Komppula, M., Krejci, R., Laborde, M., Lampilahti, J., de Leeuw, G., Pfüller, A., Rosati, B., Tesche, M., Tunved, P., Väänänen, R., and Petäjä, T.: Low hygroscopic scattering

1710 enhancement of boreal aerosol and the implications for a columnar optical closure study, Atmos. Chem. Phys., 15, 7247-7267,

https://doi.org/10.5194/acp-15-7247-2015, 2015.
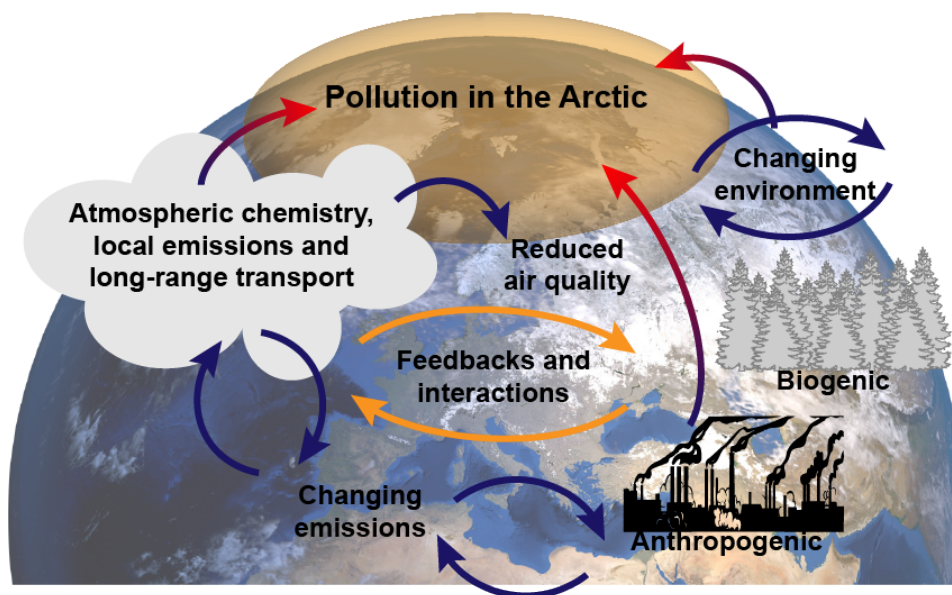
Figure 1. Atmospheric concentration of pollutants and their lifecycle in high latitudes are affected by local and regional anthropogenic activities and long-range transport from lower latitudes. Pollutant distributions and life cycles are modulated by transport patterns, changes in the biosphere, increased natural resource extraction and increased shipping in the Arctic Sea. Various feedbacks and interactions can either speed up or hinder the changes.
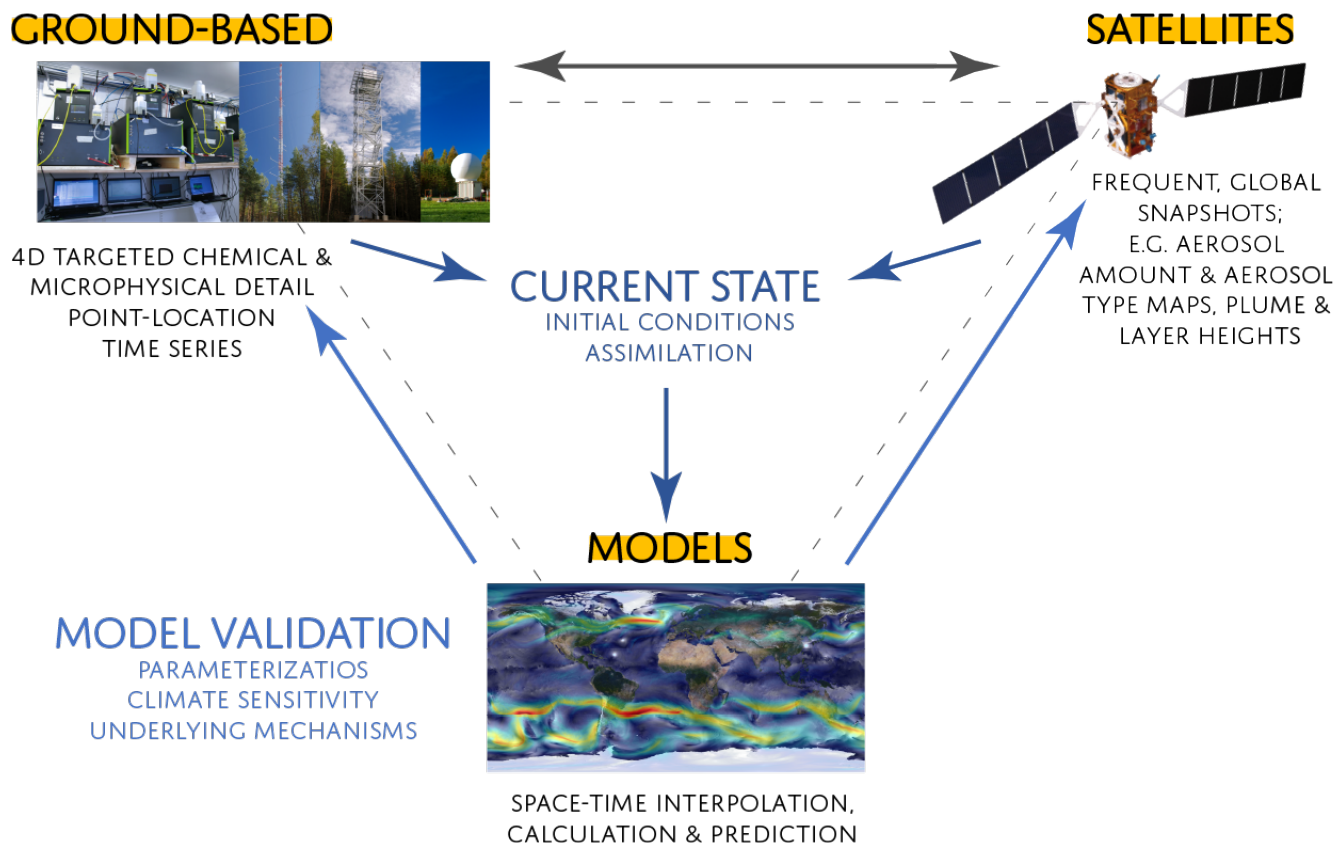
Figure 2. The integrative concept of iCUPE incorporates data and knowledge from ground-based observations, satellite remote sensing and modelling results providing a comprehensive view about the state of the environment in the polar areas.
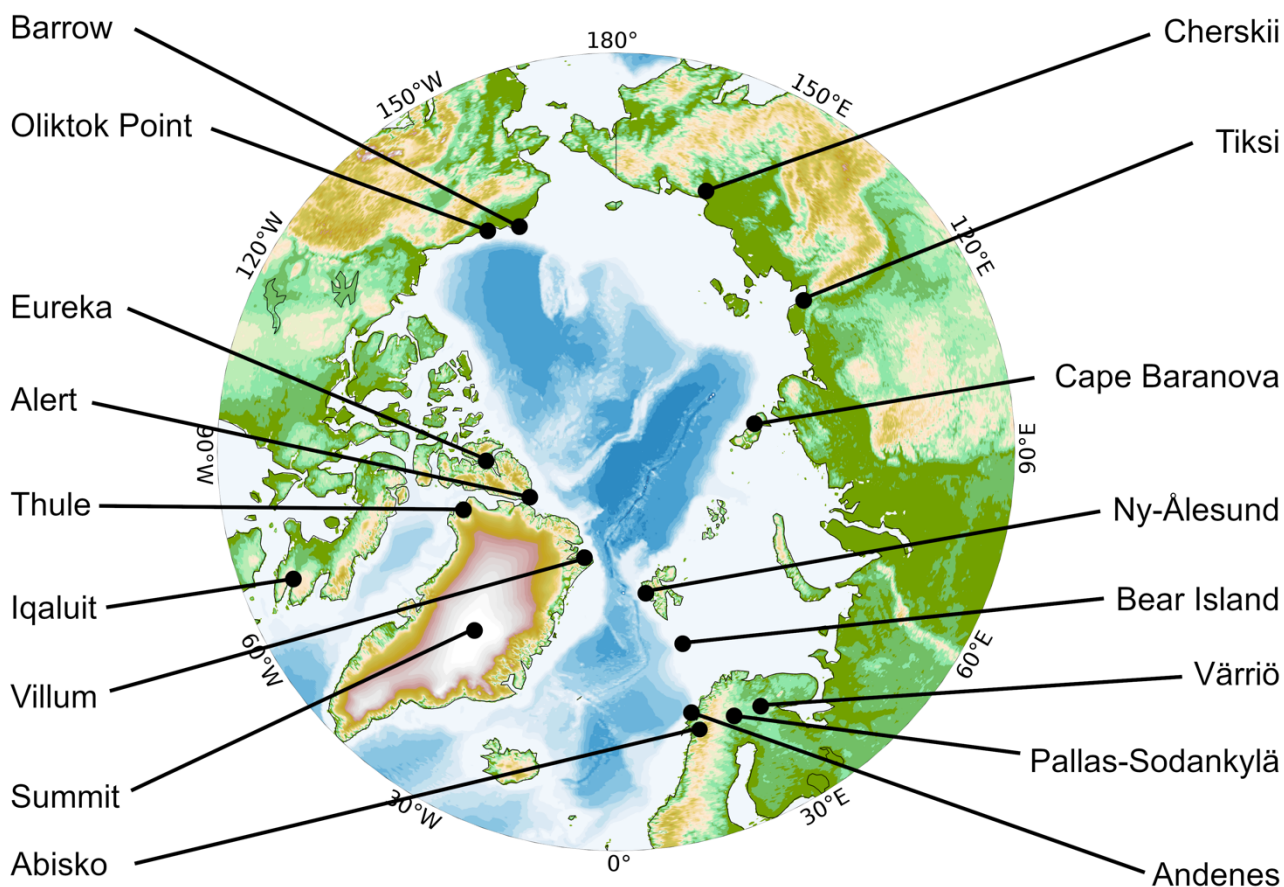
Figure 3. A map of stations with year-round observations in the Arctic with atmospheric aerosol measurements.
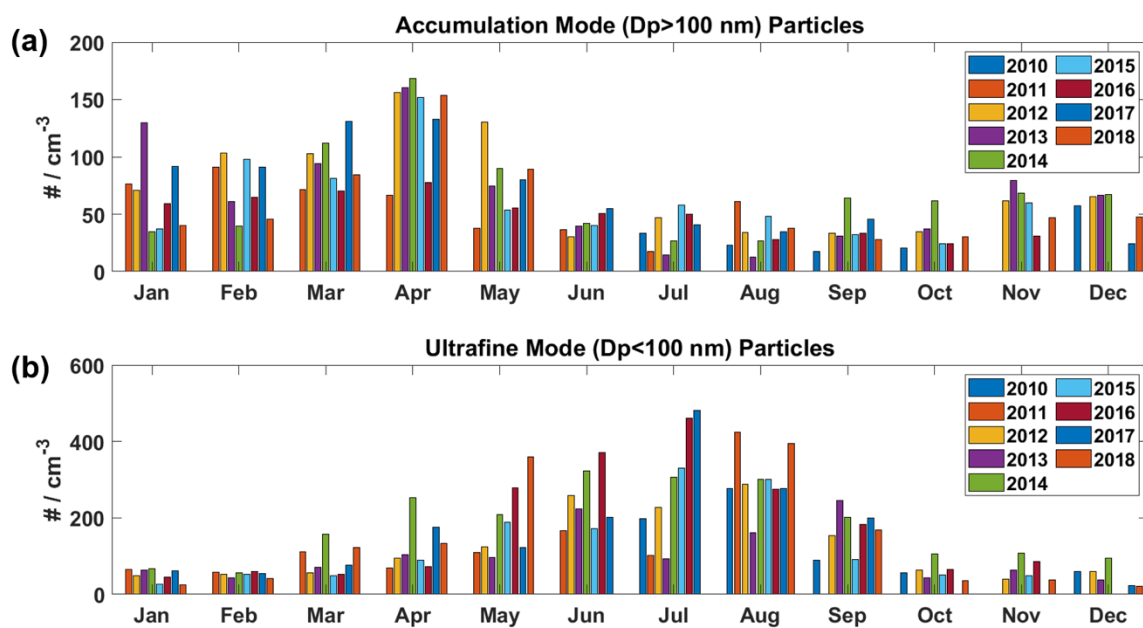
Figure 4. Monthly mean accumulation mode **(a)** and ultrafine mode **(b)** number concentration (# / cm^{-3}) measured at VRS from 2010 to 2018. Note the difference in scale of the y-axis for each panel.
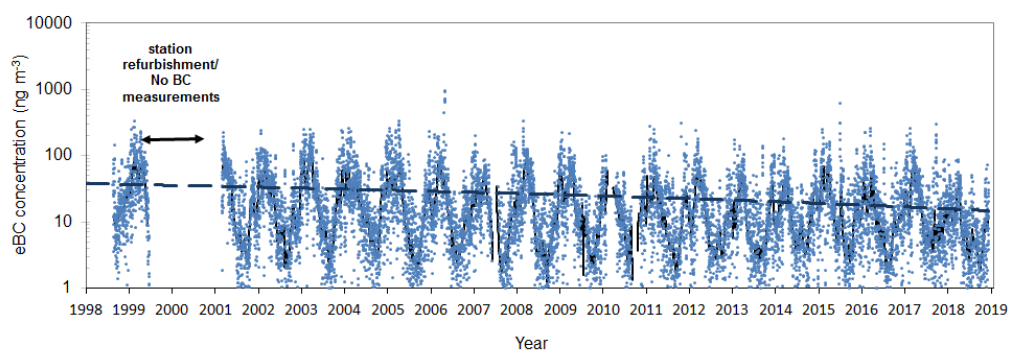
Figure 5. Equivalent Black Carbon concentration time series obtained by a 7-wavelength aethalometer at Zeppelin station. (Data before 2000 are obtained by an AE-9 aethalometer)
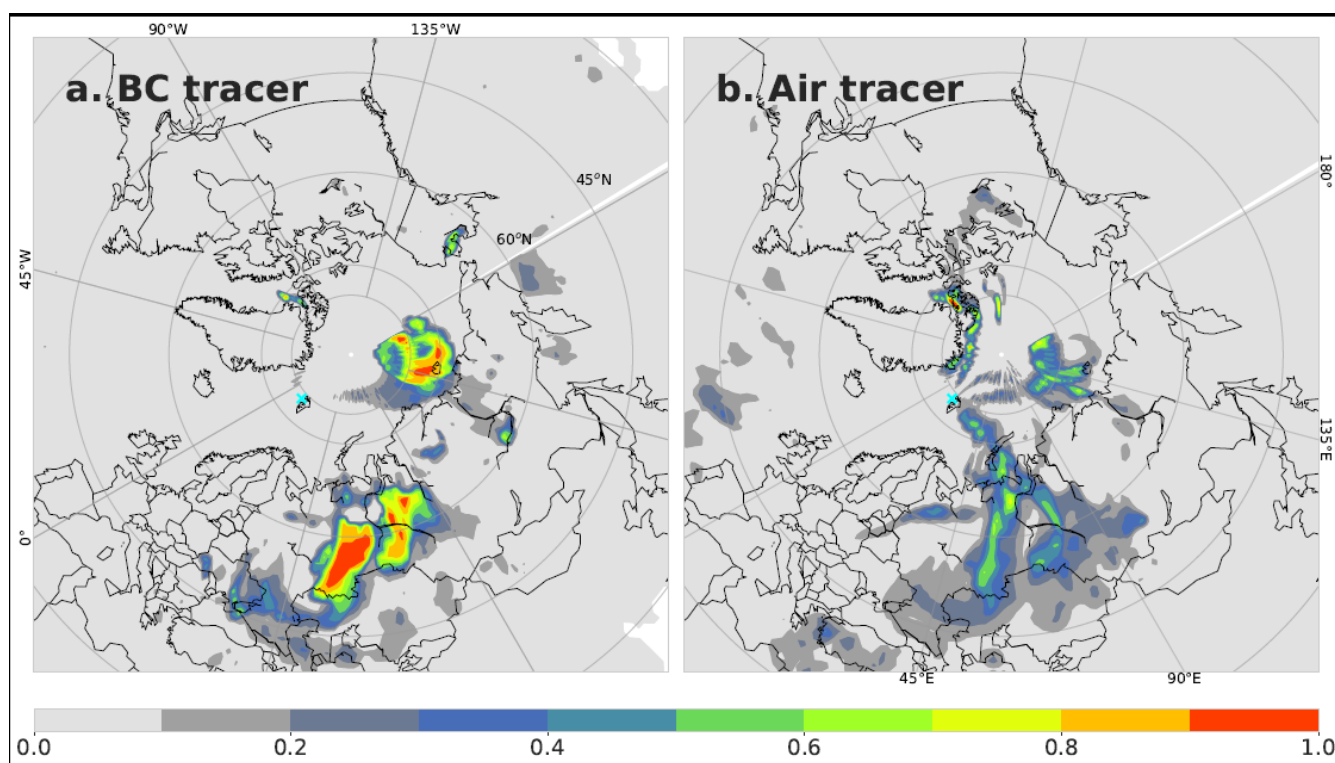
1730   **Figure 6.** Potential source contribution areas for BC observations at Zeppelin station Svalbard. The color scale represents statistical potential (1:100%) for 90th percentile of observed values to originate from certain areas of the Northern hemisphere. **(a)** and **(b)** corresponds to the air mass transport calculations using FLEXPART-model with the BC tracer and Air tracer respectively.
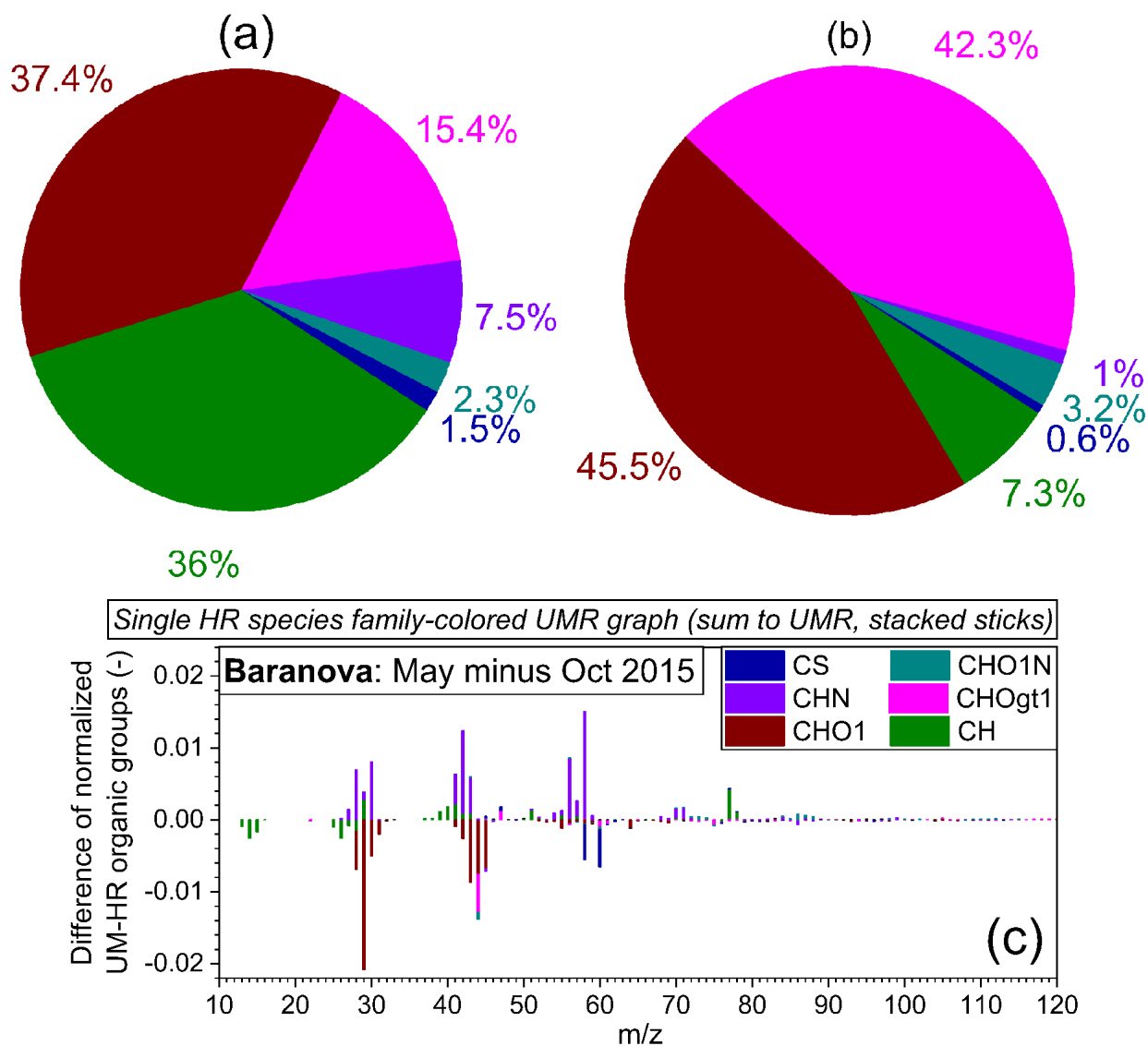
Figure 7. Offline AMS-based fractional contribution of the different organic aerosol families for **(a)** Cape Baranova (H:C = 1.53, O:C = 0.53) and **(b)** Alert (H:C = 0.81, O:C = 1.64) during October 2015. **(c)** Single organic species family-colored (stacked sticks) difference of the May minus October 2015 normalized mass spectrum. The former sample is expected to be influenced by pollution transport from mainland Russia. Data were taken and analyzed at high resolution, but are summed to unit mass resolution for display.
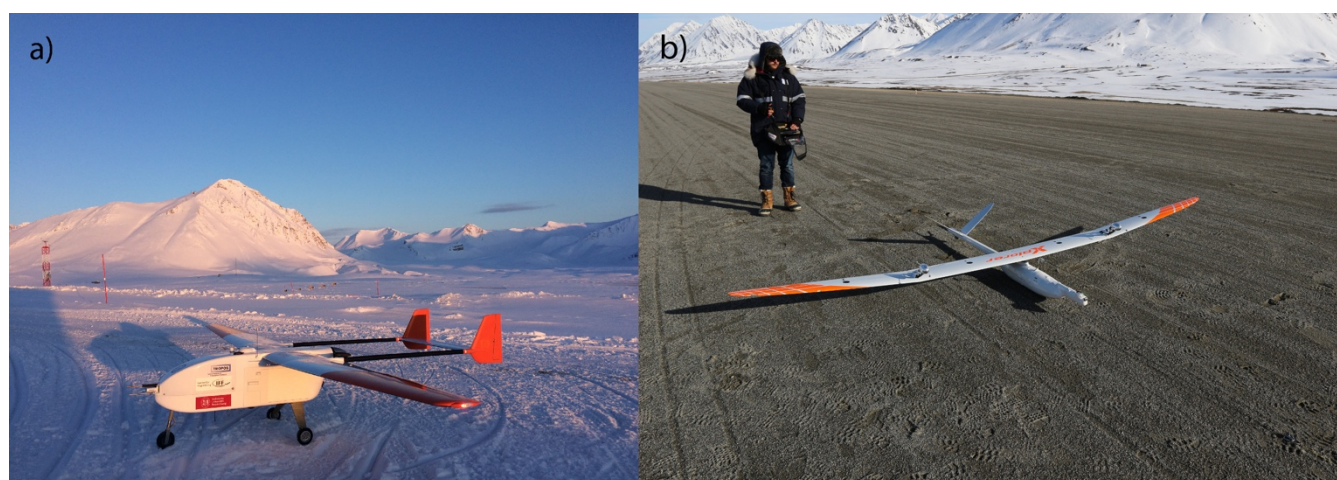
Figure 8. (a) The UAS ALADINA, **(b)** the UAS MASC3, both at the airport in Ny-Ålesund.
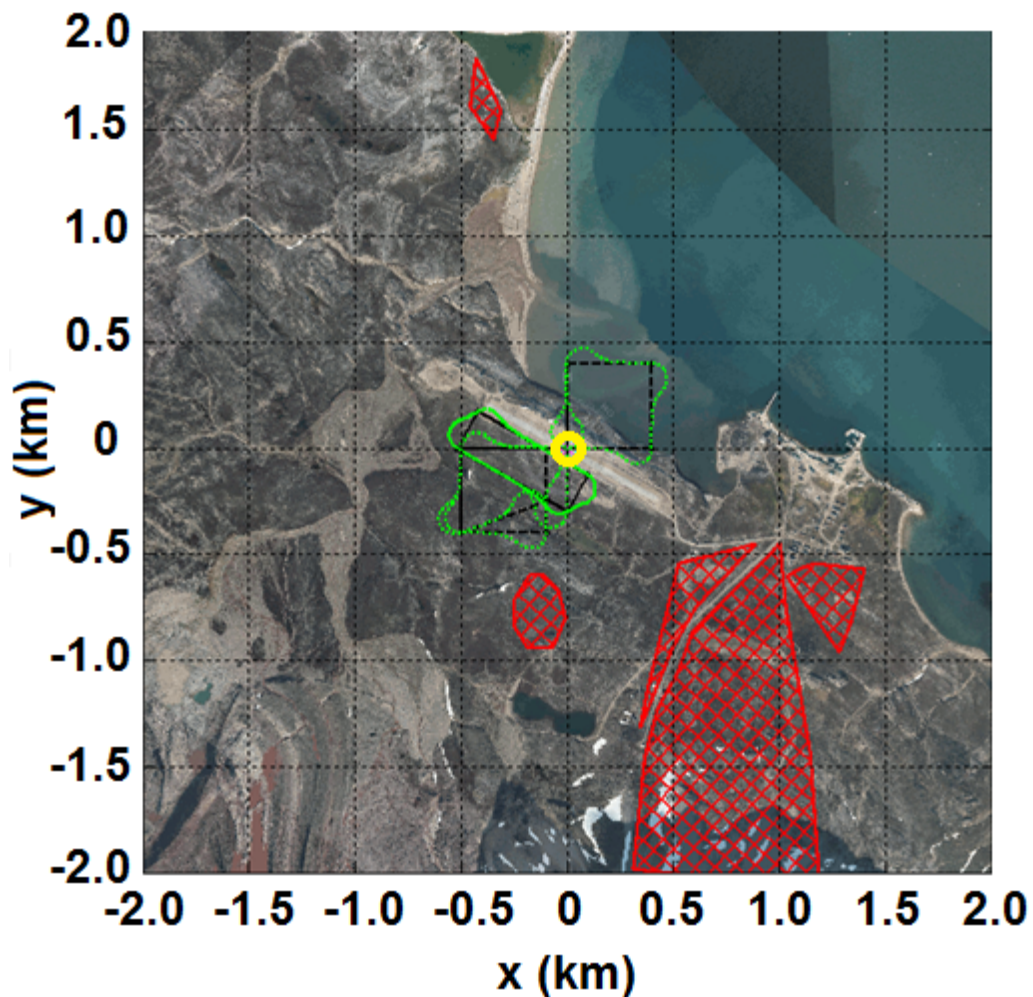
Figure 9. Flight path of the UAS ALADINA (start point in the center, marked in yellow) in order to study the vertical and horizontal distribution of aerosol particles above ice surfaces near glacier and over open water. Research flights were spatially limited by restricted areas (hatched in red), like bird sanctuary near coast, instrument areas south of Ny-Ålesund and no activity was performed over inhabited buildings of the village. The TopoSvalbard map is obtained from Norwegian Polar Institute, retrieved from http://toposvalbard.npolar.no. ©
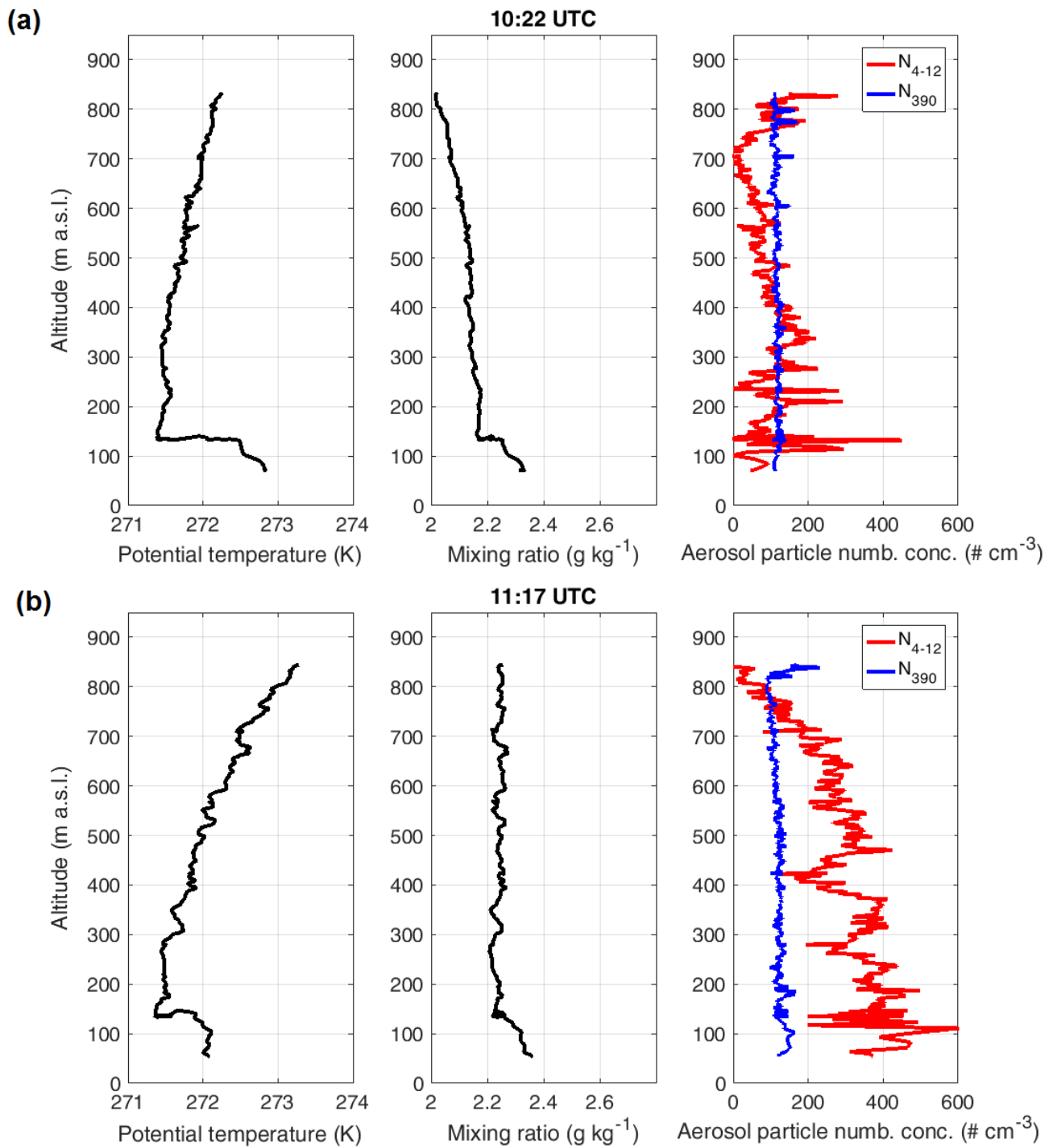
Figure 10. Selected profiles measured on May 23, 2018 in Ny-Ålesund for **(a)** 10:22 UTC and **(b)** 11:17 UTC. The panels show vertical profiles of potential temperature, water vapor mixing ratio and aerosol particle number concentrations between 4 and 12 nm and above 390 nm.
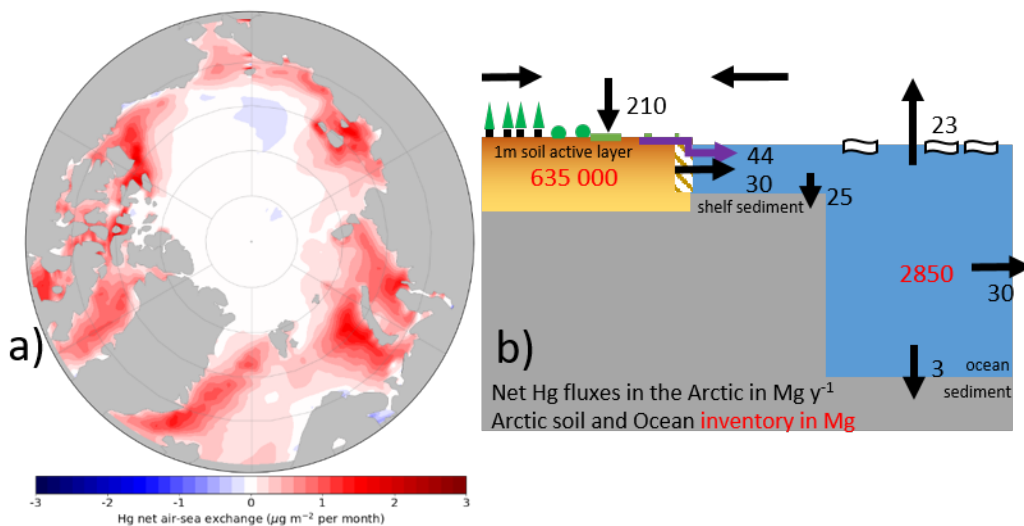
Figure 11. (a) Modeled net air–sea exchange of Hg (μg·m⁻²·month⁻¹) across the Arctic Ocean basin for the months June−July from the coupled GEOS-Chem/MITgcm Hg chemistry and transport model. Positive numbers (red) indicate a flux to the atmosphere. **(b)** The modern Arctic Hg cycle, showing net fluxes (metric tons per year, in black) between the different terrestrial, marine and atmospheric reservoirs (metric tons, in red). The hatched area represents the coastal erosion Hg flux. The large river Hg flux (purple arrow) confirms a new paradigm where tundra vegetation and soil uptake mid-latitude Hg atmospheric emissions and transfer them to rivers and the Arctic Ocean. Reproduced from Sonke et al., 2018.
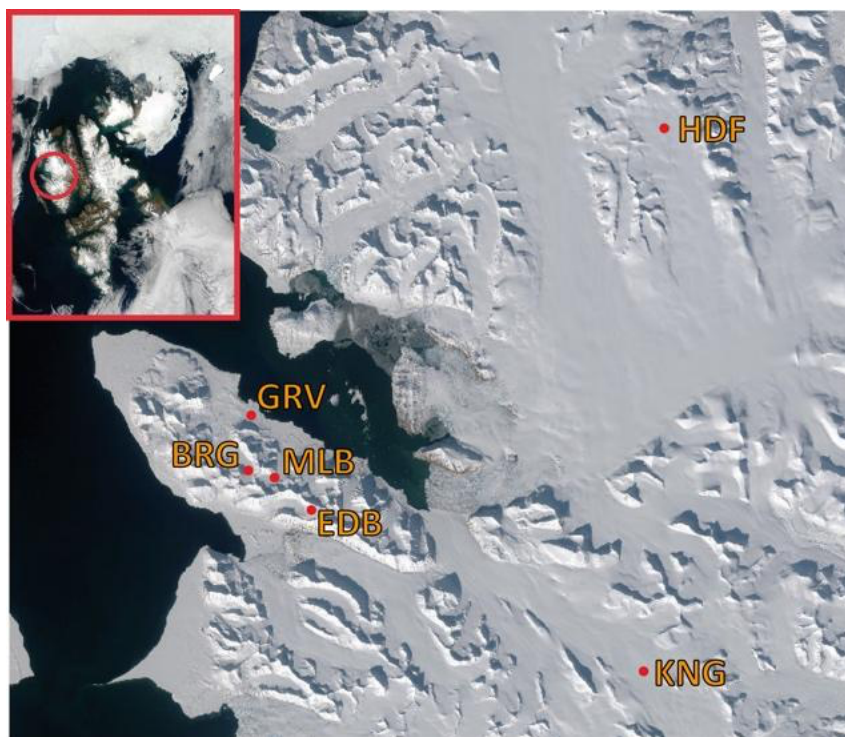
Figure 12. Snow sampling locations in the Svalbard Archipelago. BRG - Austre Broggerbreen glacier; MLB - Midtre Lovenbreen glacier; EDB - Edithbreen glacier; KNG - Kongsvegen; HDF - Holthedalfonna ice field. The TopoSvalbard map is obtained from ©Norwegian Polar Institute, retrieved from http://toposvalbard.npolar.no.
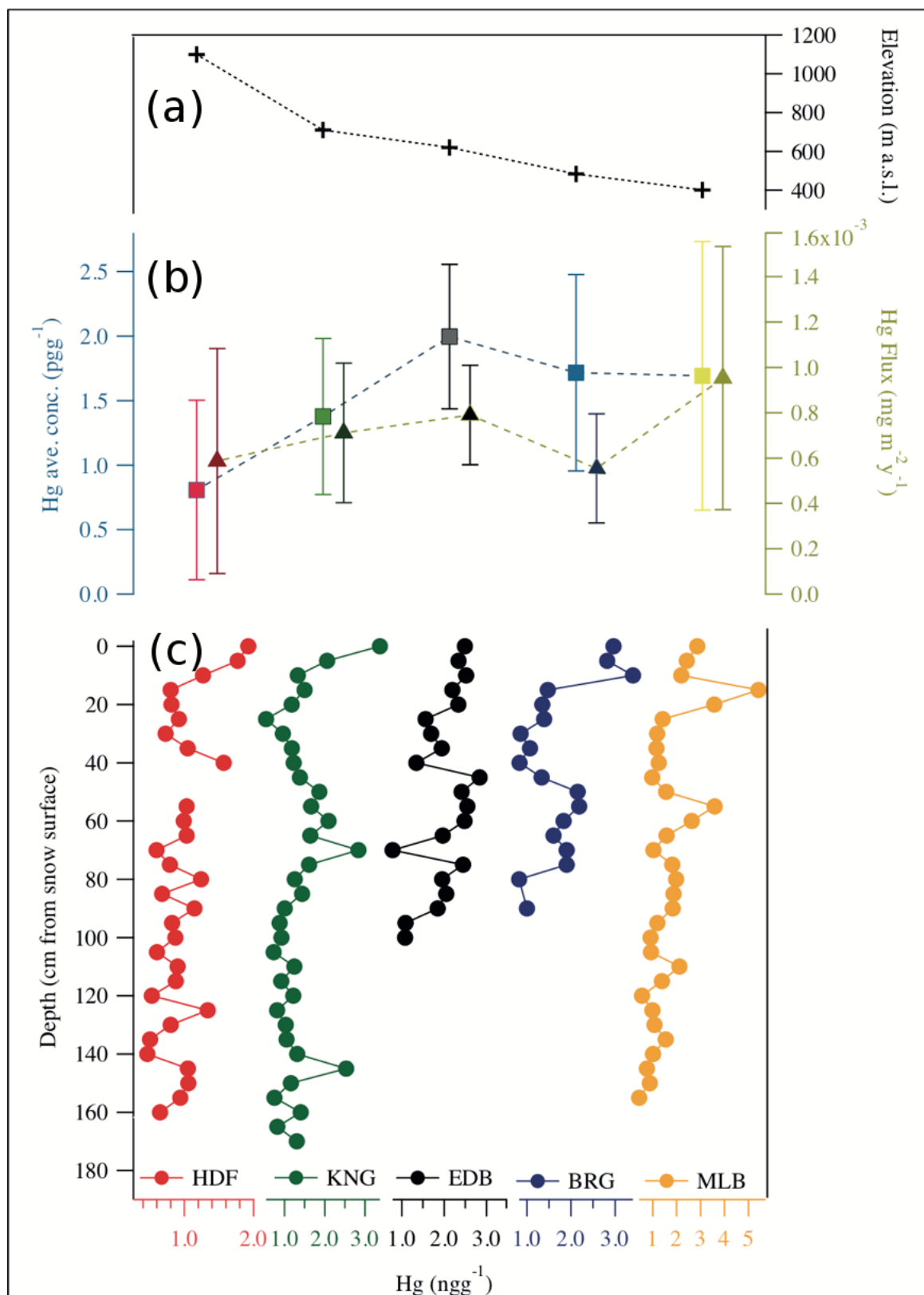
Figure 13. The upper panel (a) shows the elevation of the snow pit sampling sites. The lower panel (c) depicts Hg concentrations in the annual snowpack expressed in pg g^{-1}. The depth scale is expressed in cm and the snow surface is set at 0 cm. Samples have a constant resolution of 5 cm to the bottom. Middle panel (b): mean Hg concentration (color square) and total flux (color triangles), vertical bars indicate one standard deviation.
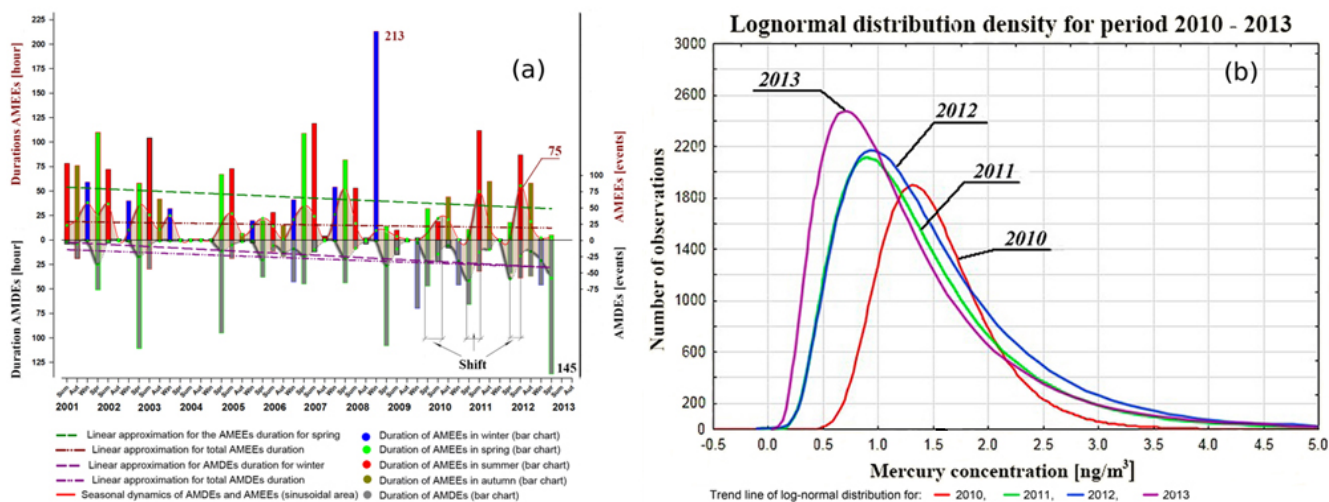
Figure 14. **(a)** Seasonal dynamics of AMDEs and AMEEs during the monitoring period from 2001 to 2013 (sinusoidal area). Duration of AMDEs and AMEEs (bar chart, the red color - summer, green - spring, dark yellow - autumn, blue - winter). Linear approximation for the AMEEs duration for spring (green dashed line), and AMDEs duration for winter (purple dashed line); for total AMEEs duration (brown dash with two dots) and for total AMDEs duration (purple dash with two dots). **(b)** The lognormal distribution of the atmospheric Hg^0 concentration during the monitoring period from June 2010 to October 2013.
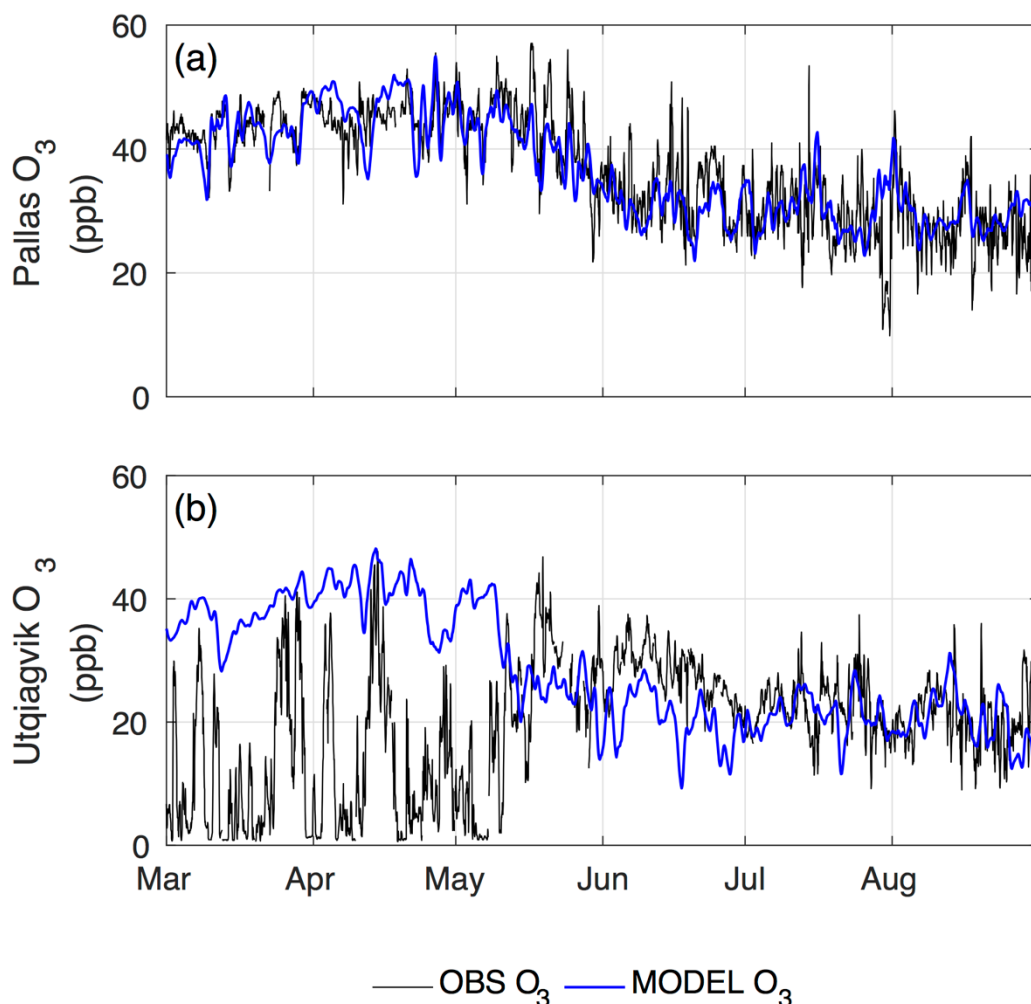
Figure 15. Observed and model predicted ozone concentrations at two Arctic surface stations for March–August 2012. WRF-Chem in blue and observations are in black. The model does not capture ozone depletion events observed at Utqiaġvik during Arctic spring. At Pallas, an inland site where no bromine activation is expected, the model in the present state captures the full spring-summer seasonal cycle of ozone.
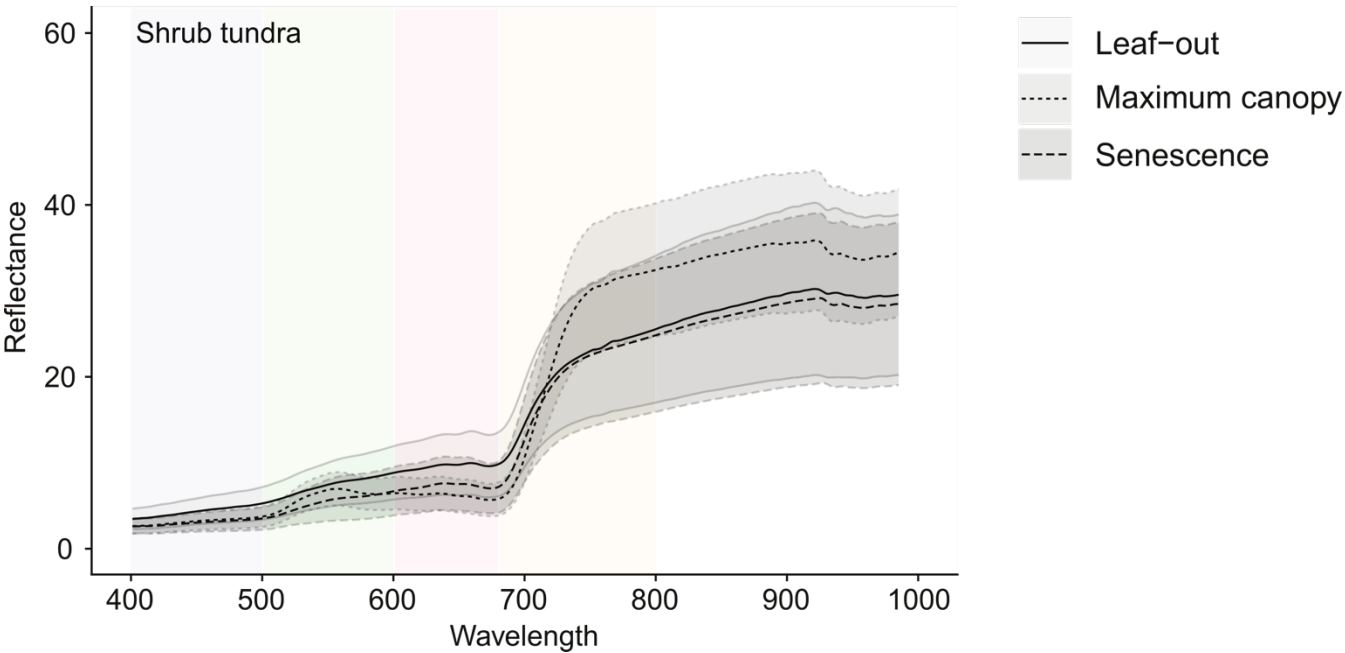
Figure 16. Canopy-level spectral reflectance from a dwarf shrub community at three major phenological phases of leaf-out, maximum canopy, and senescence (Beamish et al., 2017).
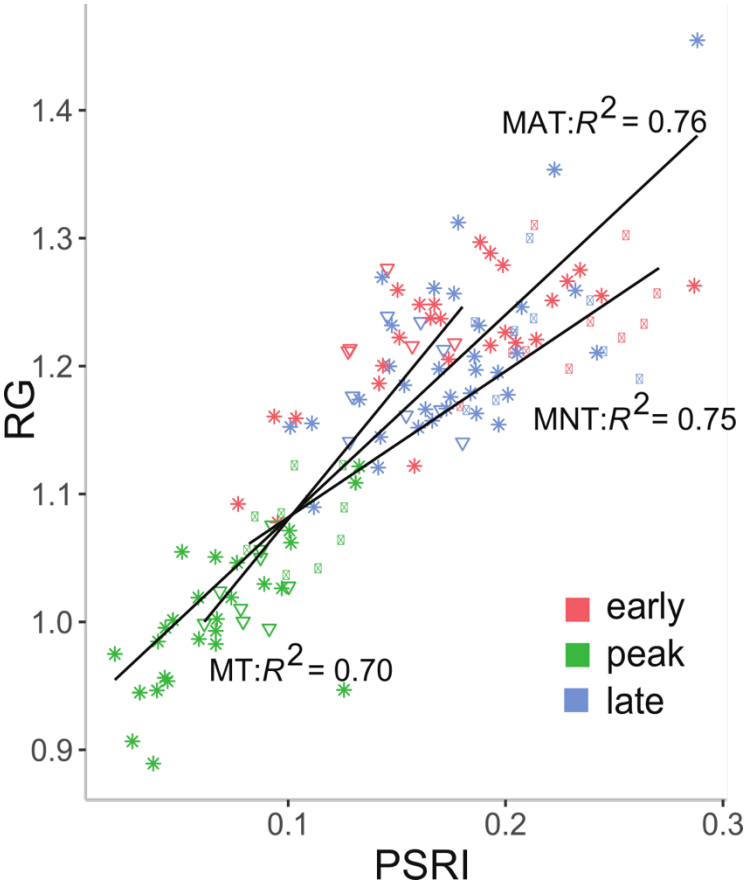
 Figure 17. The relationships between pigment driven spectral indices of Plant Senescence Reflectance Index (PSRI) calculated from canopy level spectral reflectance and the simple normalized Red Green index calculated from the digital camera data in three dominant vegetation communities. MNT: Moist non-acidic tundra; MAT: Moist acidic tundra; MT: Moss tundra. PSRI is used to track plant senescence related to the degradation of chlorophyll pigments (Beamish et al., 2018).
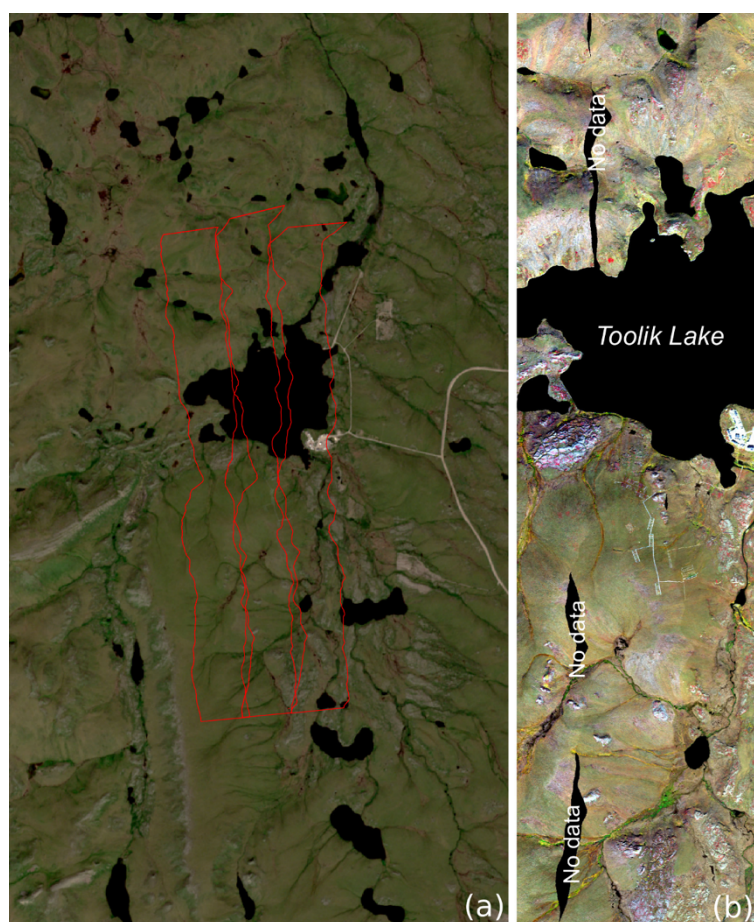
Figure 18. Toolik Lake, Alaska. (a) Sentinel-2 image (21.07.2016) with airborne hyperspectral flight lines in red; (b) AISA Eagle hyperspectral image (1.3 m) (Beamish et al., 2019b).
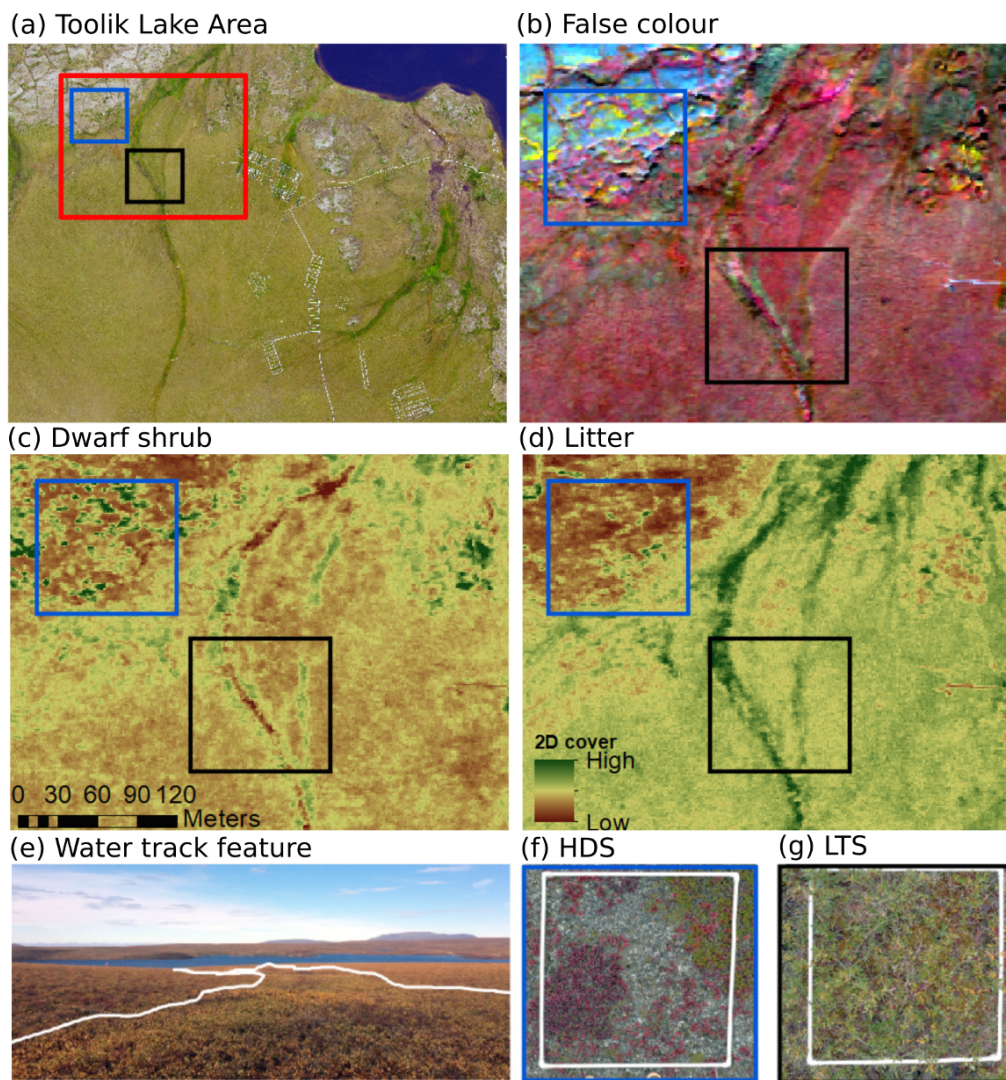
Figure 19. a) A 50 cm aerial photograph of the Toolik vegetation grid (Toolik Lake Environmental Data Centre, https://toolik. alaska.edu/edc/, 2017), inset represents the extent of hyperspectral imagery below; b) a false color composite of the north west corner of the study area, R: 812, G: 686, and B: 546 nm; c) Dwarf shrub 2D cover estimated by NRI λ1: 550 λ2: 650 nm; d) Litter 2D cover estimated by NRI λ1: 525 and λ2: 600 nm; e) field photo of a water track feature from the study area; f) Hemiprostrate and prostrate dwarf-shrub, forb, moss, fruticose-lichen tundra; g) Low and tall shrublands (Beamish et al., 2019b). The airborne image is provided by ©Toolik Lake Environmental Data Centre (https://toolik. alaska.edu/edc/, 2017).
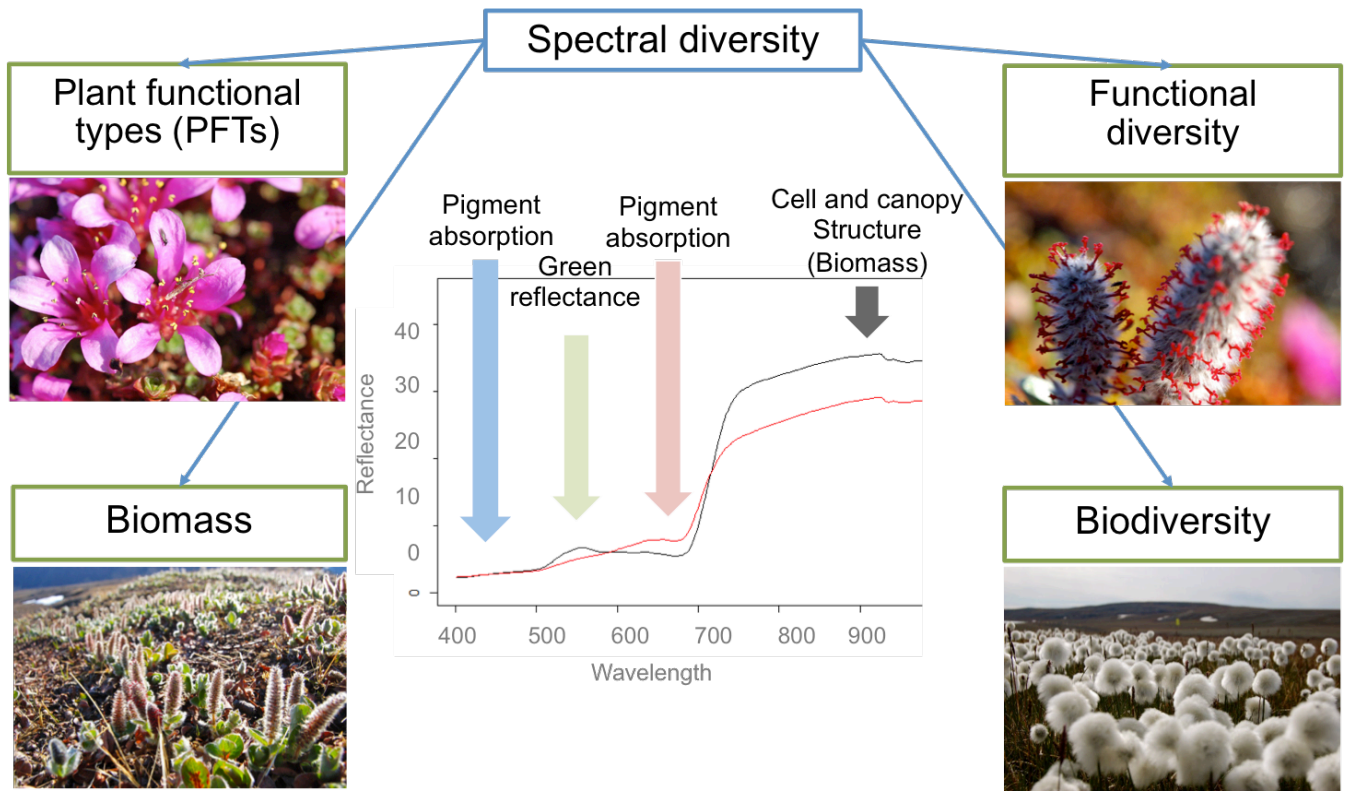
Figure 20. Spectral characterization of key biophysical and biochemical variables can inform interpretation of airborne and satellite hyperspectral remote sensing.
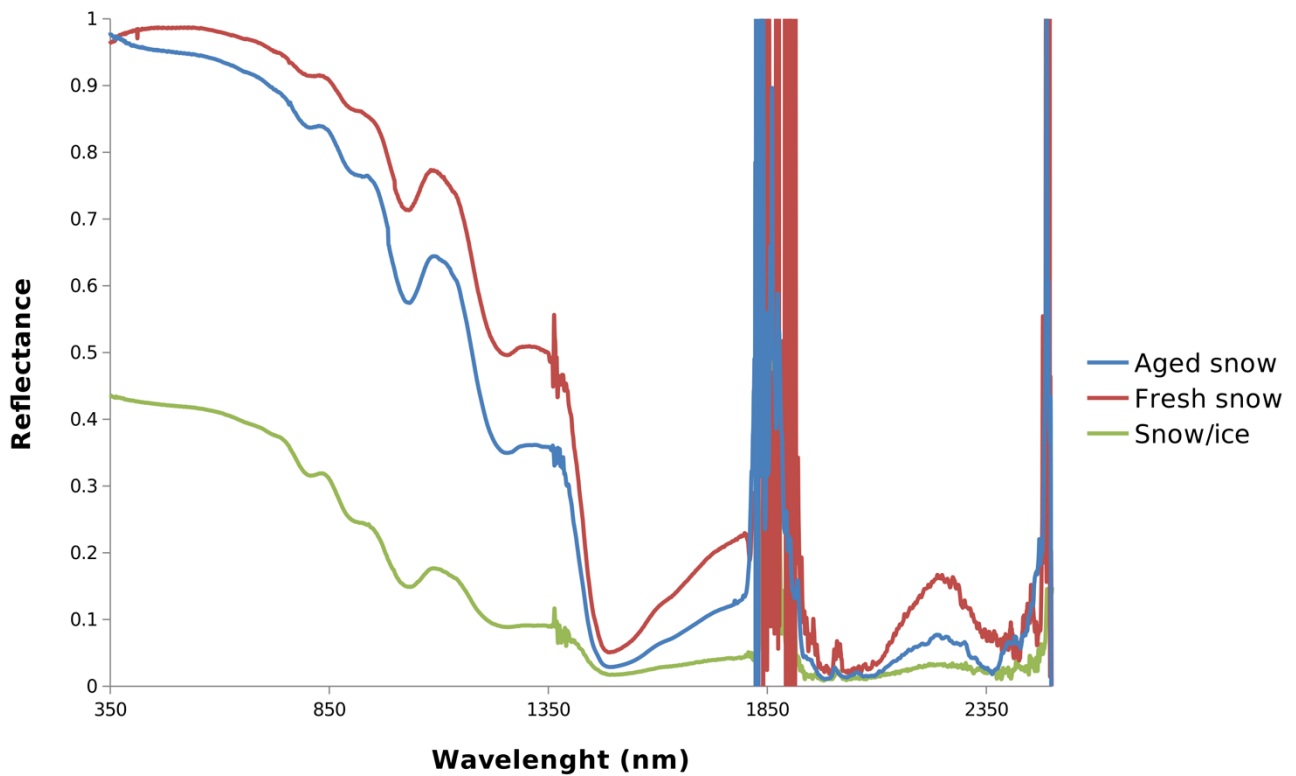
1805   **Figure 21.** Spectral behavior of different snow covers.
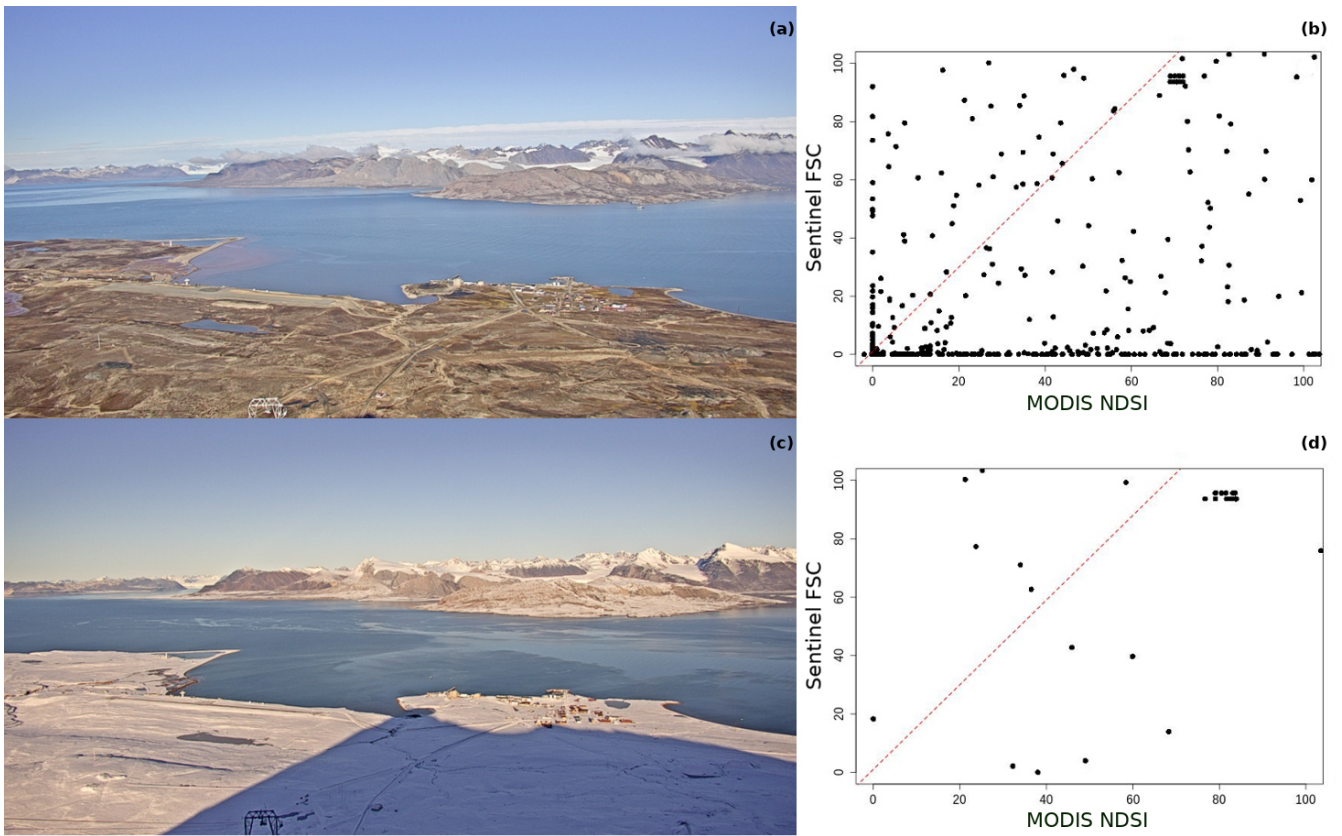
Figure 22. The snow cover at Ny-Ålesund during two different seasons: (a) August 20th 2018; (c) September 17th 2018. Relationship between the spectral index of snow (NDSI) obtained by MODIS data, and the Fractional Snow Cover estimated by Sentinel-2 and detected by terrestrial photography (b,d) (Pedersen, 2013).

1810
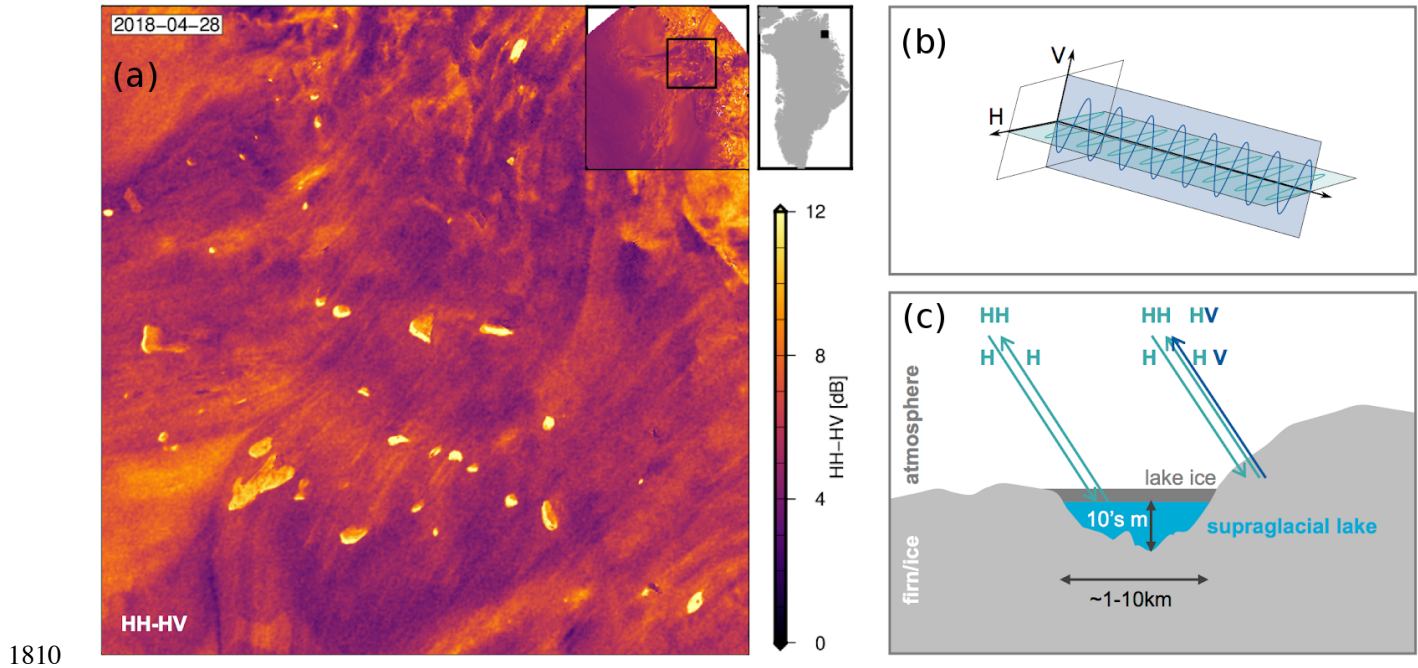
Figure 23. (a) Detection of supraglacial lakes using polarimetry using Sentinel-1. Bright yellow colors denote surface scattering, which is arising from the flat transition between lake ice and water, as shown schematically in the right panel. (b) and (c) a schematic representation of principle of polarimetric method.
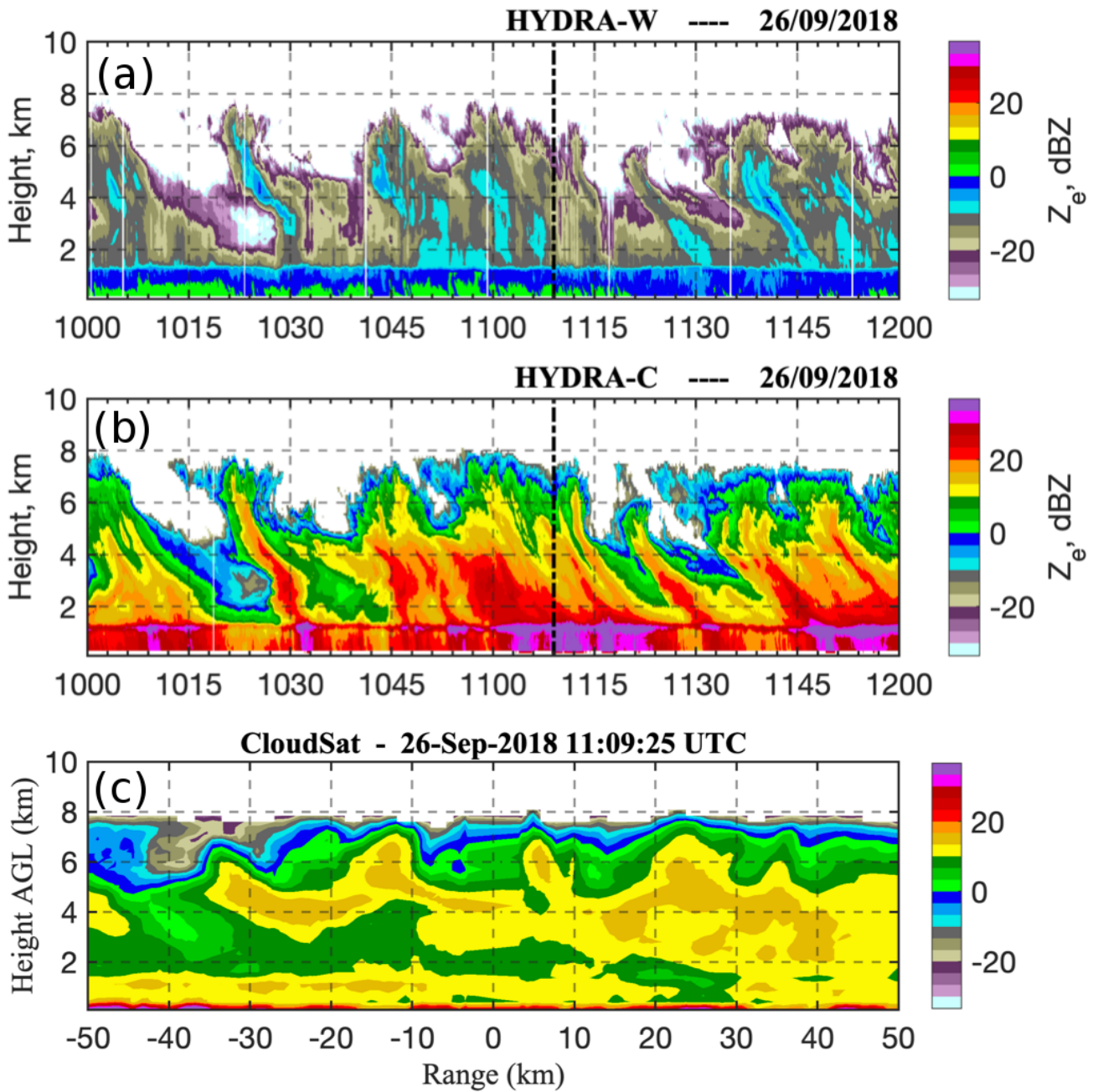
1815 **Figure 24.** Observations of clouds and precipitation using Hyytiälä **(a)** cloud, **(b)** precipitation radars and **(c)** CloudSat cloud profiling radar, the bottom panel. The vertical dash-dotted line in the panels indicates the CloudSat overpass time. The x axis in the CloudSat panel shows the distance between the Hyytiälä site and the satellite ground-track.
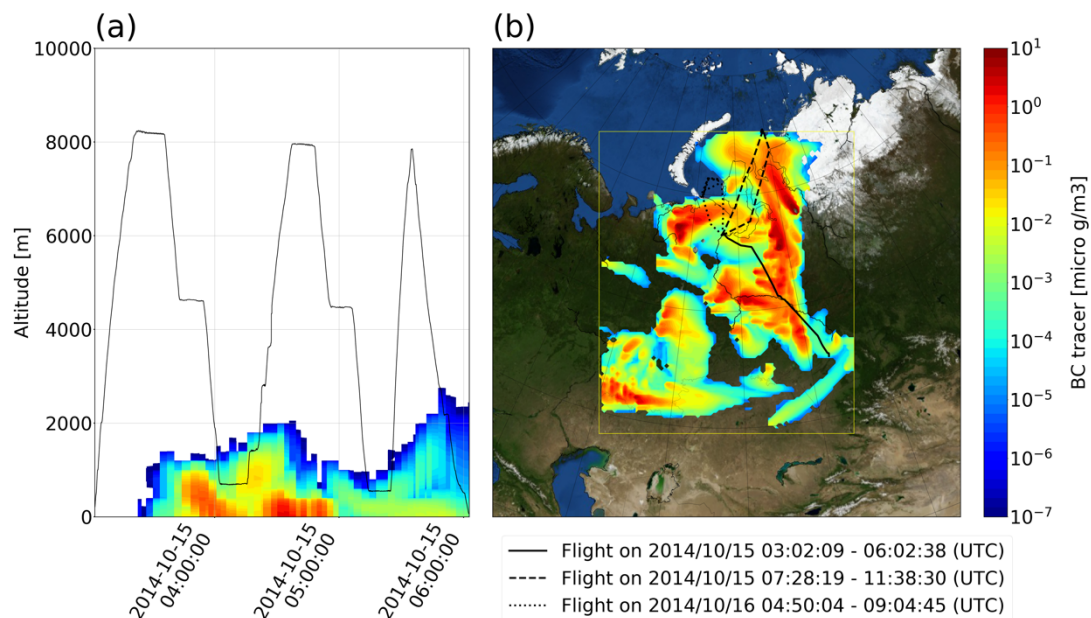
Figure 25. Simulated concentrations of BC tracer with 5 day lifetime in micro g m^{-3} **(a)** along YAK flight on 15 October 2014 (flight altitude also given, white line), and **(b)** at the surface at 05 UTC on 15 October 2014, flight tracks are also shown. BC tracer concentrations are normalised to the total BC emissions from Huang et al. (2015) over the model domain and emitted based on annual mean flaring locations using VIIRS data.
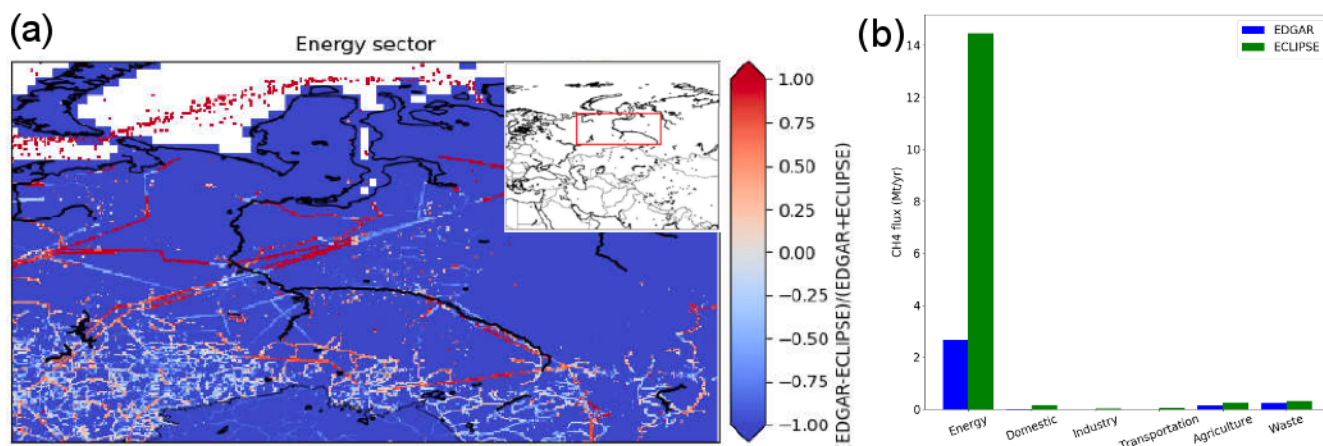
Figure 26. Comparison of the EDGAR v4.3.2 and ECLIPSE v5a inventories for methane. **(a)** spatial distribution normalized difference **(b)** total by sector of methane emission for the western Siberia area.
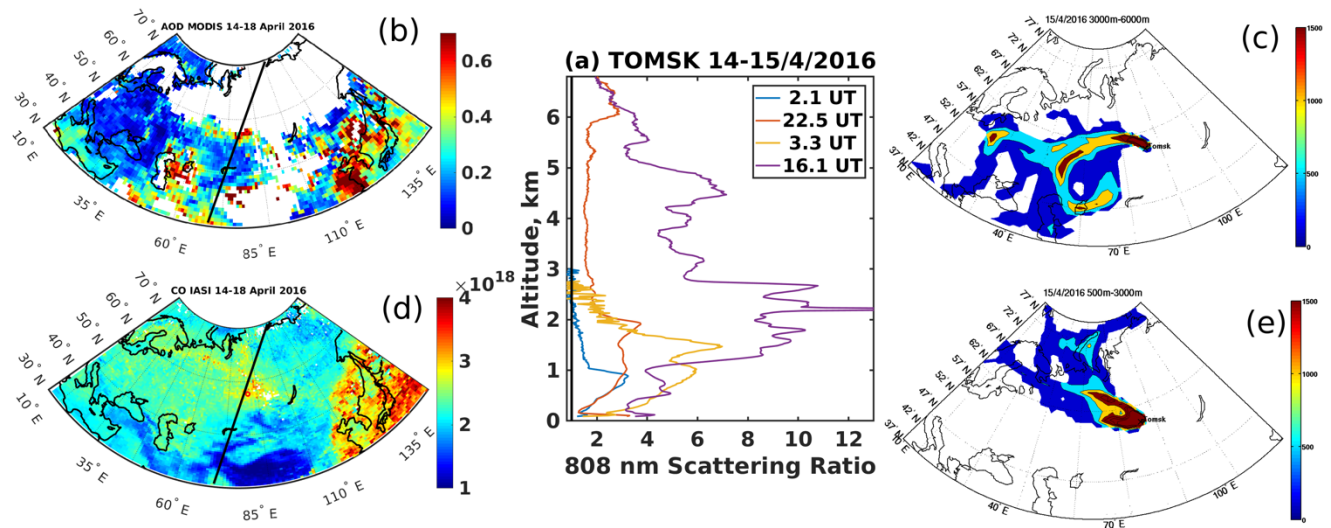
Figure 27. Vertical profiles of scattering ratio on 14 and 15 April 2016 from Tomsk lidar (a) and corresponding 5-day average map of AOD at 532 nm from MODIS (b) and of CO total column in molecules cm^{-2} from IASI observations (d). The red circle is Tomsk and the black thick lines are the CALIOP overpass over Tomsk on April 14 at 21 UTC. Potential emission sensitivity (PES) distributions of an aerosol tracer averaged for 9 days before the Tomsk lidar aerosol layer observations below 3 km (e) and above 3 km (c) are calculated with backward simulations of the FLEXPART model using dry and wet deposition of the tracer during backward transport.
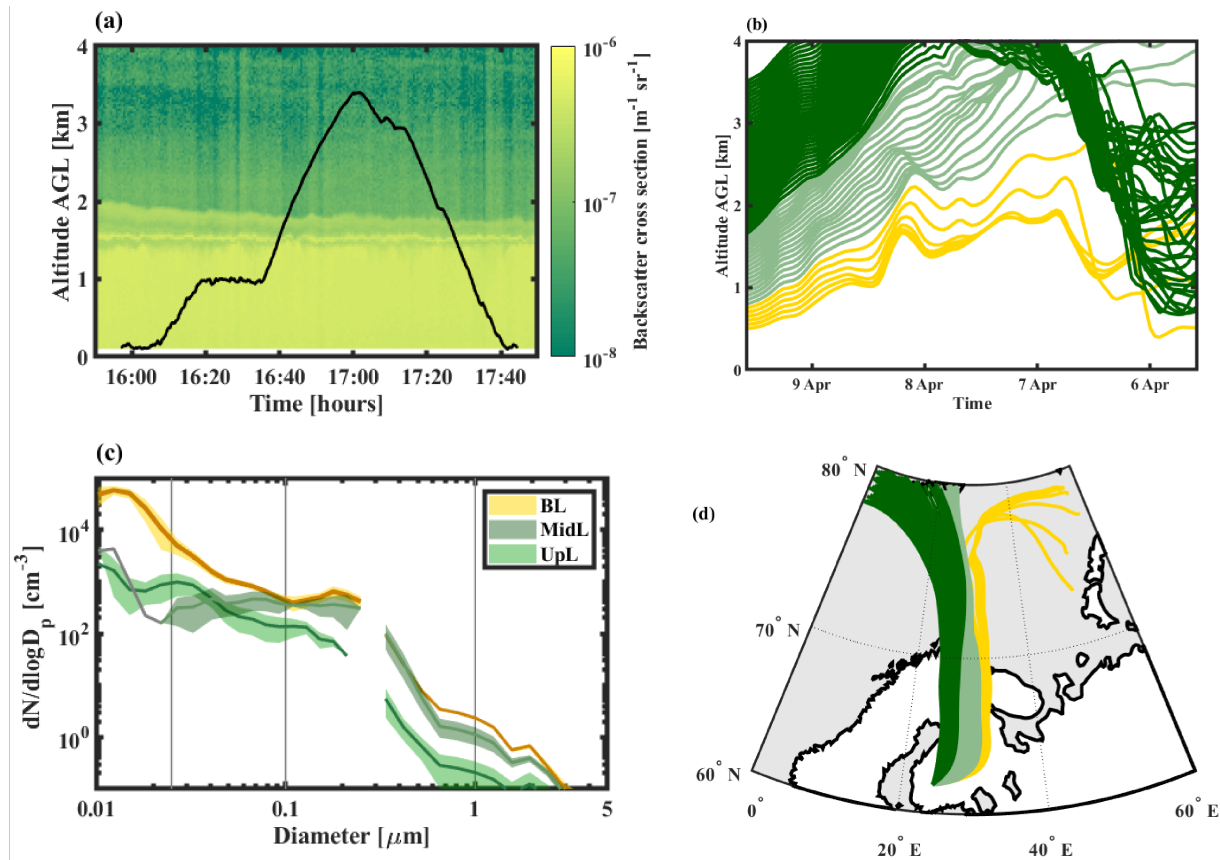
Figure 28. Clear sky case study during 9 April 2014 at SMEAR II station, Finland: **(a)** HSRL backscatter coefficient with Cessna flight altitudes in black; **(b)** 96h backward trajectories calculated every 50 m and combined into layers according to

similarities in the travelling path; **(c)** aerosol size distribution measured onboard during the flight and combined into layers, shown with 1 standard deviation; **(d)** spatial coverage of backward trajectories.
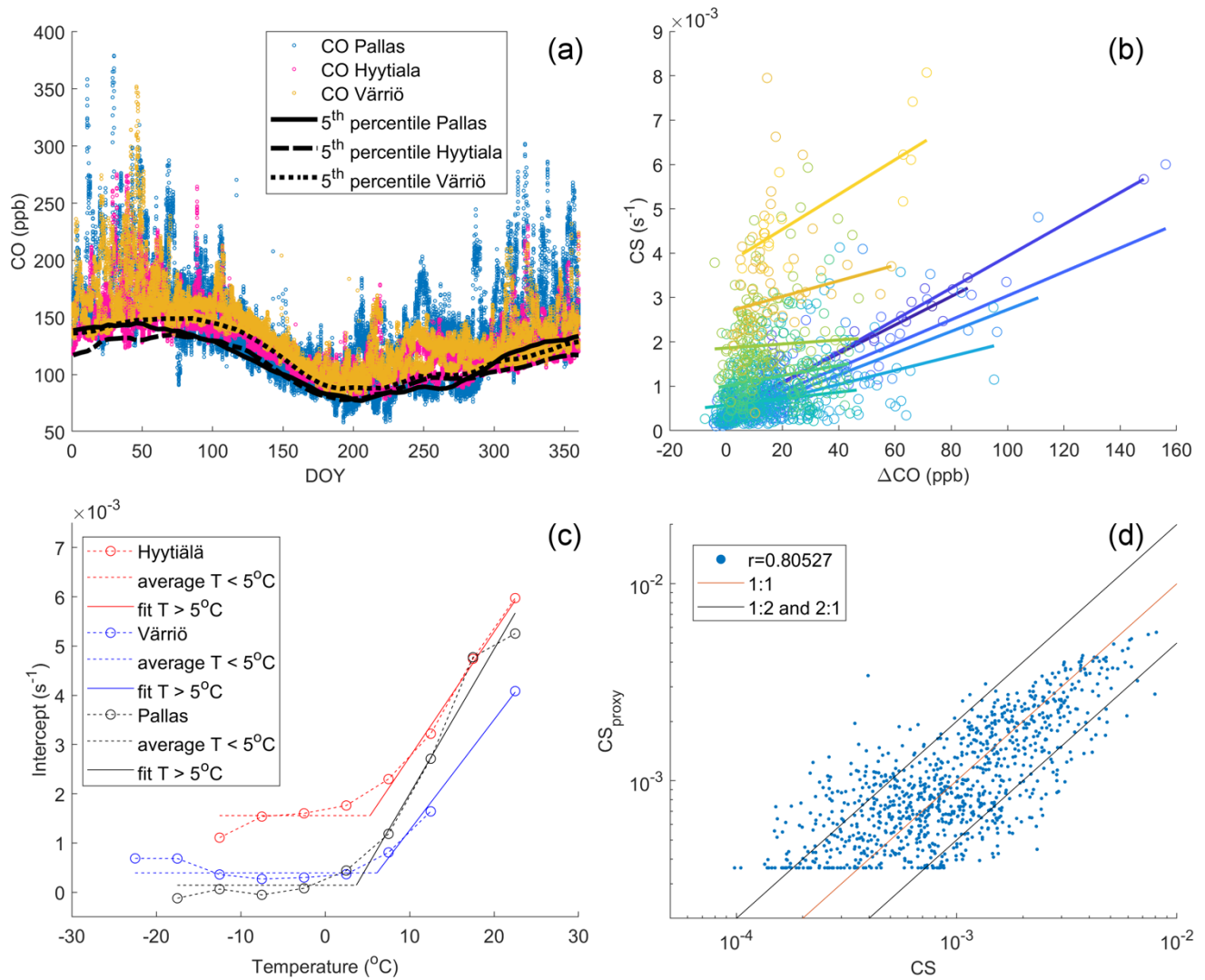
1840 **Figure 29.** Derivation of proxy for condensation sink (CS) based on carbon monoxide (CO) concentration and air temperature. **(a)** annual pattern of CO concentration and its 5th percentiles at the observation sites, **(b)** observed CS in Värriö as a function of the difference between observed CO and the 5th percentiles from panel (a) in 5 °C temperature bins (blue colors for T < 5°C, green and yellow for T > 5°C), **(c)** intercepts $a_i(T)$ in fittings to data in panel (b), when slopes are forced to their average b_{ave}, as functions of temperature, and **(d)** the resulting proxy as shown in Eq. 3.

1845
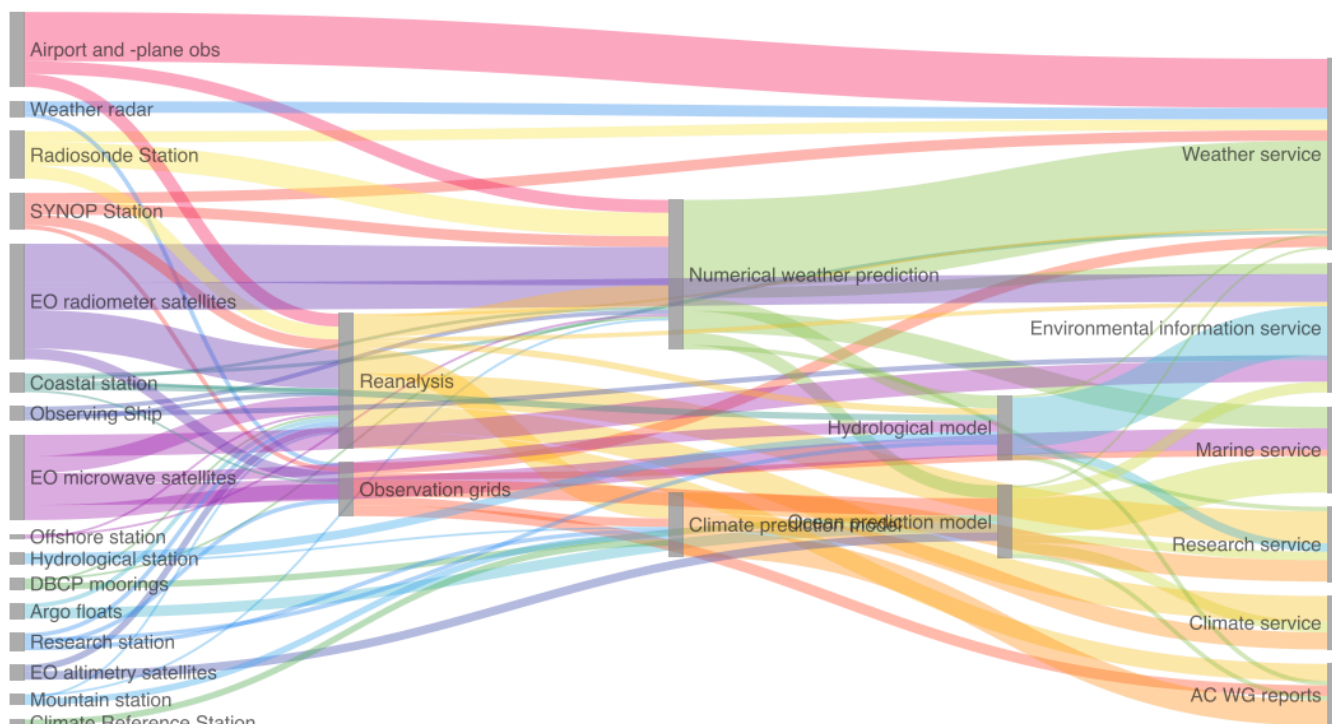
Figure 30. The observations, modelling and services parts of the value tree - the source tree. iCUPE actions are represented in research stations, EO satellites and observation grids supporting research services. The framework foresees 3 levels, but modelling is feeding its own components, which adds more depth to the tree.

 Table 1. iCUPE products as datasets resulted from research activities of the project as well as collaboration with PEEX Russian partners. First dataset was delivered in December 2018.

N	iCUPE products as datasets on:
1	Emerging organic contaminants in air from the Arctic
2	Ground based measurements for particle number, black carbon mass and ozone concentration
3	Black carbon and aerosol absorption of Arctic research infrastructures
4	Anthropogenic contaminants in snow from polar regions
5	Anthropogenic contaminants in ice cores
6	Emerging organic contaminants in snow from the Arctic
7	Emerging organic contaminants in water from the Arctic
8	Snow spectral reflectance
9	Aerosol vertical profiles from ground-based and satellite observations in Finland and Russia
10	Arctic atmospheric mercury observations: updated GMOS database
11	Blueprint for novel proxy variables integrating in situ and satellite data
12	Arctic parameters based on ground-based remote sensing and airborne platforms
13	Precipitation in the high-latitudes
14	Novel optical remote sensing products on snow and on vegetation and gas flaring mapping in selected sites
15	Arctic atmospheric mercury isotope observations
16	Time series of lakes' size changes in Northeast Greenland
17	Aerosol reanalysis for SMEAR-II
18	Organic aerosols in the Arctic based on source apportionment
	Datasets resulted from collaboration with PEEX Russian partners
20	Mercury measurements at Amderma station of the Russian Arctic
21	Elemental and organic carbon over the northwestern coast of the Kandalaksha Bay of the White Sea
22	Micro-climatic features and Urban Heat Island Intensity in cities of the Arctic region
23	Atmospheric composition at Fonovaya Observatory, West Siberia

Table 2. WMO Oscar statistics on operational stations in 30° latitude slices, iCUPE stations are mostly non-affiliated

Latitude slice	total stations	WIGOS	co-sponsored	non-affiliated	area %	land %
60°N-90°N	2 218	1 352	853	13	6,53	3,04
30°N-60°N	13 070	7 436	5 472	162	18,37	8,79
0°N-30°N	8 062	2 820	5 222	20	25,1	6,81
0°S-30°S	5 805	2 300	3 432	73	25,1	5,66
30°S-60°S	4 120	917	3 199	4	18,37	0,91
60°S-90°S	712	165	547	0	6,53	2,53